Climate across scales: the downscaling of precipitation for a basin in a tropical mountain region in the Andes of Southern Ecuador

kumulative Dissertation
zur Erlangung des
Doktorgrades
der Naturwissenschaften
(Dr. rer. nat.)

dem Fachbereich Geographie
der Philipps-Universität
Marburg
vorgelegt von

Lenin Campozano
aus Cuenca - Ecuador

Marburg / Lahn, 2016

Vom FACHBEREICH GEOGRAPHIE
der PHILIPPS-UNIVERSITÄT MARBURG
(Hochschulkennziffer 1180)
als Dissertation am 30.01.2017 angenommen

Erstgutachter: Prof. Dr. Jörg Bendix (Marburg)
Zweitgutachter: Prof. Dr. Peter Chifflard (Marburg)

Tag der mündlichen Prüfung am 02.02.2017

Preface

To understand the climatic system to the point where we can compute reliable climatic projections for decades into the future is a great achievement of a civilization. Certainly the immense development of the computing power has underpinned such advancement and scientific development. Just a few years ago it seemed an utopia to work on the downscaling of global climate models in Ecuador, a developing country where, for instance, the scarce monitoring networks and limited computing power, hampered scientific research in climate sciences. Such limitations added to the complexities of the atmospheric processes occurring in tropical mountain regions, as the Andes of Ecuador, made the task even more daunting. However at the end, I have achieved the objective.

My PhD was developed in several stays between the Laboratory for Climatology and Remote Sensing at Philipps-University of Marburg, LCRS, and Departamento de Recursos Hídricos y Ciencias Ambientales de la Universidad de Cuenca, IDRHICA. This modality stimulated the development of important projects, as the Third National Communication on Climatic Change, presented to the IPCC, which projections were calculated about 80% in IDRHICA, from which I'm proud of such contribution.

In writing these words I remember some rewarding and difficult moments during my PhD. At the same time I remember many people who helped me along the way, to whom I keep deep gratitude. Firstly, a profound appreciation to my supervisor, Prof. Dr. Jörg Bendix, who guide me in crucial moments during my PhD. I also have to express my great admiration and gratitude for his great humanity. I thank to Dr. Katja Trachte, for detailed and sharp observations, which always helped to bring the results to the highest standards. Thanks and gratitude to Dr. Rolando Célleri, for his very valuable support and advice as an expert in mountain regions. Profound admiration for Dr. Esteban Samaniego, his deep criticism helped me to find important answers on this research. Thank to his influence I could use the cluster from CEDIA for installation and use of WRF model. Special thanks to Prof. Jan Feyen, a key figure in the development of research at the University of Cuenca, who backed me and gave me valuable advice. Thanks to friends and colleagues both at the LCRS and IDRHICA. To Wolfgang Obermeir, Eva-Marie Schönmann and Benedict Spaan special thanks for translating the summary into German language and to Sandro Makowski and Giulia Curatola for their friendship and support in many stages during my PhD.

I gratefully acknowledge to SENESCYT, which made this work possible through a doctoral scholarship, due to a historic initiative of the Ecuadorian government to improve the education at all levels.

I thank to my father Lenin and my sister Karla, for their support, and specially my mother, Maria Ines, my referent of effort and sacrifice. Above all special

thanks to my beloved wife Jenny, for her constant support, she was who took full responsibility of our home during the long months of my stay abroad. Finally, with love I dedicate this work to my children David, Rafaela, Dominick and Micaela, who I have seen grow during this period of hard work, they were my sincere inspiration to pursue towards my goal.

Lenin Campozano.·.
Cuenca, Dezember 2016

Contents

List of Figures

List of Tables

1 Introduction

Earth's climate is determined by several factors: its orbital characteristics and rotation rate, the emission of radiation from the Sun, the composition of the atmosphere, the interactions between other components of the planet and the atmosphere, among other things (Wallace & Hobbs 2006). The climatic system is highly non-linear, displaying complex interactions among the climatic variables, which cause complex oscillatory signals. As a consequence, the prediction of future climate scenarios is challenging.

After the industrial revolution, and especially after 1950 the mean temperature of planet Earth has suffered an unparalleled raise over decades to millennia (IPCC, 2014). The global averaged increase of land and ocean surface temperature data shows a warming of 0.85 °C from 1880 to 2012 (IPCC, 2014). The IPCC attributes global warming to human activity with around 95% certainty (IPCC, 2014). The increase in temperature is due to the increase in green house gases concentrations, which are the highest in at least 800000 years (IPCC, 2014). Such increase in green house gases concentrations helps to add more energy to the atmosphere, thus yielding a more dynamic climatic system and consequently climate change (CC). Projections of precipitation indicate a not uniform impact of CC. For instance, in many mid-latitude and subtropical dry-regions, precipitation will decrease. Contrarily, the tropics under CC conditions, especially over wet regions, are very likely to present more intense and more frequent extreme precipitation events (IPCC, 2014). In summary, CC will have varying influences across diverse regions and societal aspects.

Projections of climate are generated by the use of Global Climate Models (GCMs). GCMs solve the so-called primitive equations: the momentum balance, the conservation of energy, the conservation of dry air mass and all phases of moisture, as well as the equation of state for a perfect gas (Kalnay, 2002). For the representation of sub-grid processes, parameterizations of land surface, vegetation, planetary boundary layer and turbulence, convection, microphysics, radiation in clear skies, cloud cover and radiation in cloudy skies, and orographic drag are mainly considered (Stensrud, 2007). GCMs' typical resolution to date is roughly of 1 to 2 degree, due to computational constraints. Therefore, the climate representation skill of GCMs is region dependent, due to the fact that sub-grid processes occur differently across planet Earth. Nevertheless, GCMs are to date the best tools to estimate the dynamics of the atmosphere, especially at continental and larger scales (Randall, et al 2007). The capabilities of GCMs in simulating some aspects of the climate system have improved, e.g. El Niño-Southern Oscillation (ENSO). However, the description of other aspects of the climate signal, such as the representation of the Madden-Julian Oscillation (Randall, et al 2007), is still limited.

GCMs results present some limitations due to the misrepresentation of parameterized processes and due to their low resolution. For instance, climate in the tropics is strongly influenced by convective activity due to the excess of solar energy input on these latitudes. The function of the global climate system is to transport the excess of energy to higher latitudes (Meehl, 1992), where there is an energy deficit, caused by radiation into space. Due to the condensation of moisture in towering clouds along the tropics,

latent heat is released, which in turn, is an important source of energy to the global climate system (Meehl, 1992). Lauer & Hamilton (2012) evaluated state of the art GCMs from CMIP5 representation of cloud climatology against CMPI3 models. They found that CMPI5 models present small improvement over CMIP3 models, which present important deviations from observations, especially in the tropics and subtropics. They attribute this shortcoming to the treatment of sub-grid cloud and boundary layer processes.

On the other side, due to the low resolution of GCMs, the representation of regional climate is a challenge. In mountain regions, in addition to continentality and latitude, altitude and orography are key aspects controlling climate (Barry, 1994). Elevation, slope, aspect, and exposure may create local climates (Beniston, 2008), and mild orographic components might produce important modifications to climatic features. Nonetheless, the meteorological and climatological processes in mountain regions influence ecosystems beyond their boundaries (Beniston, 2006). Furthermore, around 40% of the population on the Earth lives in river basins, which originated in mountain regions (Beniston, 2006), providing with resources and water services. For instance, mountains supply from 50 to 90% of total discharge in arid regions and from 20 to 50% in humid regions (Viviroli, & Weingartner, 2004). Furthermore, mountain regions are susceptible to CC and thus constitute strategic regions for early detection of CC signal (Beniston, 2003). These facts make the study of CC in mountain regions a matter of major importance. However, current studies of climate on these regions require the application of downscaling of GCMs, to overcome the mismatch of spatial scales between GCMs results and the scale for impact assessment.

To assess the impact of climate change for societal concerns it is necessary to improve climate projections spatial scales. For instance, the application of downscaling techniques to precipitation fields helps to improve the resolution of GCMs results, besides the improvement of the estimates themselves (Maraun, D., et al. 2010). However, the downscaling of temperature has been applied with higher success due to the fact that precipitation presents higher spatio-temporal variability and is the result of complex nonlinear processes (Maraun, D., et al. 2010). There are mainly two approaches to downscaling: (i) Dynamical downscaling (DD), which nests a regional climate model (RCM) into the GCM solving the climate equations with higher resolution, and (ii) Statistical downscaling (SD), which aims to find statistical relations between large-scale climate variables and local variables (Maraun, D., et al. 2010). Furthermore, SD methods can be classified as: (i) Weather classification schemes, which groups weather types by synoptic similarity typically by applying clustering techniques. Examples of this approach are the Analog or hidden Markov chain method (Maraun, D., et al. 2010). (ii) Regression models, establish linear or nonlinear relations between predicted local variables and large-scale synoptic variables, which are called predictors. Examples of this approach are multiple linear regression, artificial neural networks, support vector machines and canonical correlation analysis (Maraun, D., et al. 2010). (iii) Weather generators, this approach use models, which aim to resemble statistical characteristics of observed variables, without considering the time series as a sequence of events (Wilks and Wilby, 1999).

Hitherto, mixed conceptions about the capabilities and applicability of either statistical

downscaling or dynamical downscaling exist. Despite several approaches are used for the downscaling of GCMs across the world, such procedure along mountain regions is still an active topic of research (Hamlet, et al. 2010, Hu et al. 2013, Souvignet, M., & Heinrich, J. 2011), especially in remote regions with scarce observational networks. Buytaert, et al 2010, studied the added valued of the regional climate model, PRECIS (50km resolution), for the representation of precipitation and temperature in Ecuador. Interestingly they found that the RCM results could capture the gradients better than GCMs outputs. However, they showed that RCM results were prone to higher mismatches with respect to observations than GCMs outputs. In conclusion, the author recommends an increase in the resolution of RCMs in order to capture local gradients besides the implementation of ensembles of downscaling results to assess the uncertainty involved in the procedure. The application of the RCM, Regional Climate Model version 3, RegCM3, from the The Abdus Salam International Centre for Theoretical Physics (ICTP), tends to overestimate precipitation along the Andes, despite a negative bias across South America (Pal, et al. 2007), which is in agreement with other studies, e.g. Fernandez et al. 2006. On the other side, Sachindra et al. (2015) studied the issues and challenges of statistical downscaling of GCMs to hydroclimatic variables at basin scale. The authors acknowledge several sources of uncertainty on the process e.g. (i) the predictors of statistical downscaling possess high uncertainty due to limitations in the mathematical representation of processes which are exacerbated by the limited knowledge on the physical processes, (ii) the formulation of several equiprobable green house gases future scenarios adds uncertainty to the climatic projections, (iii) the quality and length of observations, which are used during the calibration and validation process, (iv) uncertainty due to the specific technique used in the process of statistical downscaling, which imply a dependence of the predictor-predictand relation on the used technique. They finally concluded that although such limitations and uncertainties are involved in the statistical downscaling process, such technique is still considered as a potential method for the generation of hydroclimatology at basin scale.

1.1 Motivation

Ecuador is located in the tropical region, around the equatorial line on the northwestern part of south-America. The continental region of Ecuador is located between 1.43N-5.02S and 75.25W-81.01W. The insular region corresponds to the Galapagos Islands, located ca. 1000 km west of the coastal line in the Pacific Ocean. Ecuador is divided by the Andes cordillera, which is formed by two ridges corresponding to the western (cordillera occidental) and eastern cordillera (cordillera oriental). It is located from north to south along 600 km, and from 150 to 180 km wide (Coltorti & Ollier, 2000). To the northeast there is a third ridge, which develops it maximum elevation in Colombian territory. The Andes separate the coast form the Amazon region. Between both cordilleras the inter-Andean depression is located.

The climate in Ecuador presents a conspicuous variability. However, a main climatic influence is the Inter-Tropical Convergence Zone (ITCZ) enhancing convective precipitation across the country. The Andes cordillera, which acts as a weather divide

(Bendix & Lauer, 1992), shapes three natural regions, with their own climatic influences: the Amazonian, the coastal, and the inter-Andean region. The coastal regions are strongly influenced by the ITCZ, the Pacific Ocean, and the Southeast Pacific anticyclone. On the other hand, the Amazonian region is strongly influenced by the ITCZ, the easterlies, and abundant moist air from the Amazon. The inter-Andean region receives a mix influence from both regions depending on elevation and orographic features, e.g. exposure, slope, aspect. Also, Vuille et al. (2000) found teleconnections of precipitation in the inter-Andean region, with the Atlantic Sea Surface Temperature (SST) Anomalies. They proposed a dipole-like mechanism where positive Atlantic SST anomalies south of the ITCZ, and negative Atlantic SST anomalies north of the ITCZ, produced more rainfall over the eastern cordillera. They also showed that the temperature in the Andes is linked to the SST in the Tropical Pacific regions El Niño 3 and Niño 3.4 with one-month lag.

In Ecuador, the main source inter-Annual precipitation variability is ENSO. (Bendix, 2000, Bendix & Bendix, 2006b, Rossel et al, 1998, Pavón, J. D., & Dorado, J. 2008). The El Niño events produce anomalous positive rainfall in the coastal region, and weak negative anomalies in the Amazon region (Bendix et al, 2011, Vuille et al. 2000). On the other hand, La Niña events produce anomalous positive rainfall in the Amazon and drought in the coastal region. The influence of ENSO on the precipitation of the inter-Andean region is weakly related Niño 3.4 region (Recalde-Coronel, et al. 2014, Morán-Tejeda et al, 2015, Vicente-Serrano, et al., 2016). Thus further research related to the drivers modulating climate in the inter-Andean region is necessary.

Currently, GCMs present shortcomings in representing climate change signals in tropical mountain regions. This is mainly due to limitations in convection parameterization and low resolution. Furthermore the downscaling of GCMs is necessary to study CC impact at basin scale. Thus, the evaluation of the skill of downscaling approaches in reproducing present day precipitation and future projections in regions of complex spatio-temporal variability of precipitation, as the inter-Andean region in Ecuador, is scientifically interesting, challenging, and still is a major concern.

Besides the scientific value of such studies, they also have a strategic importance for Ecuador's economy. Around 54% of energy in Ecuador comes from hydroelectric production (CELEC EP, 2014), and around 87% of hydroelectricity is generated from inter-Andean watersheds. Furthermore, the spatio-temporal availability of accurate rainfall data also for future projections would be of utmost importance for planning Ecuador's energy production. However, due to the challenges described above, this is not realized to date.

For instance, the Paute basin (PB), fosters two power plants (e.g. Molino 1100 MW, Mazar 170 MW), producing around 40% of Ecuador energetic demand (CELEC EP, 2014). The PB is located in the inter-Andean depression between the western and eastern cordillera from 3.3-2.3 S to 79.4 – 78.3 W (Figure 1.1). The Paute river is a tributary of Santiago river which is a tributary of the Marañón river (Amazon river) into the Amazon basin. The basin covers 6292 km^2, where the downstream ends on the flanks of the eastern cordillera and the beginning of the Amazon region. The altitudinal range of the PB varies from 895 to 4172 m asl and around 3000 m asl of mid-elevation. Páramo (tropical alpine grassland) covers almost half of the PB. Thus the PB provides water for irrigation systems, industrial and domestic uses besides of providing water for

hydroelectric production. Due to these facts, the PB is one of the best-monitored basins countrywide, thus facilitating research and helping water management institutions in charge of the water resource to be leading institutions in the country and regionally.

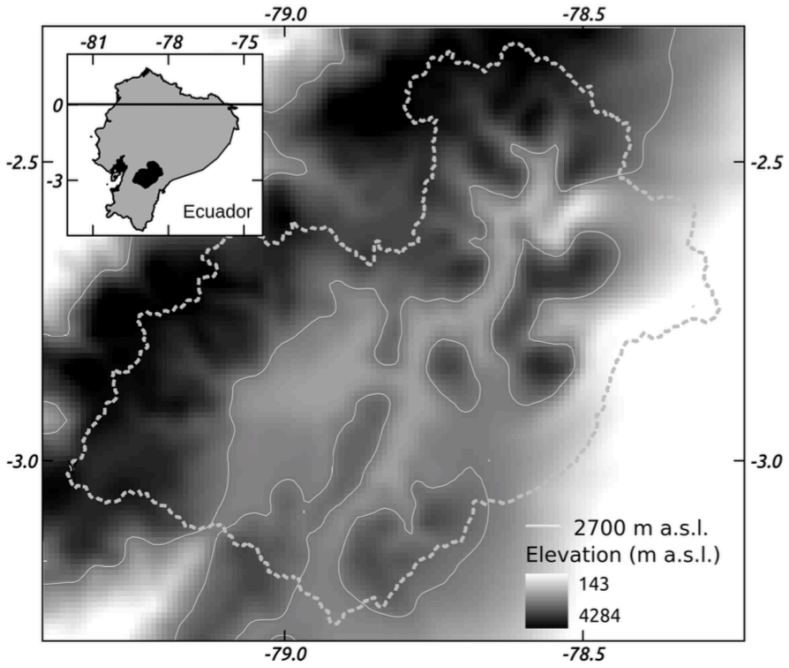

Figure 1-1: The Paute river basin located in the Andes of Ecuador (dashed grey line)

The climate in the PB presents a complex spatio-temporal variability and is probably the most studied basin in the country. For instance, Celleri et al, 2007, studied the precipitation regimens across the PB. Using correlation analysis they determined the existence of four regimens: (i) the bi-modal 1 regime present in the inter-Andean regions, which present rainy season in March-April and October-November, and very dry August-September, with a mean annual precipitation between 660 and 1100 mm, (ii) the bi-modal 2 regime, with similar seasonality as bi-modal 1, but less pronounced dry season. This regime is located on higher elevations, presenting a mean annual precipitation from 1000 to 1800 mm, (iii) the uni-modal 1 regime, with a peak rainy season in July, presenting an average annual precipitation of from 2900 to 3400 mm, located in the lower part of the basin, and (iv) the uni-modal 2, with similar seasonality to uni-modal 1, located in the northern part of the PB, presenting an average annual precipitation from 1100 to 1600 mm. Mora & Willems, 2011, studied decadal oscillations in the PB. They showed that temperature in the PB is linked to the SST on the Pacific Ocean, with higher influence on stations with higher elevations, especially from December to February. However they claim that the influence in precipitation depends on other factors as, e.g. aspect orientation, slope, and hydrological regime. The climatic complexity of the PB is the result of interactions between the synoptic scale and orographic factors, making the PB a natural laboratory to evaluate the downscaling of precipitation at basin scale in tropical mountain regions.

In summary, the climatic influences in Ecuador, mainly due to the ITCZ, ENSO, SST from the Pacific and Atlantic Ocean, added to the complex orography of the Andes, produce complex spatio-temporal variability. The inherent complexity in the climatic

systems of this region, added to the low resolution of GCMs and limited representation of convective processes, cause a poor climate representation of GCMs especially at the scale of CC impact. Thus it is necessary to evaluate the application of downscaling techniques under these limiting conditions.

To the best knowledge of the author, to date, just a few studies have evaluated the improvement of climate representation by the downscaling of GCMs in this region. For instance, Buytaert, et al 2010, studied the added valued of the regional climate model, PRECIS (50km resolution), for the representation of precipitation and temperature in Ecuador. They concluded that the RCM results could capture the gradients better than GCMs outputs. However RCMs results were prone to higher mismatches with respect to observations than GCMs outputs. The author finally recommends the application of RCMs with higher resolution in order to capture local gradients. This study also recommends the implementation of ensembles of downscaling results to assess the uncertainty involved in the procedure. A shortfall of Buytaert, et al 2010, might be the lack of a specific sensitivity analysis of sub-grid scale parameterizations, which may be even more necessary in the tropics, where the convective precipitation represents a larger proportion of the total precipitation. On the other side, the application of ensembles of downscaling results to evaluate inter-model related uncertainties in fact is necessary. However, limitations in computational capabilities hampered such investigations. A more specific study was conducted by Mora, et al 2012. They evaluated the representation of temperature and rainfall of IPCC AR4 GCMs and RCM PRECIS (50 Km) in six stations of the PB. The analysis was conducted at annual, monthly and daily scales. Several statistical criteria such as the relative mean squared error, bias and Pearson correlation were used to evaluate models performance. They showed that no model performed well for all the statistical criteria. However some models performed better than others in general, differing from station to station. They found that several GCMs performed better that PRECIS RCM, concluding that the increase of spatial resolution do not necessarily results in a more accurate description of climate. The author finally encourages the evaluation of statistical downscaling techniques for climate representation in the region.

To have a better understanding of regional or global climate models limitations on the representation of precipitation in the region, it is necessary to study the dynamics of clouds and rainfall. However very limited climatic monitoring networks make difficult to convey such investigations. Furthermore the monitoring based on ground stations in complex terrain in remote regions bring further complications. Thus satellite products may be an option for the study of climate in this region. Bendix, et al 2004, presented a threshold technique for cloud detection in the tropical mountainous area of Ecuador based on National Oceanic and Atmospheric Administration Advanced Very High Resolution Radiometer (NOAA-AVHRR) data. Maps of relative cloud frequency base on 155 images where generated for Ecuador and adjacent areas. Clear relations between topography, main airflow and cloudiness due to barrage and lee-effects were found. In another study, Bendix, et al 2006a, used a 3 yr data set of NOAA-AVHRR (Advanced Very High Resolution Radiometer) imagery to investigate cloud frequency, cloud-top height and cloud liquid water path for the Ecuadorean area, with special emphasis on the Andes of southern Ecuador. They found significant correlation between cloudiness and rainfall seasonal cycle. They also showed that the complex topography of the Andes cause a local spatial structure of cloud frequency and cloud properties, as is the case along the eastern Andean slopes, where a line of high cloud frequency and rain is

caused by the barrage effect of the Andes. Interestingly the average cloud-top height revealed a clear division between the Pacific area west of the western Cordillera chain, and the eastern parts of the country. Increase values of average cloud-top height towards the Amazon are an indication of enhanced convective cloud formation processes. However the study of satellite cloud products and its potential use to derive precipitation products at basin scale needs further investigation.

1.2 Aims and Outlines

Based on the current knowledge gaps summarized in the previous section, the purpose of the present work is to investigate the downscaling of precipitation at basin scale in a Tropical mountain region in Andes of south Ecuador. Given the context presented in previous sections, it is necessary in the first place to investigate the dynamics of clouds and rainfall in the Paute basin. It is assumed that two factors, the orography and the climatic synoptic conditions, influence the development of several specific rainfall regimes across short distances, e.g. uni-modal and two-modal regimes. Such investigation will illuminate the added value expected from the application of downscaling procedures, given that, for instance, statistical methods do not provide information about orographic features, whereas the dynamical approach adds the orographic influence by resolving the atmospheric processes using high-resolution terrain information. Secondly, in order to isolate the orographic component, statistical downscaling to the station will be applied. Such procedure will be evaluated in stations with diverse precipitation regimes. It is expected to gain more knowledge about the stations and regimens with greater synoptic climatic influence over stations with local influence. After the evaluation of the statistical downscaling techniques, which isolate the orographic component, in third place, the evaluation of the dynamical downscaling approach, e.g. using a RCM, will be conducted. The application of a RCM in comparison with a statistical downscaling approach will provide evidence about the real value of incorporating the orographic information, besides the added value of including sub-grid processes as parameterizations of the regional climate model. Finally, after the evaluation of the strengths and weaknesses of each technique, both approaches combined, e.g. the statistical and the dynamical downscaling, will be applied and evaluated for a specific use, as is the generation of future precipitation scenarios for the Paute basin.

Thus, the main hypotheses of the present study are:

- **H1:** In the Paute basin the interplay between the synoptic climatic influences and the orography produce shifts in rainfall regimens at local scale.
- **H2:** Statistically downscaled estimates of precipitation have an improved representation of observations in stations with greater synoptic climatic influence in the Paute basin.
- **H3:** Dynamically downscaled estimates of precipitation will surpass the skill of statistical downscaling estimates in the Paute basin, due to the incorporation of the orographic information.
- **H4:** The combined application of dynamical and statistical downscaling of precipitation improves the representation and reliability of downscaled estimates of precipitation in the Paute basin.

To verify the main hypothesis presented above, the main aims of this work are:

- To investigate the dynamics and cross-scale generation processes of clouds and rainfall at basin scale in the Paute basin.
- To evaluate several approaches of statistical downscaling of precipitation at basin scale, in stations with diverse orographic characteristics and precipitation regimes.
- To evaluate the added value of incorporating orography in the downscaling of precipitation by using regional climate modeling.
- To evaluate the estimations of the combined, dynamical and statistical downscaling approaches, for precipitation in the Paute basin.

Current difficulties of this investigation are:

- To date the study of the climatic and orographic influences, which produce the complex precipitation seasonality in the Paute basin is not fully understood.
- There is a gap of knowledge about the capabilities of downscaling approaches, particularly in tropical high mountains such as the Andes.
- There is low spatio-temporal representativity of data availability.
- There is limited computational power for the implementation of regional models.

To study the downscaling of precipitation at basin scale in the Paute river basin in Ecuador is important, both from a scientific perspective as well as for water resource management and planning assessment.

The present work is structured in 7 chapters. In chapter 2 the conceptual design is described. Within this chapter (section 2.1) the elaboration of hypotheses to working packages is presented, followed by some theoretical background on downscaling methods in section 2.2, and in section 2.3 information about the data and methodological aspects of working packages is finally explained.

The following four chapters are supporting working packages from 1 to 4, summarized in the following publications. The analysis of the orographic and synoptic influences on the precipitation and clouds variability of the Paute basin is conducted in **Campozano, L.,** Célleri, R., Trachte, K., Bendix, J., & Samaniego, E. (2016). Rainfall and Cloud Dynamics in the Andes: A Southern Ecuador Case Study. Advances in Meteorology, 2016, 15. doi:10.1155/2016/3192765, corresponding to chapter 3. In chapter 4 the evaluation of the downscaling of precipitation in the Paute basin by the statistical approach is presented in **Campozano, L**., Tenelanda, D., Sanchez, E., Samaniego, E., & Feyen, J. (2016). Comparison of Statistical Downscaling Methods for Monthly Total Precipitation: Case Study for the Paute River Basin in Southern Ecuador. Advances in Meteorology, 2016, 1–13. doi:10.1155/2016/6526341. The evaluation of the dynamical and statistical approaches is presented in Ochoa, A., **Campozano, L**., Sánchez, E., Gualán, R. and Samaniego, E. (2016), Evaluation of downscaled estimates of monthly temperature and precipitation for a Southern Ecuador case study. Int. J. Climatol., 36: 1244–1255. doi:10.1002/joc.4418, corresponding to chapter 5. In chapter 6, the combined application of the dynamical and statistical downscaling approaches is evaluated in the Paute basin, followed by the generation of climatic projections of precipitation and temperature. This work is presented in the publication, Mora, D. E.,

Campozano, L., Cisneros, F., Wyseure, G., & Willems, P. (2014). Climate changes of hydrometeorological and hydrological extremes in the Paute basin, Ecuadorean Andes. Hydrology and Earth System Sciences, 18(2), 631–648. doi:10.5194/hess-18-631-2014.
Finally, the conclusions and outlook is presented in chapter 7.

References

Barry, R. G., 1994. Past and potential future changes in mountain environments: a review. In Beniston, M. (ed.), Mountain Environments in Changing Climates. Routledge Publishing Company, London and New York, 3–33.

Bendix, J., & Lauer, W. (1992). Die Niederschlagsjahreszeiten in Ecuador und ihreklimadynamische Interpretation. Erdkunde, 46, 118–134.

Bendix, J. (2000). Precipitation dynamics in Ecuador and northern Peru during the 1991 / 92 El Nino : A remote sensing perspective. International Journal of Remote Sensing, 21(3), 533–548.

Bendix, J., Rollenbeck, R., & Palacios, W. E. (2004). Cloud detection in the Tropics--a suitable tool for climate-ecological studies in the high mountains of Ecuador. International Journal of Remote Sensing, 25(21), 4521–4540. doi:10.1080/01431160410001709967

Bendix, J., Rollenbeck, R., Göttlicher, D., & Cermak, J. (2006a). Cloud occurrence and cloud properties in Ecuador. CLIMATE RESEARCH, 30(2004), 133–147.

Bendix, A., & Bendix, J. (2006b). Heavy rainfall episodes in Ecuador during El Niño associated regional atmospheric circulation and SST patterns. Advances in Geosciences, 43–49.

Bendix, J., Trachte, K., Palacios, E., Rollenbeck, R., Goettlicher, D., Nauss, T., & Bendix, A. (2011). El Niño meets La Niña – anomalous rainfall patterns in the "traditional" El Niño region of southern Ecuador. Erdkunde, 65(2), 151–167. doi:10.3112/erdkunde.2011.02.04

Beniston, M. (2006). Mountain weather and climate: A general overview and a focus on climatic change in the Alps. Hydrobiologia, 562(1), 3–16. doi:10.1007/s10750-005-1802-0

Beniston, M. (2003). Climatic change in mountain regions: a review of possible impacts. … Change in High Elevation Regions: Past, Present & …, 5–31. doi:10.1023/A:1024458411589

Buytaert, W., Vuille, M., Dewulf, A., Urrutia, R., Karmalkar, A., & Célleri, R. (2010). Uncertainties in climate change projections and regional downscaling in the tropical Andes : implications for water resources management. Hydrology and Earth System Sciences, 1247–1258. doi:10.5194/hess-14-1247-2010

CELEC EP, 2014, Informe de rendición de cuentas.

Celleri, R., Willems, P., Buytaert, W., & Feyen, J. (2007). Space–time rainfall variability in the Paute basin, Ecuadorian Andes. Hydrological Processes, 21(August), 3316–3327. doi:10.1002/hyp

Coltorti, M., & Ollier, C. D. (2000). Geomorphic and tectonic evolution of the Ecuadorian Andes. Geomorphology, 32(1-2), 1–19. doi:10.1016/S0169-555X(99)00036-7

Fernandez, J. P. R., S. H. Franchito, and V. B. Rao, 2006: Simulation of the summer circulation over South America by two regional climate models. Part I: Mean climatology. Theor. Appl. Climatol., 86, 247–260.

Hamlet, A. F., Salathé, E. P., & Carrasco, P. (2010). Statistical downscaling techniques for global climate model simulations of temperature and precipitation with application to water resources planning studies. Final Rep. for the Columbia Basin Climate Change Scenarios Project, 27 pp. [Available online at www.hydro .washington.edu /2860/products/sites/r7climate /study_report/CBCCSP_chap4_gcm_final.pdf.]

Hu, Y., Maskey, S., & Uhlenbrook, S. (2013). Downscaling daily precipitation over the Yellow River source region in China: A comparison of three statistical downscaling methods. Theoretical and Applied Climatology, 112(3-4), 447–460. doi:10.1007/s00704-012-0745-4

IPCC, 2014: Climate Change 2014: Synthesis Report. Contribution of Working Groups I, II and III to the Fifth Assessment Report of the Intergovernmental Panel on Climate Change [Core Writing Team, R.K. Pachauri and L.A. Meyer (eds.)]. IPCC, Geneva, Switzerland, 151 pp.

Kalnay E (2002) Atmospheric modeling, Data Assimilation and Predictability. Camebridge University Press, 364 pp

Lauer, A., & Hamilton, K. (2013). Simulating clouds with global climate models: A comparison of CMIP5 results with CMIP3 and satellite data. Journal of Climate, 26(11), 3823–3845. doi:10.1175/JCLI-D-12-00451.1

Maraun, D., et al. (2010). Precipitation downscaling under climate change: Recent developements to bridge the gap between dynamical models and the end user. Reviews of Geophysics, 48(2009RG000314), 1–38. doi:10.1029/2009RG000314.1.INTRODUCTION

Meehl, G., (1992). Effect of tropical topography on global climate. Annu. Rev. Earth Planet. Sci. 20:85-112.

Mora, D. E., & Willems, P. (2011). Decadal oscillations in rainfall and air temperature in the Paute River Basin—Southern Andes of Ecuador. Theoretical and Applied Climatology, 108(1-2), 267–282. doi:10.1007/s00704-011-0527-4

Mora, D. E., Liu, T., Cisneros, F., Wyseure, G., and Willems, P. (2012). Statistical Analysis on the Performance of Global and Regional Climate Models for the Paute

River Basin in the South-Ecuadorian Andes, Proceedings of 10th International Conference on Hydroinformatics, Hamburg, Germany2012.

Morán-Tejeda, E., Bazo, J., López-Moreno, J. I., Aguilar, E., Azorín-Molina, C., Sanchez-Lorenzo, A., … Vicente-Serrano, S. M. (2015). Climate trends and variability in Ecuador (1966-2011). International Journal of Climatology. doi:10.1002/joc.4597

Pal, J. S., Giorgi, F., Bi, X., Elguindi, N., Solmon, F., Gao, X., … Steiner, A. L. (2007). Regional climate modeling for the developing world: The ICTP RegCM3 and RegCNET. Bulletin of the American Meteorological Society, 88(9), 1395–1409. doi:10.1175/BAMS-88-9-1395

Pavón, J. D., & Dorado, J. (2008). Intraseasonal Variability of Rainfall Over Northern South America and Caribbean Region. Earth Sciences, 12(2), 194–212.

Randall, D.A., R.A. Wood, S. Bony, R. Colman, T. Fichefet, J. Fyfe, V. Kattsov, A. Pitman, J. Shukla, J. Srinivasan, R.J. Stouffer, A. Sumi and K.E. Taylor, 2007: Cilmate Models and Their Evaluation. In: Climate Change 2007: The Physical Science Basis. Contribution of Working Group I to the Fourth Assessment Report of the Intergovernmental Panel on Climate Change [Solomon, S., D. Qin, M. Manning, Z. Chen, M. Marquis, K.B. Averyt, M.Tignor and H.L. Miller (eds.)]. Cambridge University Press, Cambridge, United Kingdom and New York, NY, USA.

Recalde-Coronel, C. G., Barnston, A. G., & Muñoz, Á. G. (2014). Predictability of december-april rainfall in coastal and Andean Ecuador. Journal of Applied Meteorology and Climatology, 53(6), 1471–1493. doi:10.1175/JAMC-D-13-0133.1

Rossel, F., Mejía, R., Ontaneda, G., Pombosa, R., Roura, J., Le Goulven, P., … Calvez, R. (1998). RÉGIONALISATION DE L'INFLUENCE DU EL NIÑO SUR LES PRÉCIPITATIONS DE L'ÉQUATEUR. Bull. Inst. Fr. Études Andines, 643–654.

Sachindra, D. A., Huang, F., Barton, A., & Perera, B. J. C. (2015). Potential improvements to statistical downscaling of general circulation model outputs to catchment streamflows with downscaled precipitation and evaporation. Theoretical and Applied Climatology, 122(1-2), 159–179. doi:10.1007/s00704-014-1288-7

Souvignet, M., & Heinrich, J. (2011). Statistical downscaling in the arid central Andes: Uncertainty analysis of multi-model simulated temperature and precipitation. Theoretical and Applied Climatology, 106(1-2), 229–244. doi:10.1007/s00704-011-0430-z

Stensrud, D. J. (2007). Parameterization schemes : keys to understanding numerical weather prediction models. Cambridge [etc.]: Cambridge University Press.

Vicente-Serrano, S. M., Aguilar, E., Martínez, R., Martín-Hernández, N., Azorin-Molina, C., Sanchez-Lorenzo, A., … Nieto, R. (2016). The complex influence of

ENSO on droughts in Ecuador. Climate Dynamics, 1–23. doi:10.1007/s00382-016-3082-y

Viviroli, D., & Weingartner, R. (2004). The hydrological significance of mountains: from regional to global scale. Hydrology and Earth System Sciences, 8(6), 1017–1030. doi:10.5194/hess-8-1017-2004

Vuille, M., Bradley, R. S., & Keimig, F. (2000). Climate Variability in the Andes of Ecuador and Its Relation to Tropical Pacific and Atlantic Sea Surface Temperature Anomalies. Journal of Climate, 13(Hastenrath 1981), 2520–2535. doi:10.1175/1520-0442(2000)013<2520:CVITAO>2.0.CO;2

Wallace, J. M., & Hobbs, P. V. (2006). Atmospheric science: An introductory survey. Amsterdam: Elsevier Academic Press.

Wilby, R.L. et al.. 2004: Guidelines for Use of Climate Scenarios Developed from Statistical Downscaling Methods. IPCC Task Group on Data and Scenario Support for Impact and Climate Analysis (TGICA)

Wilks DS, Wilby RL. 1999. The weather generation game: a review of stochastic weather models. Progress in Physical Geography 23: 329 – 357.

2 Conceptual Design

2.1 Elaboration of Hypotheses to Working Packages

The purpose of the present work is to investigate the downscaling of precipitation at basin scale in the Paute river basin, in the Tropical Andes of Southern Ecuador. Given the context presented above, it is necessary to explore the dynamics of clouds and rainfall in the Paute basin. It is assumed that two factors, the orography and the climatic synoptic conditions, produce precipitation regime shifts at local scale. For instance, uni-modal and bi-modal regimens are found across short distances (e.g. in regions few kilometers apart). Such investigation will illuminate the added value expected from the application of downscaling procedures. Secondly, in order to isolate the orographic component, statistical downscaling to the station will be applied. Such procedure will be evaluated in stations with diverse precipitation regimens. It is expected to gain knowledge about the stations and regimens with grater synoptic climatic influence over stations with local influence. After the evaluation of the statistical downscaling techniques, in third place, the evaluation of the dynamical downscaling technique through the use of a RCM is conducted. The application of a RCM in comparison with a statistical downscaling approach will provide evidence about the real value of incorporating a finer orographic representation besides the added value of including sub-grid processes parameterizations. Finally, after the evaluation of strengths and weaknesses of the precedent techniques applied independently, the combined application of both approaches, e.g. the dynamical and the statistical downscaling approaches, will be evaluated in the Paute basin, and future precipitation scenarios will be generated.

To evaluate the hypothesis presented in section 1,2, from H1 to H4, the working packages are devised as follows:

- **WP1:** Develop monthly precipitation models considering satellite clouds products as well as orographic variables in order to conduct a regionalization of precipitation in the PB. Analysis of the relation between synoptic climatic variables to explain types of rainfall seasonality across the PB.
- **WP2:** Implement state of the art statistical downscaling models in order to evaluate and analyze their skill in representing the seasonality in stations of diverse precipitation regime.
- **WP3:** Implementation of a regional climate model in the PB with high resolution e.g. 15 km and comparison with statistical downscaling results. Following WP3 the representation of the seasonality will be evaluated.
- **WP4:** Based on the comparative skill between statistical and dynamical downscaling approaches, develop the implementation of a combined application of dynamical and statistical downscaling approaches to generate projections of precipitation in the PB.

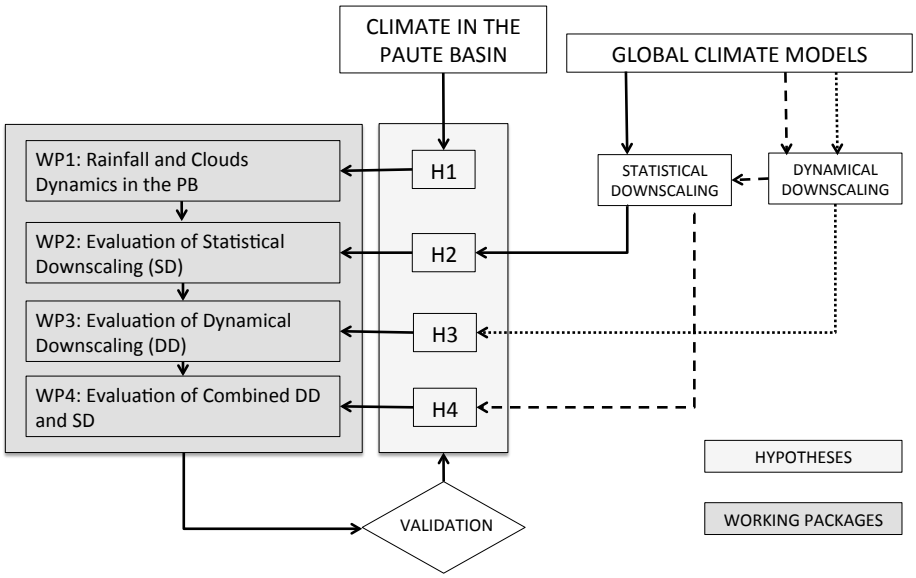

Figure 2-1: Conceptual design of doctoral project

2.2 Data and methodological aspects of working packages

- **WP1:** Pronounced spatiotemporal precipitation variability is characteristic in mountain regions worldwide. In the present WP the relation between clouds and rainfall seasonality types in the PB with orography and synoptic conditions is studied. Firstly the regionalization of precipitation types is conducted. In regions as the PB, scarce monitoring networks hamper our understanding of the precipitation and clouds generation processes involved. Thus, the use of satellite and GIS data may be suitable for the generation of data-driven statistical models to study spatiotemporal rainfall seasonality. In WP1 the satellite products used are based on 452 NOAA- AVHRR scenes retrieved during 2002 and 2004. The data set consist of cloud frequency (CF), cloud top height (ZMIT) and cloud liquid water path (LWP) on 1 km resolution. For more details on the generation of the data set the reader may refer to (Bendix et al. 2004 & Bendix and Bendix 2006). The Global 30 Arc-Second Elevation (GTOPO30) is used for terrain information (Data available from the U.S. Geological Survey). Also, data from 15 rainfall stations of the Ecuadorian National Institute of Meteorology and Hydrology, INAMHI, delivering daily values for the period January 2000 to December 2009 were available. Data from 4 rainfall stations of the Empresa Municipal de Telecomunicaciones, Agua Potable y Saneamiento, ETAPA, delivering hourly values for the period December 2001 to December 2009 were also available. The observational data was previously quality controlled and checked for homogeneity (Campozano et al. 2014). Then, several multiple linear

regression models were devised and regionalization was conducted by pixel-wise correlation with precipitation regimen types.

- Secondly, to study the relation between the precipitation types in the PB with the orography and synoptic influences, (i) the synoptic analysis of dynamical variables and its relation to seasonal clouds products, and (ii) the evaluation of normalized precipitation types (NPRs) along a representative transect in the Paute river basin, is conducted. For (i), the analysis of the synoptic conditions is conducted using Hovmöller diagrams across a zonal transect from 270º to 300º, averaged from latitude -5º to latitude 5º vs the month of the year. NCEP/NCAR 40-year reanalysis 1 project (Kalnay 1996), from Omega, zonal wind, meridional wind and specific humidity during the 1981 - 2010 period is used. The dynamical variables omega at 600 hPa as a proxy for air vertical velocity influencing cloud formation, zonal and meridional winds at 600 hPa, influencing advection and orographic cloud and rain formation, and specific humidity at 600 hPa, are studied to explain the atmospheric processes throughout the year. The influence of synoptic conditions on the spatial distribution of CF, LWP and ZMIT, for the seasons March to May and June to August, is studied. March-April-May period is important because it is the rainiest season of the year for BM regions. Contrarily, June-July-August is the rainiest season for UM regions, and the driest season for BM and TM regions. For (ii), the correlation between cloud products and NPRs across a representative transect in the Paute basin is calculated. An East-West transect is considered because year around easterlies are among the main climatic influence in the North-South oriented Andean mountains.

- **WP2:** H1 validation is underpinned on the development and results of WP1. Thus, the degree of influence that a specific station may have from the synoptic or local conditions is studied in the previous WP. For H2 it is expected that downscaling results are station dependent, with higher skill for some stations belonging to precipitation types with more synoptic influence over precipitation types with more local influence. It is worth noticing that the information on the performance of downscaling methods in the Andean mountain region is limited. In order to have more robust results and to asses about the uncertainty related to the technique used for downscaling, the intercomparison of several statistical downscaling methods is conducted, e.g. the statistical downscaling model (SDSM), artificial neural networks (ANNs), and the least squares support vector machines (LS-SVM). For the statistical evaluation of the results, the representation of the climatological median and variance of the 30-year observations (e.g. from 01-1980 to 12-2009) is conducted in 5 climate stations from diverse precipitation regimens, located in the Paute River basin in southern Ecuador.

- **WP3:** In WP2 the evaluation of downscaling methods without considering terrain information is conducted to validate H2. WP3 is devised to evaluate the added value of RCMs against the statistical downscaling counterpart based on ANN. For dynamical downscaling, the RCM, WRF model version 3, with high-resolution orography (e.g. 15km) is implemented. Because, to a certain extent, the value added of RCMs is to consider more detailed terrain information, the study region included the PB and the Jubones basin (Fig. 5-1), which present higher altitudinal gradients, thus providing a scientifically interesting location

for exploring how well the scale effects are captured. For WRF, a sensitivity analysis is conducted following the parameterizations recommended from several studies available in the literature, which consider microphysics, convective and shallow clouds, surface layer, land and urban surface, planetary boundary layer, long wave radiation, short wave radiation. The comparison of dynamical and statistical downscaling methods is not straightforward. Thus, in order to make a more fairly comparison we devised two versions of the statistical downscaling approach. One of them includes regional orographic variables as predictors to allow for spatial extrapolation, and the other is purely local. For the evaluation, some predictive capabilities regarding the generation of station-scale mean monthly rainfall and temperature of both, the statistical and the dynamical downscaling approaches are assessed.

- **WP4:** From WP3, which validates H3, the added value of incorporating orographic information in the downscaling processes is assessed. Thus, finally WP4 is devoted to the evaluation of the combined application of the dynamical and statistical downscaling approaches, and to the generation of future precipitation and temperature projections in the PB. The inputs from GCMs and RCMs from the IPCC AR4 and the IPCC SRES future scenarios A1B, A2 and B1 are considered for the period 2045 - 2065.

References

Bendix, J., Rollenbeck, R., & Palacios, W. E. (2004). Cloud detection in the Tropics--a suitable tool for climate-ecological studies in the high mountains of Ecuador. International Journal of Remote Sensing, 25(21), 4521–4540. doi:10.1080/01431160410001709967

Bendix, A., & Bendix, J. (2006). Heavy rainfall episodes in Ecuador during El Ni no associated regional atmospheric circulation and SST patterns. Advances in Geosciences, 43–49.

Campozano, L., Sánchez, E., Aviles, A., & Samaniego, E. (2014). Evaluation of infilling methods for time series of daily precipitation and temperature: The case of the Ecuadorian Andes. MASKANA, 5(1), 99–115. Retrieved from http://dspace.ucuenca.edu.ec:8080/handle/123456789/5586

Kalnay, E. (1996). The NCEP/NCAR 40-year reanalysis project. Bulletin of the American Meteorological Society, 77, 437–471. Retrieved from http://journals.ametsoc.org/doi/abs/10.1175/1520-0477(1996)077%3C0437:TNYRP%3E2.0.CO;2

3 Rainfall and cloud dynamics in the Andes: a southern Ecuador case study

This chapter is published in Advances in Meteorology, 2016, 15.
Received: 11 November 2015 / Accepted: 20 December 2015

Rainfall and cloud dynamics in the Andes: a southern Ecuador case study

Lenin Campozano[1,2,3], Rolando Célleri[1,4], Katja Trachte[3], Joerg Bendix[3], and Esteban Samaniego[1,2]

[1] Departamento de Recursos Hídricos y Ciencias Ambientales, Universidad de Cuenca, Cuenca, Ecuador

[2] Facultad de Ingeniería, Universidad de Cuenca, Av. 12 de Abril s/n, Cuenca, Ecuador

[3] Laboratory for Climatology and Remote Sensing (LCRS), Faculty of Geography, University of Marburg, Deutschhausstr. 10, D-35032 Marburg, Germany

[4] Facultad de Ciencias Agropecuarias, Universidad de Cuenca, Av. 12 de Abril s/n, Cuenca, Ecuador

Corresponding author: lenin.campozano@ucuenca.edu.ec

Abstract Mountain regions worldwide present a pronounced spatio-temporal precipitation variability. Such variability added to scarce monitoring networks limits our understanding of precipitation dynamics and generation processes. To improve our understanding of clouds and precipitation dynamics and cross-scale generation processes in mountain regions, we analyzed spatio-temporal rainfall patterns using satellite cloud products (SCP). The Paute basin (900 - 4200 m a.s.l. and 6481 km2) in the Andes of Ecuador was chosen as the study site due to its good combination of rainfall complexity and monitoring infra-structure (the best monitored basin country-wide). Precipitation models using SCP (based on NOAA-AVHRR images) and GIS data, reveal the spatial extension of three regimes: A tri-modal (TM) mainly present across the basin, a bi-modal (BM), typical for sheltered valleys, and a uni-modal (UM) at windward slopes of the eastern cordillera. Once these regimes are spatially located, the spatio-temporal analysis is performed. Using synoptic information we show that the dry season of the BM regime during boreal summer is caused by strong subsidence inhibiting convective clouds formation. Meanwhile, in UM regions, low advective shallow cap clouds mainly cause precipitation, highly influenced by water vapor from the Amazon and year around easterlies, stronger during boreal summer. TM regions are transition zones from UM to BM, and zones on the windward slopes of the western cordillera. These results highlight the suitability of satellite and GIS data-driven statistical models to study spatio-temporal rainfall seasonality in highly complex terrain as the Andes, especially in regions of scarce monitoring. Although models cannot be a substitute for observations, the application of high-resolution mesoscale models might

be required to fully explain the spatial distribution of cloud and rain forming processes, and further investigations will be oriented on this direction for future studies.

Keywords: convective precipitation, Paute basin, rainfall in mountain regions, model of rainfall, Andean Occurring System.

3.1 Introduction

Mountain regions provide diverse resources and services worldwide. Of especial importance is the provision of water for several uses like irrigation and drinking water (Viviroli et al., 2007). However, the assessment of water resources in mountain regions is uncertain due to the combination of high spatio-temporal precipitation variability and, scarce monitoring networks. These also hinder the understanding of the precipitation processes. In particular the Andes represent a privileged region for studying the processes involved in clouds formation and rainfall development (Pourrut & Gómez, 1998).

The Andes cordillera in Ecuador, is oriented from north to south, and is formed by two mountain ranges, which are sharply pronounced in the northern and central part, and hardly established in the southernmost part of the country (Coltorti & Ollier, 2000). The Andes acts as a weather divide in Ecuador (Bendix & Lauer, 1992). Towards the west of the cordillera, in the coastal plains, one rainy season occurs from December to April, which is mainly modulated by the Pacific Ocean sea surface influence, especially by the region Nino 1+2, and by the evolution of the Inter-tropical Convergence zone (ITCZ). In the Amazon, towards the eastern part of the Andes, the rainfall is present year around, with two periods of higher rainfall during March-May and October-November, modulated by the ITCZ and moist air from the Amazon basin. The inter-Andean valleys between the two mountain ranges, present a bi-modal regime of rainfall, with a dry period during boreal summer. The wind field in the eastern Andes is generally characterized by a very high frequency of easterlies (75%) all year around, (Rollenbeck & Bendix, 2011) and the east facing slopes without shelter are frequently exposed to the main air stream. These climatic influences added to the complex topography of the Andes, make their study scientifically important and challenging.

Nonetheless, there are some studies that deal with the characterization of rainfall dynamics in this region. For instance, in the Paute basin (PB, 6481 km2) in the Southern Andes of Ecuador, Mejia et al. (1996), used 35 stations to study the annual precipitation variability, identifying 7 homogeneous regions. Not all sub-catchments could be considered because of a lack of data. Célleri et al. (2007) analyzed 23 rainfall stations to study the spatial variability of annual rainfall, the relation of precipitation and altitude as well as intra-seasonal rainfall variability / trends for 11 stations with longer time series. They identified two main annual rainfall regimes in space, a bi- (BM) and a uni-modal (UM) type, including subtypes BM1, the inter-Andean valley stations, with a marked dry season during JJA and BM2, a high mountain regime with higher amounts of annual precipitation. Because no spatial precipitation information was available, delineation of the regions was conducted by using a digital terrain model. With respect to the dependence of precipitation on elevation they could not find a clear relation. Buytaerd et al. (2006) studied spatial and temporal rainfall patterns in the west part of

the PB (3500 - 4100 m asl) using 14 stations installed from 2001 to 2005. They found that only stations within 4 km distance are strongly correlated. Also they found that seasonal variation was low, around 100 mm between the wettest and the driest month. With respect to the relation between average daily rainfall and orographic features as slope and aspect, significant correlations were found. For inter-annual precipitation variability, the Rio Paute system is also influenced by quasi-periodic oscillations of the ENSO system (Bendix et al., 2011). Therefore, Mora & Willems (2012) studied decadal oscillations on time series of monthly precipitation (25 stations) and temperature (16 stations). They found that rainfall variations were negatively correlated with the sea surface temperature anomalies of El Niño 1+2 region. The stations from the BM2 region with a northeast aspect showed strong anomalies in similar periods as Amazon regime stations. BM1 stations revealed similar behavior with lower correlation to large-scale circulation. These facts highlight the influence of orographic features in the rainfall spatial distribution. Therefore, depending on the climatic influences, orography complexity and data accessibility, the instauration of adequate monitoring networks to properly understand rainfall distribution and generation processes may be difficult and sometimes impossible.

The lack of adequate monitoring networks for studying such rainfall variability makes necessary the use of remotely sensed data and / or regional climate modeling. With reference to a specific mountain region in the Andes of southern Ecuador, Bendix et al. (2006) investigated cloud frequency, cloud-top height and cloud liquid water path using a dataset of NOAA-AVHRR (Advanced Very High Resolution Radiometer) imagery in 1 km resolution. In general they found that the seasonal cycle of cloudiness is significantly correlated to the spatial occurrence of the rainy seasons. However, the complex topography of the Andes, with dynamic effects at the windward and lee sides, as well as thermal breeze-systems, cause a specific spatial structure of cloud frequency and cloud properties. Regarding rainfall, Ochoa et al. (2014) evaluated a big data set of surface precipitation stations against data from the Tropical Rainfall Measuring Mission (TRMM) 3B42 V7 and its predecessor V6, and the North Western South America Retrospective Simulation (OA-NOSA30), covering 21 sub-catchments situated in the westernmost axis of South America, the Pacific-Andean Basin into Ecuador and Peru. They found that only the southern sub-catchments of Ecuador and northern Peru were relatively well estimated by both methods. However, the accuracy of both approaches was quite poor in the northern and central basins in the region of study (0-3.6 S), limiting the possibility of its use. Particularly the model based OA-NOSA30 was inferior in generating the spatial distribution of the mean annual precipitation. Considering regional climate modeling, Ochoa et al. (2015), aimed at reproducing temperature and rainfall seasonality for 3 stations in the PB and 2 stations in the Jubones basin, located towards the south. Although the seasonal patterns were represented, improving those of reanalysis data, however monthly amounts were strongly overestimated. Finally, the uncertainties in climate change projections as derived by climate models for the Andes of Ecuador and the Paute system are shown to be enormous. For instance, for precipitation, climate models differ considerably in the region of study: some models project positive anomalies meanwhile others project negative anomalies (Mora et al., 2014). This is due, in part, to climate models non-adapted to the complex topography which is required to resolve rainfall formation processes cross different scales (Buytaerd et al., 2009; Buytaerd et al., 2010; Bendix et al., 2009; Trachte & Bendix, 2012). In addition, climate models need observational data to be adequately calibrated, which, in the case of the PB, is still required.

In summary, different rainfall regimes exist in the Rio Paute catchment area, but to date a spatial explicit delineation is still lacking due to the scarcity of the station network. Furthermore, no study hitherto exists that links the zonation to potential rainfall generation processes and the varying influences ranging from global circulation patterns to mesoscale atmospheric processes, which might be responsible for rainfall formation in time and space. Hence, the main aim of the present study is to understand the spatio-temporal dynamics of precipitation and clouds, and the potential cross-scale generation processes of rainfall in the Paute basin. In section 2, the study area and data are presented. Section 3 describes the methods used in this study, while section 4 introduces the results and discussion. Finally, section 5 presents a summary, which is followed by the conclusions in section 6.

3.2 Study area and data

The study region is the Paute river basin (Fig. 3.1), 6481 km2. The Paute basin is located in the inter-Andean depression between the western and the eastern Andean escarpments of southern Ecuador (Coltorti & Ollier, 2000). Its elevation range varies from 900 - 4200 m a.s.l. and around 40% of the basin is covered by Páramo (Célleri et al., 2007). The páramo is a neotropical alpine wetland ecosystem covering the upper Andean region of Venezuela, Colombia, Ecuador and Peru (Buytaerd & De Bievre, 2012). Ecosystem services provided by the páramo include high water regulation capacity and carbon sequestration. Particularly, several cities along the Andes like Quito and Bogotá (De Bievre, 2003) and irrigation systems benefit from water yielded from the páramo. Its high water regulation capacity (Mosquera et al., 2015) originates from a combination of its soil properties (mainly Andosols and Histosols, with high organic matter content) that can store large volumes of water (Buytaerd, et al., 2006), the climate (rainy, cold and cloudy) (Padrón et al., 2015; Córdova et al., 2015) and the vegetation (mainly tussock grasses and cushion plants). Predicted changes in the climate will lead to negative changes in its water regulation (Buytaerd et al., 2011) and therefore they are considered a very fragile component of the high Andean ecosystems. The Paute river basin feeds several hydroelectric power plants, Amaluza (1075 MW), El Labrado y Chanlud (38.4 MW), Mazar (162.6 MW) and Sopladora (500 MW), generating around 40% of the Ecuadorian national hydroelectrical production. Several cities in the region depend directly on diverse hydro-ecological services of the basin.

The topography shows main ridges of the Andean western Cordillera bordering the basin to the South and East. Two lower ridge systems are striking SW-NE, separated by river valleys as the one of the Rio Paute. The lowest part in the Northeast marks the outflow of the river system toward the Amazon lowlands. The eastern part of the Paute basin, is located on the escarpments of the eastern cordillera. In this region the Paute basin is influenced by the Andean Occurring System (AOS), which is a band of clouds and rain located along the eastern escarpments of the eastern cordillera.

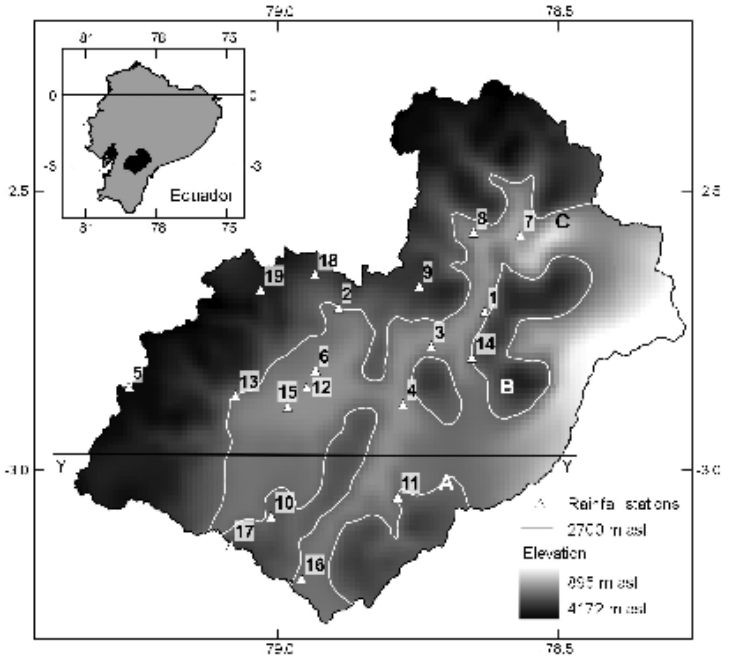

Figure 3-1: The Paute river basin in south Ecuador. Profile Y-Y black line. Prominent orographic features are: Mount El Calvario(A), Mount Bellavista (B) and Paute canyon (C).

Data from 15 rainfall stations of the Ecuadorian National Institute of Meteorology and Hydrology, INAMHI, delivering daily values for the period January 2000 to December 2009 were available (Table 3.1). Data from 4 rainfall stations of the Empresa Municipal de Telecomunicaciones, Agua Potable y Saneamiento, ETAPA, delivering hourly values for the period December 2001 to December 2009 were also available (Table 3.1). For the quality control of the data, time series with less than 10 % of gaps during the study period was considered in first place. Then homogeneity was checked with the package RHTestsV3 (Wang, 2008a; Wang, 2008b) on monthly data, since daily time series can be very noisy. The software change point detection test is based on the penalized maximal F-test. Finally infilling of gaps in homogeneous time series was conducted using a multiple regression model with the stations of higher correlation (Campozano et al., 2014).

The satellite products used in this study are based on 452 NOAA- AVHRR scenes acquired during 2002 and 2004. The data set has a spatial resolution of 1 km and consists of cloud frequency (CF), cloud top height (ZMIT) and cloud liquid water path (LWP). For more details on the generation of the data set the reader may refer to Bendix et al. (2004) and Bendix & Bendix (2006). For elevation terrain information the Global 30 Arc-Second Elevation (GTOPO30) was used (Data available from the U.S. Geological Survey). Also, reanalysis data from 1981 to 2010 period was used. Omega, zonal wind, meridional wind and specific humidity from NCEP/NCAR 40-year reanalysis 1 project was used (Kalnay et al., 1996).

Table 3-1 : Precipitation stations of the Paute river basin. INAMHI (Instituto Nacional de Meteorología e Hidrología) stations with daily data, and ETAPA (Empresa Pública Municipal de Teléfonos, Agua Potable y Alcantarillado de Cuenca) with hourly data. (*) Stations used for validation of rainfall models.

#	Code	Name	Lat (deg)	Log (deg)	Altitude (m asl)	Institution
1	M045	PALMAS	-2.716	-78.63	2400	INAMHI
2	M137	BIBLIAN	-2.709	-78.892	2640	INAMHI
3	M138	PAUTE	-2.778	-78.726	2289	INAMHI
4	M139	GUALACEO	-2.882	-78.776	2360	INAMHI
5	M141	EL LABRADO	-2.85	-79.267	3260	INAMHI
6	M197	JACARIN	-2.821	-78.933	2700	INAMHI
7	M217	PEÑAS COLORADAS	-2.579	-78.566	2000	INAMHI
8	M410	MAZAR RIVERA	-2.574	-78.65	2450	INAMHI
9	M414	CHANIN	-2.67	-78.747	3020	INAMHI
10	M418	CUMBE	-3.083	-79.0128	2720	INAMHI
11	M424	SIGSIG INAMHI	-3.048	-78.786	2600	INAMHI
12	M426	RICAURTE	-2.851	-78.949	2545	INAMHI
13	M427	SAYAUSI	-2.866	-79.076	2710	INAMHI
14	M431	SEVILLA DE ORO	-2.798	-78.653	2360	INAMHI
15	M067	CUENCA AEROPUERTO *	-2.887	-78.983	2516	INAMHI
16	--	JIMA *	-3.194	-78.958	2898	ETAPA
17	--	PORTETE *	-3.134	-79.084	3174	ETAPA
18	--	LA ESMERALDA *	-2.649	-78.934	3171	ETAPA
19	--	CHANLUD *	-2.677	-79.031	3485	ETAPA

3.3 Methods

To improve our understanding of spatio-temporal dynamics of precipitation and clouds, and the potential cross-scale generation processes of rainfall in the Paute basin, the present study was conducted in two stages. First, we pursue the delineation of precipitation regimes across the basin, based on cloud products and GIS data. We considered that the identification of precipitation regimes by regions might help to differentiate influences in precipitation at synoptic, meso and local scales. Secondly, we analyzed the rainfall dynamics and the relation to cloud dynamics and orography using reanalysis data and cloud products to understand further the synoptic conditions influencing precipitation in the PB.

3.3.1 Spatial delineation of rainfall seasonality

The work flow for spatial data set generation of seasonality is presented in Fig. 3.2. The approach consists of five consecutive steps including (i) generation of normalized precipitation regimes (NPR), (ii) area-wide seasonal delineation using satellite derived variables CF, LWP, ZMIT, (iii) the development of a model of rainfall based on principal component analysis (PCA) applied to CF (CFM) to generate seasonality delineation, (iv) the development of a multiple linear regression model of rainfall (MLRM) to generate seasonality delineation, and (v) the pixel-wise evaluation of regionalization obtained from CF, LWP, ZMIT, CFM and MLRM against zonation from Célleri et al. (2007). Kendall's tau correlation is a robust non-parametric estimate of similarity between two ranked series. Therefore, no a-priory assumption about the distribution is necessary. Because NPRs and CF, LWP, ZMIT, MLRM, CFM, exhibit non-Gaussian asymmetric distributions, the Kendall's tau correlation was calculated and tested at 0.05 significance level. The relation between rainfall and the variables used from cloud products is complex. Therefore to detect at least low linear correlations between them is important. Thus, to represent the seasonal delineation, the evaluation of the maximum Kendall's tau correlation greater than 0.3 comparing the three NPRs with CF, LWP, ZMIT, MLRM, and CFM was conducted. In the following paragraphs these steps will be explained.

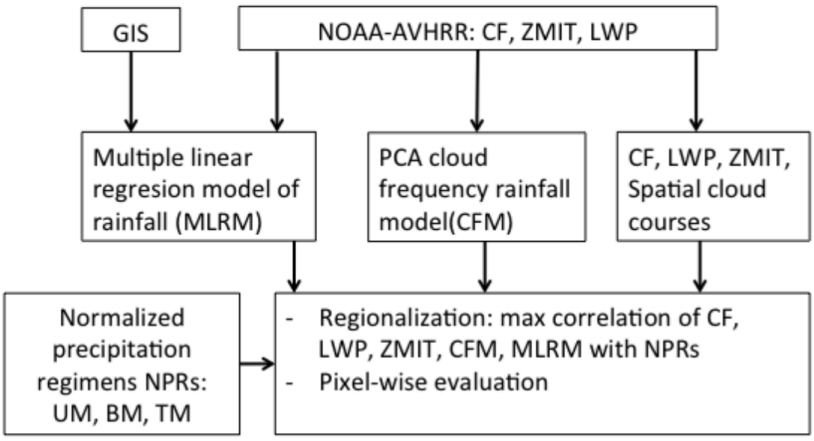

Figure 3-2: Overall work flow of spatial data set generation of seasonality.

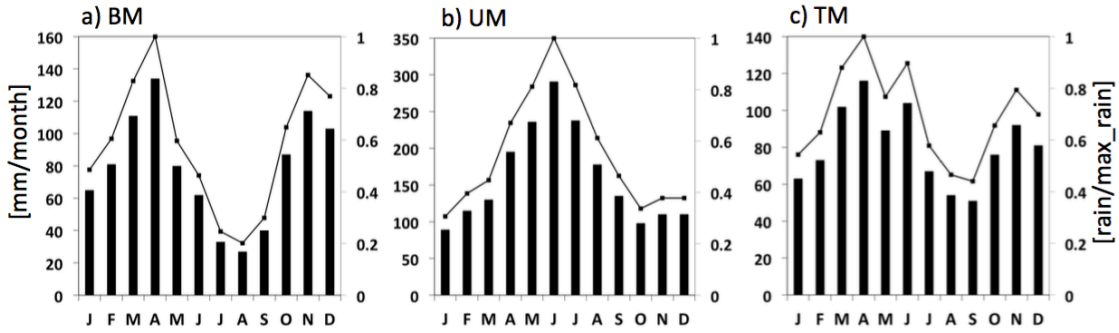

Figure 3-3: The three seasonal precipitation regimens, average monthly rainfall (left y-axis) and normalized regimens NPR (right y-axis). a) bi-modal regime, b) uni-modal regime and c) three modal regime.

3.3.1.1 Normalized observational precipitation regimes (NPR)

Stations with similar seasonality were grouped to obtain a representative pattern for each type of precipitation regime. Following Bendix & Lauer (1994) and Célleri et al. (2007), three seasonal rainfall regimes are present in the Paute river basin (Fig. 3.3), BM, UM, and three-modal (TM). While the BM regime is the typical high inter-Andean type, TM is a high mountain regime with higher amounts of annual precipitation. In order to classify monthly precipitation by signal, three normalized observational precipitation regimes (NPRs) as shown in Fig. 3.3 are defined. The normalization of precipitation was calculated dividing the average monthly precipitation from all stations of the respective regime (UM, BM, TM) by the average maximum monthly precipitation occurring in the seasonal regime.

3.3.1.2 Types of area wide seasonal regimens using satellite-derived variables

From a conceptual consideration, three variables derived from satellite data are expected to be related to monthly rainfall (Thies et al., 2008): monthly CF, average LWP, and mean ZMIT. It is expected that (i) the higher the cloud frequency in one grid cell, the higher the likelihood for rainfall (e.g. blurred by non-raining low clouds), (ii) the greater the cloud top height, the higher the likelihood for convective precipitation (e.g. blurred by strong cloud advection), and (iii) the greater the liquid water path, the greater the likelihood for big droplets forming rainfall (Thies et al., 2008). For the assessment of the satellite dataset, a pixel-wise calculation of Kendall tau correlation and significance between the NPRs UM, BM and TM NPRs and the space-borne variable is conducted.

3.3.1.3 PCA cloud frequency model of rainfall

The rainfall model based on the application of PCA to monthly cloud frequency (CFM), use the 3 main principal components as inputs and the monthly rainfall as output. These components were selected after the application of the scree test. The scores from the first 3 PCs, are the three main CF patterns, and their occurrence thru the 12 months is represented by the weights Therefore the product of the scores multiplied by the weights represent the monthly influence of each PC, as a weighted score. In order to map the weighted scores to rainfall amounts, an exponential fitting is applied to monthly observed precipitation of 14 stations, generating pixel-wise monthly rainfall data. Because precipitation is a variable with positive values, the fitting to an exponential function was conducted.

Applied pixel-wise, the CFM rainfall model for each month is in general of the form:

$$P_k = \exp(c_k + \sum_{i=1}^{n} a_{ik} s_{ik} L_{ik})$$

Where P_k is the rainfall for the month kth on a pixel, a_{ik} & c_k are regression coefficients for the kth month, s_{ij} is the score for the kth month corresponding to the ith principal component, L_{ij} is the weight for the kth month corresponding to the ith principal component.

For the validation of the model, the monthly precipitation was calculated for 5 stations not considered in the calibration group, then the bias, the slope and total variance explained by the model was calculated. Finally, area-wide seasonality of rainfall is derived from correlation analysis with NPRs.

3.3.1.4 Multiple regression model of rainfall

A multiple linear regression model of rainfall (MLRM) is applied to generate area-wide data sets of NPRs. A principal component analysis (PCA) was applied to satellite-borne and GIS based data variables, and the 5 main principal components were used as inputs to the model. As in CFM, the main components were selected after the application of the scree test. The three satellite products are the aforementioned CF, LWP, and ZMIT, while the five GIS predictor variables encompass (i) the average potential radiation per month (Lauer et al., 2003) as a proxy for the energy available for generation of local convection, (ii) the average monthly wind shelter as a proxy for the formation of advective rainfall (Wagemann et al., 2015), and (iii) latitude, longitude and elevation as important predictors accounting for orographic effects.

Therefore, the multiple linear regression model of precipitation applied pixel-wise is:

$$P_k = c_k + \sum_{j=1}^{5} a_{kj} pcs_{kj}$$

where P_k is the precipitation corresponding to the kth month, c_k is the regression coefficient independent term of the kth month, a_{kj} is the regression coefficient of the jth principal component score (pcs), corresponding to the kth month, and pcs_{kj} is the jth pcs of kth month. It is important to observe that prior to PCA application, the variables derived from cloud products and GIS were normalized by subtracting the mean and then dividing by the standard deviation.

The MLRM model was calibrated using the monthly precipitation for a group of 14 stations from UM, BM and TM regimens. For the validation of the model, the monthly precipitation was calculated for 5 stations not considered in the calibration group, then the bias, the slope and total variance explained by the model was calculated. Then, area-wide seasonality of rainfall is derived from correlation analysis with NPRs.

3.3.2 Rainfall dynamics and the relation to cloud dynamics and orography

In order to study the relation between rainfall dynamics with clouds dynamics and orography, we conducted (i) the synoptic analysis of dynamical variables and its relation to seasonal clouds products, and (ii) the evaluation of NPRs along a representative transect in the Paute river basin. For (i), the analysis of the synoptic conditions was conducted using Hovmöller diagrams across a zonal transect from 270º to 300º, averaged from latitude -5º to latitude 5º vs the month of the year. The dynamical variables omega at 600 hPa as a proxy for air vertical velocity influencing cloud formation, zonal and meridional winds at 600 hPa, influencing advection and orographic cloud and rain formation, and specific humidity at 600 hPa, are studied to explain the atmospheric processes throughout the year. To study the influence of synoptic conditions on the spatial distribution of CF, LWP and ZMIT, the seasons MAM and JJA, were studied. To concentrate on MAM is important because MAM is the rainiest season of the year for BM regions. On the other hand, JJA is the rainiest season for UM regions, and the driest season for BM and TM regions. For (ii), we calculated the correlation between cloud products and NPRs across a representative transect in the Paute basin. A East-West transect was considered because year around easterlies are among the main climatic influence in the North-South oriented Andean mountains (profile location presented in Fig. 3.1).

3.4 Results and discussion

3.4.1 Delineation of seasonal regimes

Based on the evaluation of the maximum Kendall's tau correlation greater than 0.3, comparing the three NPRs with CF, LWP, ZMIT, CFM and MLRM, the representation of precipitation regimens delineation are presented in Fig. 3.4) a-e. Also, the pixels significant at 0.05 level where plotted in Fig. 3.4 f-j. As a reference for evaluating NPRs

spatial delineation, the regionalization proposed by Célleri et al. (2007) was used, due to the lack of basin-wide rainfall observations availability. It was assumed that UM is UM1 and UM2, BM is BM1, and TM is BM2 in the present and Célleri et al. (2007) work respectively. The study area on Célleri et al. (2007), present less area than the area used in the present study. However it is important to mention that delineation of rainfall seasonality furnished in Célleri et al. (2007) was based mostly in topographic features and a limited number of stations. It must be stressed that significance of correlation is given but only based on 12 values representing the monthly climatology. This means that correlation is very sensible to outliers and thus, not a full spatial coverage of significant correlations can be expected. Also, it is important to highlight that although precipitation in complex terrain is highly variable in time and space, the spatial delineation of rainfall regimes using clouds products with 1 km resolution may be appropriate when considering the climate scale.

The results of the regionalization and pixels significant at 0.05 level using CF is presented in Fig. 3.4 a,f. Correlation with UM NPR is not represented. Correlation with TM present an irregular spotty pattern in the centre of the Paute basin. Correlation with BM, significant at 0.05 level, is shown in the centre of the Paute basin around BM stations Gualaceo and Jacarín, on the north, on the west near by TM station El Labrado, and on the south next to TM station Cumbe. Although BM regime is depicted, however a clear delineation of seasonality is not represented. For LWP, regionalization and significant pixels at 0.05 level are presented in Fig. 3.4 b, g. Isolated regions of BM towards the west near to BM station Sayausí, UM towards the north around UM stations Peñas Coloradas, and Palmas, and TM to the south west is presented. However a clear delineation of seasonality is not represented as well. Further, significant values at 0.05 level are present in just a few pixels. The regionalization of ZMIT (Fig. 3.4 c), represent the BM NPR in almost the full extent of the Paute basin. However significant values at 0.05 level (Fig. 3.4 h), are presented, in the centre to the west region. NPRs UM and TM are not represented by ZMIT. This fact, points to a pronounced influence of convective clouds with greater top heights producing strong rainfall during MAM and SON. At the same time, regimes with enhanced rainfall during JJA are not represented by ZMIT. This fact might be due to the presence of low clouds.

Table 3-2: Multiple linear regression coefficients for the 5 main PCs.

Month	c	a1	a2	a3	a4	a5
Jan	63.10	3.24	5.80	-7.45	3.20	-5.69
Feb	75.84	-0.84	4.27	-5.69	3.31	7.17
Mar	103.78	-2.28	-9.78	-0.78	4.45	-10.15
Apr	127.35	1.25	10.96	-8.24	-4.52	-0.47
May	95.23	-8.50	12.70	15.82	0.97	-4.52
Jun	102.10	5.47	-17.48	22.95	-27.38	21.41
Jul	66.13	-21.30	-5.13	-3.02	-14.41	1.83
Aug	53.04	-7.39	-5.71	17.49	15.44	10.53
Sep	52.82	6.05	3.67	-1.71	-10.09	-11.60
Oct	80.50	-0.12	-0.41	-10.16	-1.65	0.77
Nov	99.25	-1.53	-11.52	-4.87	-6.41	-9.29
Dec	88.62	0.90	-1.01	5.70	11.68	15.59

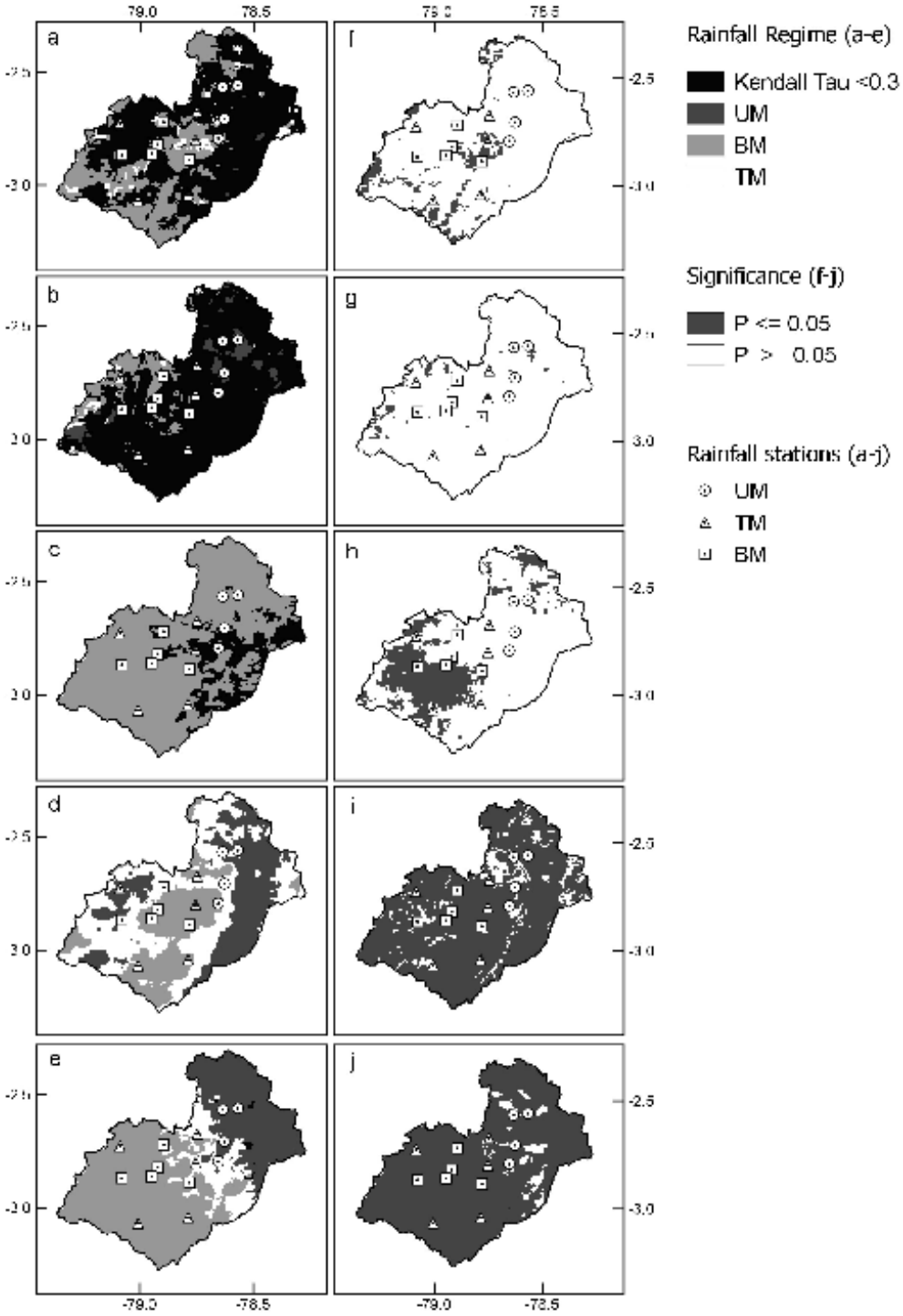

Figure 3-4: Pixel-wise maximum Kendall tau correlation between NPRs UM, BM, TM for CF (a), LWP (b), ZMIT (c), CFM (d), MLRM (f). Only correlations greater than 0.3 are plotted. Corresponding significance of maximum correlation at 0.05 level for CF (f), LWP (g), ZMIT (h), CFM (i), MLRM (j).

For CFM the regionalization based on the maximum Kendall's tau correlation with NPRs, and significant pixels at 0.05 level are presented in Fig. 3.4 d,i. CFM was calibrated using the multiyear monthly mean precipitation of 14 stations, and validated against 5 stations. The regression coefficients are presented in Table 3.4. The r2, bias, and slope is presented in Table 3.5. Although R2 is low 0.357 in average, the spatial pattern of NPRs is similar to Célleri et al. (2007) regionalization, assuming that TM is BM2 in the cited work. CFM regionalization highlights the importance of orography in precipitation seasonality. UM regime in CFM is located in parallel to the orientation of the Eastern cordillera, along the AOS. However in the region in front of the Paute canyon, UM regime enters the basin, highlighting the influence of this orographic feature for the climate of the basin. The region with the UM regime is important for the Paute hydroelectric power production and thus, of mayor importance for the Ecuadorian economy. Therefore it is an important feature that must be properly captured by any rainfall delineation scheme.

Table 3-3: Validation parameters for MLRM. Multi-year monthly mean precipitation observed vs modeled with MLRM. R^(2), bias and slope.

Name	Bias	Slope	R2
Esmeralda	-35.90	0.92	0.72
Chanlud	-1.33	0.54	0.17
Cuenca aeropuerto	5.51	0.92	0.85
Portete	-34.81	0.59	0.54
Jima	-61.33	0.79	0.22
Average	-25-57	0.75	0.50

A drawback of CFM is the overrepresentation of UM regime on a short extension in the western part of the basin, but it is important to acknowledge that the model captures the enhancement of rainfall on the eastern flanks of the eastern and the western cordillera. This enhancement of rainfall might be due to the orographic lifting of air on the windward side of the cordillera, forcing convection and rainfall. For CFM, TM is mainly present across the Paute basin, and BM regime is located only in regions sheltered by the eastern cordillera. Also, the TM regime divides the basin due to the influence of the passage of clouds between Mounts Bellavista and El Calvario (Fig. 3.1). This feature is absent in Célleri et al. (2007), but still necessary to be confirmed. The CFM model points out that TM is a transition state between UM and BM regimens. Therefore on the unsheltered eastern flanks of the cordillera UM and TM NPRs are expected, and BM NPR is more present in isolated sheltered regions.

Table 3-4: CFM regression coefficients for the 3 main PCs.

Month	c	a1	a2	a3
Jan	3.90	-0.55	0.01	0.12
Feb	4.18	0.27	-0.01	0.04
Mar	4.58	-0.12	0.00	-0.04
Apr	4.76	-0.28	-0.02	-0.07
May	4.83	0.14	-0.01	0.05
Jun	4.82	0.15	0.04	-0.29
Jul	4.59	0.09	-0.42	1.21
Aug	4.06	0.09	-0.05	0.93
Sep	4.20	0.10	-0.03	-0.03
Oct	4.35	-0.65	-0.02	0.16
Nov	4.60	0.10	-0.03	0.04
Dec	4.21	0.10	-0.23	0.33

Table 3-5: Validation parameters for CFM. Multi-year monthly mean precipitation observed vs modeled with CFM. R^(2), bias and slope.

Name	Bias	Slope	R2
Esmeralda	31.34	0.63	0.21
Chanlud	-68.24	1.21	0.49
Cuenca aeropuerto	26.80	0.58	0.61
Portete	18.52	0.26	0.32
Jima	32.99	0.34	0.16
Average	8.28	0.60	0.36

The regionalization based on maximum Kendall's correlation greater than 0.3 and significance at 0.05 level of MLRM with NPRs are presented in Fig. 3.4 e&j. As CFM, the MLRM was calibrated using multi year monthly mean precipitation of 14 stations, and validated with 5 stations. The regression coefficients are presented in Table 3.2. The R2, bias, and slope between the model results and the observations of 5 stations are presented in Table 3.3. The delineation of MLRM presents the BM regime located toward the west and southwest of the basin. UM is depicted on the north and northeast. TM regime is located between BM and UM regions, rightly represented as a mix between these two regimes. However, there is a lack of representation of TM on the eastern flank of the western cordillera on higher elevation slopes, missing therefore the enhancement of precipitation during JJA due to orographic features. It is interesting to observe that MLRM captures UM region on the Paute canyon area. This fact might be due to the consideration of orographic variables. A drawback of the model is the overestimation of UM influences in the northern part of the basin, where BM regime

was found by Célleri et al. (2007). In comparison with CFM regionalization, where UM is located in parallel to the eastern flanks of the eastern cordillera, MLRM lack UM representation along this regions.

To summarize the previous results, in Table 3.6 the pixel-wise evaluation of seasonality of CF, LWP, ZMIT, MLRM, and CFM was conducted against regionalization proposed by Célleri et al. (2007), presupposing that TM is BM2 on their study. It is important also to highlight that the region considered in Célleri et al. (2007) study covers less area than the region considered in the present study. The station-wise evaluation of seasonality representation by the models was also possible, but this approach does not give information about the extended spatial delineation representation. Therefore, in order to make a distributed evaluation score, pixels with a perfect match were assigned a value of 1 and 0 otherwise. In order to calculate the total concordance the summation of all pixels is calculated and then divided by the number of pixels. The results show that MRLM and CFM outperformed CF, LWP and ZMIT, with CFM presenting a slightly higher concordance score.

Table 3-6: Concordance of seasonal regimens of cloud frequency, liquid water path, average cloud top height, multiple linear regression model of rainfall and PCA cloud frequency model of rainfall against Célleri's regionalization.

Approach	Concordance (%)
CF	17.05
LWP	19.52
ZMIT	16.71
MLRM	46.88
CFM	53.67

The spatial representation of the seasonality of rainfall in the Paute basin was better conveyed by the MLRM and CFM models of rainfall. Quantitatively, regarding the pixel-wise evaluation of seasonality representation (Table 3.6), the two models present similar coincidences, CFM with slightly higher values, although is important to stress that the evaluation was developed against Célleri et al. (2007) based mostly on topographical features, besides the fact that the region considered for evaluation do not covers the eastern slopes of the Paute basin toward the Amazon, where strong differences in seasonality representation between the two models arise. Furthermore, the validation of the two rainfall models was conducted against the monthly rainfall of 5 stations, displaying on average similar results. Qualitatively, MLRM is able to represent UM, BM and partly TM regions in the transition zone from the lower to the upper part of the Paute basin. However, the lack of representation of TM regions on the western slopes of the Paute basin oriented to the east, is an important drawback of the MLRM model.

With regard to CFM, it is able to represent UM, BM, and the transitional TM region: the seasonal delineation resembles the one presented in Célleri et al. (2007) (considering TM as equivalent to BM2). A remarkable capability of this model is the good representation of the BM regime in the sheltered regions to the easterlies. Another important feature is the representation of the shift of seasonality from UM to TM on the

northernmost part of the basin towards higher elevations. A drawback of this model is the overrepresentation of UM on a small area in the western slopes of the western Cordillera eastward oriented. As a general finding, the NPRs delineation highlighted the relation between the precipitation regime and the orographic features in the PB. Thus, in order to understand the spatio-temporal dynamics of precipitation and clouds, and the potential cross-scale generation processes of rainfall in the PB, further analysis is conducted.

3.4.2 Spatio-temporal analysis of cloudiness and consequences for rainfall seasonality related to orography

3.4.2.1 Analysis of synoptic conditions and seasonal cloud products

To understand the atmospheric conditions producing rainfall and clouds in the Paute river basin, the long-term 1981-2010 multiyear monthly mean omega, zonal wind, meridional wind and specific humidity was studied. We used Hovmöller diagrams across a zonal transect from 270º to 300º averaged from latitude -5º to latitude 5º vs the month of the year (Fig. 3.5). Omega negative values (up oriented) mean ascending air, enhanced convection, the development of clouds, therefore more probability of rainfall. On the other hand, positive values of omega (down oriented) imply subsidence, producing inhibition of clouds formation and rainfall. From Fig. 3.5-a, is evident a relative peak of omega, from February to April. Therefore higher cloud formation and rainfall of convective nature is expected during this season. This is related to the rainy season MAM. On the other hand, from June to September, omega positive values mean subsidence, inhibiting cloud formation and rainfall, accounting for the drier season for BM regions. Also, due to subsidence lower clouds are expected. From October, omega values are low negative again until December, where higher negative values are presented. Although subsidence during JJA account for the drier season in BM regions, however, JJA is the rainiest season for UM regions, and TM regions present a shallow peak in rainfall in June. To account for JJA precipitation in UM and TM regions, the analysis of horizontal winds and specific humidity are important. Fig. 3.5-b, shows that easterly winds influence the Paute basin throughout the year, with values markedly stronger during JJA. Further, in Fig. 3.5-c, the highest values of specific humidity are present from April to July. This fact points to strong easterlies with high content of moist, are cooled adiabatically due to the raising air along the eastern slopes of the cordillera, enhancing clouds and precipitation along the escarpments of the cordillera. Similar situation might occur, to a lesser extent, on the eastern slopes of the western cordillera, accounting for a shallow peak in clouds and rainfall in June. We also, studied meridional winds, however results are not presented, because, intra-annual variation was not significant.

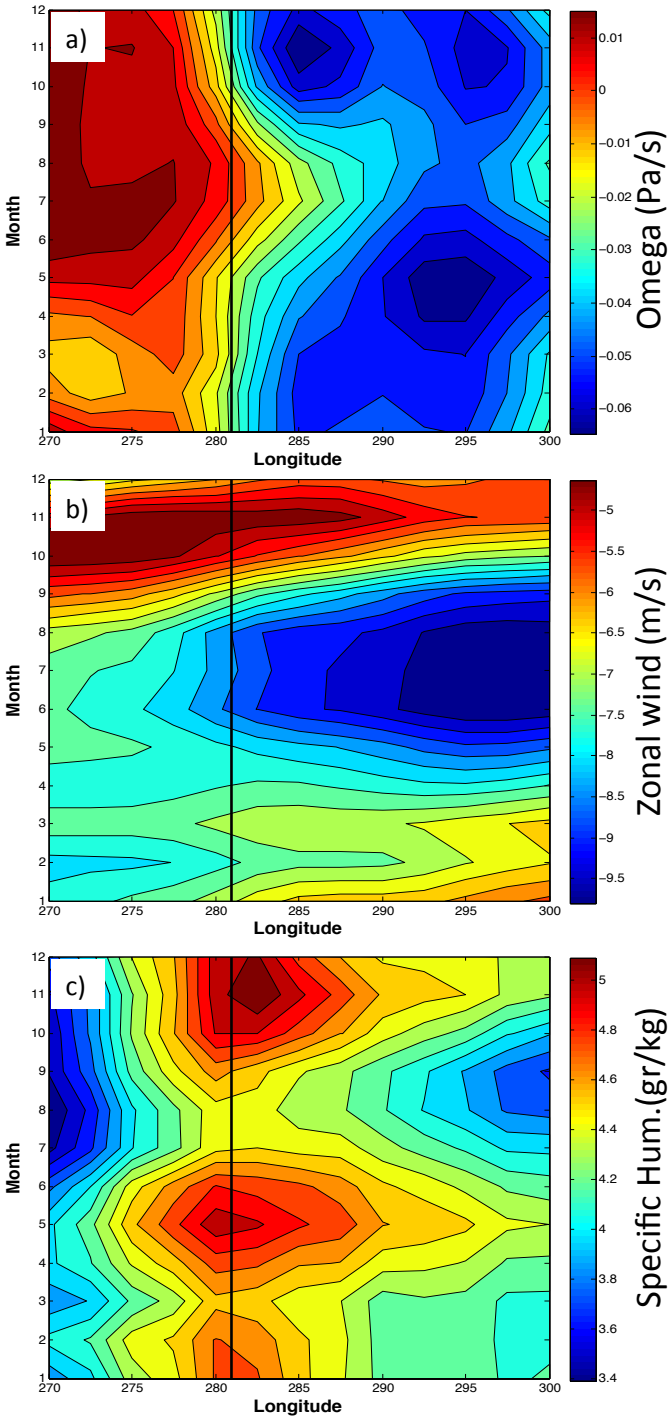

Figure 3-5: Hovmöller diagram across a longitudinal transect from 270E to 300E averaged from 5S to 5N of: a) omega 600hPa, b) zonal velocity wind 600 hPa, c) specific humidity 600 hPa vs the months of the year. The black line located at 281E represents the Paute basin.

Therefore, in order to explain the rainfall dynamics of the seasonal regimens in the study area, the driving macro and mesoscale mechanisms should be considered. Rainfall seasonality near the equator around the world is mainly BM with local variations (Basalirwa, 1995; Basalirwa et al., 1999; Poveda et al.,2001). This seasonal regime is characterized by two rainy seasons, i.e. one during March-April and the second one during October-November with a dry season during June-July. The rainfall behavior is related to the evolution of the ITCZ, and thus, the rainfall mainly develops due to convective processes. To support this fact, we used omega as a proxy for vertical velocity which influence convection (Fig. 3.5-a). This fact is also confirmed by the study of outgoing longwave radiation in tropical regions by Wang (1994). Rainfall seasonality toward the east of the Paute basin, on the Amazon basin is reported to be BM near equatorial areas (Ronchail et al., 2002). On the contrary, toward the west in the coastal plains of Ecuador, the precipitation regime observed describes one rainy season from December to April with its maximum in March. The second rainy season during October is suppressed (Bendix & Lauer, 1994). Therefore considering the UM regime with its maximum in June-July, available on the eastern part of the Paute river basin, rainfalls are expected to develop due to local effects. On the other side, subsidence in JJA, is due to a intensified Walker-Circulation, producing advective low clouds rather than the formation of deep convective activity. Thus, the June-July precipitation maximum for UM and TM regions are strongly linked to the synoptic scale state of the Walker circulation. UM or TM with the June-July maximum should be related to unsheltered windward sides of the slopes where local to mesoscale forced convection counteracts macroscale subsidence induced by the seasonality of the Walker-Circulation, as explained before. Because of the northward shift of the ITCZ during this season, stronger easterlies are enabled to enhance the advection of moisture toward the eastern slopes of the Andes (Figs. 3.5-b,c). These findings are supported by the study of Laraque et al., (2007). They found that the east-west water vapor flux is highest for May-June (215 kg m^-1 s^-1) at 2.5ºS, 77.5W) with a zonal orientation, increasing the precipitation on the windward side of the cordillera.

To study the influence of the atmospheric synoptic conditions on cloud products, the average CF, LWP, and ZMIT for MAM and JJA are presented in Fig. 3.6 for the Paute catchment. CF for MAM and JJA is presented in Figs. 3.6a&b, respectively. During MAM, CF is high across the Paute basin pointing out to a generalized convective situation, affecting UM, BM and TM stations. During MAM, the wetter season for BM and TM regimes, convective cloud formation is common due to ITCZ passages. Toward the coastal plains increased values of CF coincide with the rainiest season during MAM. For JJA, CF is much lower with respect to MAM, with exception of the regions along the eastern slopes. This fact reveals that (i) across the basin the dry season is present during JJA and more evidently marked on the sheltered inter-Andean valleys, and (ii) that there is a band like pattern of enhanced CF and rainfall along AOS, where UM regime could be dominant. Therefore clouds and rainfall are strongly dependent on the easterlies exposure in the Paute basin. As a confirmation to this fact, on the western escarpment of the western cordillera toward the coastal plains, a lee effect is evident during JJA for CF and LWP (Fig. 3.6 b&d). It is striking the resemblance between CF patterns during JJA with CFM seasonality delineation (Fig. 3.6), pointing to the importance of the Amazon influence in seasonality of precipitation and climate for the basin

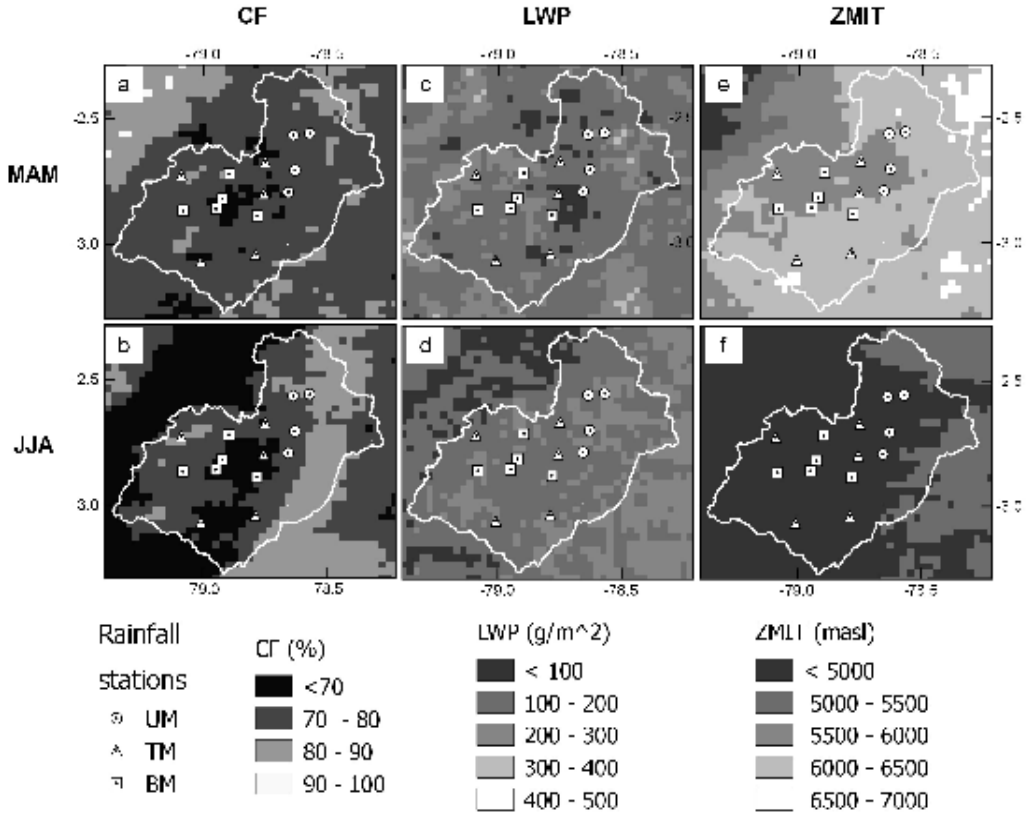

Figure 3-6: Seasonal average for CF, LWP and ZMIT (left, center and right columns) during MAM and JJA seasons (top and bottom rows).

For liquid water path, a more patchy structure can be observed during MAM due to convective cloud formation. In JJA LWP is depicted as an east to west decreasing gradient Fig. 3.6 c&d). This points to advective clouds with high content of water originating from the Amazon influencing the Paute basin. During JJA UM stations are affected as well as TM stations located at the eastern escarpment of the western cordillera. The strong decrease in LWP and CF toward the west of the basin in the western flanks of the western cordillera confirms the findings of Bendix & Lauer, (1992) that the Andes act as a weather divide. For ZMIT, values during MAM are higher due to the generally more convective predisposition compared to JJA. At the average, ZMIT in JJA is around 80% the value of annual mean of ZMIT for the stations selected in the present study. This is due to the general tendency for a subsiding air in the Walker circulation during this season. Thus, inhibition of convective cloud formation accounts for lower ZMIT values of the prevailing lower advective clouds.

3.4.2.2 The influence of orography on cloud products

Regarding the relation between orography, cloud frequency and rainfall, in Fig. 3.7 a west-east cross-section through the Paute basin generally depicts five different zones: (i) The eastern foothills show a tendency that CF is more related to BM and TM NPR. (ii) This changes at escarpment heights around 2300 m asl where high cloudiness in BM and TM means low precipitation. The weak positive correlations between CF and UM point out that UM rainfall is concomitant with a peak in CF possibly related to AOS

region running parallel to the Andes. (iii) At the windward side of the western crest altitude (at approx. 3000 m asl), TM and BM NPRS positively correlates very similar with CF which means that this is the most distinct area where different cloud processes leading to BM and UM NPR are blended. (iv) The basin between the eastern and the western crest altitudes are most dominated by BM related cloud processes, UM is clearly negatively correlated to CF which means rain minima in JJA are a result of minima in CF. (v) The western slopes of the eastern crest at 3000 m asl clearly resemble the situation of the blended UM/BM TM regime of (iii).

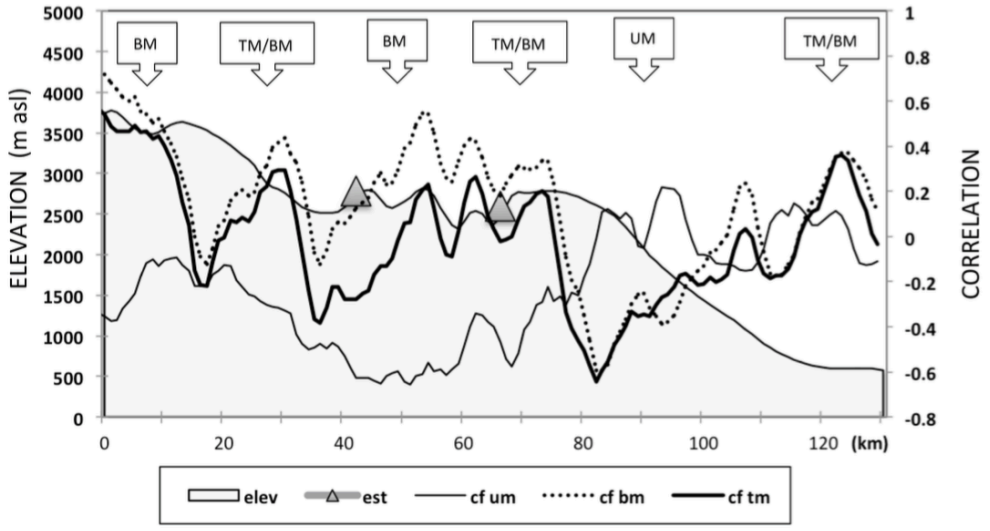

Figure 3-7: Profile of elevation and Pearson correlation of CF with UM, BM, TM normalized observational precipitation regimenes. (For the location of the profile line refer to figure 3.1).

3.5 Summary

In the Paute river basin three defined precipitation regimes can be differentiated: UM, BM, and TM. AOS might produce the UM regime in the Paute basin due to the air masses coming from the Amazon through the Paute Canyon, diminishing its influence toward higher elevations, shifting the seasonality of rainfall to TM regime. Therefore, the AOS influence on the eastern slopes of the cordillera is important, and a clear BM seasonality is possible just in the inter-valley locations most sheltered against the influence of the easterlies. An indirect influence from the Amazon is evident for TM stations on the eastern oriented slopes of the western cordillera as El Labrado, Chanin, and, to a lesser extend, for Biblian (Fig. 3.1). Also a direct but weaker influence is detectable for the stations Sigsig and Cumbe due to the passage of clouds between Mount Bellavista and El Calvario, although there is a high inter-annual variability of the June-July peak (Fig. 3.1).

Similar climatological conditions, as those occurring the Paute basin, are expected along the Andes cordillera in tropical latitudes. For instance, in Bendix & Lauer, (1992) UM regime was found to be located in elevations greater than 1000 m asl on the eastern slopes along the eastern cordillera, as stations Papallacta(3160 m asl), Baños (1843 m

asl) and Sucua (910 m asl). Confirming these results UM stations in the present study were found above 1000 m asl in stations Palmas (2400m), Sevilla de Oro (2360m), Peñas Coloradas (2321m) and Mazar (2450m). This fact confirms that UM regime along the eastern slopes of the cordillera might be due to the influence of AOS, and further, is evident that the presence of UM regime in the lower part of the Paute basin might be more related to the local influence of AOS (Bendix & Bendix, 2006). With respect to the transitional regime between UM and BM, TM, in Bendix & Lauer, (1992) was found toward the east in lower elevations such as Puyo (960masl), Sangay (880 m asl), Tena (665 m asl) concluding that TM regime is confined between 700 and 1000 m asl in basins with outlet toward the eastern cordillera. However, in the present study TM was found toward the west in higher elevations, as El Labrado (3335 m asl), Chanin (3270 m asl). In consequence, it seems plausible that the TM regime is present above and below the rain and clouds band produced by the AOS. Further studies are necessary on the processes and influence for cloud formation and rainfall on AOS along the eastern slopes of the eastern cordillera in Ecuador, even more importantly knowing that rainfall along this region could influence strategic hydro-electrical projects for the Ecuadorian economy.

Based on these findings, Fig. 3.8 describes a conceptual model of rainfall seasonality in inter-Andean basins like the Paute basin. The basin gets rainfall all over the year mainly from high convective clouds. On the eastern slopes of the eastern cordillera, a zone of advective cloud immersion exists particularly in JJA where especially moist but shallow cap clouds lead to the UM rainfall maximum. JJA rainfall at windward slopes seems therefore to be due to an advective barrage effect. The BM rainfall is of typical convective character during the equinoxes. The increase of the TM rainfall regime shows that the clear convective BM regime is blended with cloud advection where the latter also leads to some additional rainfall in JJA, mostly not exceeding the more convective rains in the BM seasons.

The high spatio-temporal variability in the Paute river basin, which is summarized as the conceptual model presented in Fig. 3.8, shows that although the ITCZ plays an important roll in enhancing convection throughout the year, the strengthening of the Walker Circulation producing subsidence during boreal summer, account for the dry season of the inter-Andean regions. Also, of major importance is the influence during boreal summer of the easterlies bringing moist air from the Amazon, which enhances the precipitation amounts on the eastward oriented slopes. The enhancement of precipitation is due to low advective shallow cap clouds along AOS. The inter-annual precipitation variability due to climatic influences as ENSO is weak in the Paute basin (Mora & Willems, 2012), due to the fact that the western cordillera, higher than the eastern cordillera around this latitude, limits the influence of the Pacific Ocean sea surface temperature, as is the case for the coastal plains of the country. These facts highlight the importance of considering the interplay between the climatic factors and the orography for determining rainfall variability in regions of complex topography.

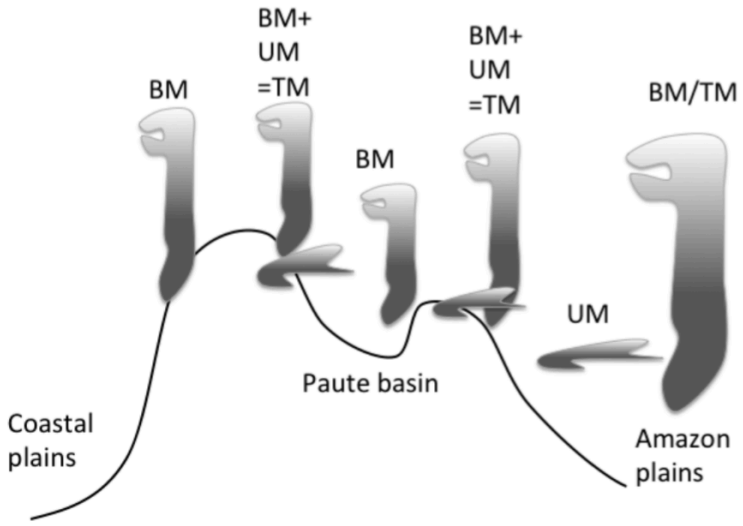

Figure 3-8: Conceptual model of seasonal rain formation for the Rio Paute catchment area.

3.6 Conclusions

The main aim of the present study was to understand the spatio-temporal dynamics of precipitation and clouds, and the potential cross-scale generation processes of rainfall in the Paute basin, located in the Andes of Ecuador. Precipitation models using satellite cloud products and GIS data, reveal the spatial extension of three regimes: A tri-modal (TM) mainly present across the basin, a bi-modal (BM), typical for sheltered valleys, and a uni-modal (UM) at windward slopes of the eastern cordillera. The spatio-temporal analysis shows that the ITCZ plays an important roll in enhancing convection throughout the year. However, during boreal summer, the strengthening of the Walker Circulation produce subsidence, accounting for the dry season of the inter-Andean regions. Of major importance is the influence during boreal summer of the easterlies bringing moist air from the Amazon, which enhances the precipitation amount on the eastward oriented slopes. Therefore, low advective shallow cap clouds mainly cause precipitation in uni-modal regions. Due to these facts, the three-modal seasonality is the main regime for this region in the Andes, where the western cordillera is higher than the eastern cordillera, while bi-modal only occurred on sheltered valleys with precipitation mainly of convective nature. Further, in altitudes from 1000 to 3000 m asl on the eastern flanks of the eastern cordillera, uni-modal features a maximum in June-July. The precipitation is mainly of advective nature related to the rainfall and clouds band, Andean Ocurring System. Therefore, three-modal is suggested to be a mixture between UM and BM, characterized by both, convective and advective influences.

The use of remote sensing showed to be a feasible tool to study climatology for case studies in highly complex terrain. Moreover, this work adds to a thin literature on convective and advective variability in the tropical Andes. Although models cannot be a substitute for observations, the use of regional climate models is also necessary to understand the underlying mechanisms occurring on such a complex terrain. However, it demands an exhaustive sensitivity analysis of the parameterizations in order to be able to represent the precipitation and cloud dynamics on this region. Further investigations will be oriented on this direction in future studies.

Appendix: List of Acronyms

Acronym	Meaning
UM	Uni-modal regime of rainfall
BM	Bi-modal regime of rainfall
TM	Three-modal regime of rainfall
NPR	Normalized precipitation regime
CFM	Cloud frequency based model of rainfall
MLRM	Multiple linear regression model of rainfall
CF	Cloud frequency
LWP	Cloud liquid water path
ZMIT	Cloud top height
ENSO	El Niño Southern Oscillation
ITCZ	Inter-tropical convergence zone
AOS	Andean occurring system
MAM	March-April-May
JJA	June-July-August

Acknowledgments

LC was funded by a grant provided by SENESCYT (Secretaría Nacional de Educación Superior, Tecnología e Innovación). Complementary funding was provided by MICMOR (Helmholtz Research School, Mechanisms and Interactions of Climate Change in Mountain Regions). We acknowledge the institutions that provided data: INAMHI (Instituto Nacional de Meteorología e Hidrología), and ETAPA (Empresa Municipal de Telecomunicaciones, Agua Potable y Saneamiento). Thanks to IERSE (Instituto de Estudios de Régimen Seccional del Ecuador) for information of the Paute basin. Special thanks to Dr. Patrick Laux for helpful comments on the manuscript. German Research Foundation (DFG) PAK825: BE1780/38-1, TR1201/1-1.

References

Basalirwa, C. (1995). Delineation of Uganda into climatological rainfall zones using the method of principal component analysis. International Journal of Climatology, 15(10), 1161–1177. doi:10.1002/joc.3370151008

Basalirwa, C. P. K., Odiyo, J. O., Mngodo, R. J., & Mpeta, E. J. (1999). The climatological regions of Tanzania based on the rainfall characteristics. … Journal of Climatology, 19(1), 69–80. doi:10.1002/(SICI)1097-0088(199901)19:1<69::AID-JOC343>3.0.CO;2-M

Bendix, J., & Lauer, W. (1992). Die Niederschlagsjahreszeiten in Ecuador und ihreklimadynamische Interpretation. Erdkunde, 46, 118–134.

Bendix, J., Rollenbeck, R., & Palacios, W. E. (2004). Cloud detection in the Tropics--a suitable tool for climate-ecological studies in the high mountains of Ecuador. International Journal of Remote Sensing, 25(21), 4521–4540. doi:10.1080/01431160410001709967

Bendix, A., & Bendix, J. (2006a). Heavy rainfall episodes in Ecuador during El Ni no associated regional atmospheric circulation and SST patterns. Advances in Geosciences, 43–49.

Bendix, J., Rollenbeck, R., Gottlicher, D., & Cermak, J. (2006b). Cloud occurrence and cloud properties in Ecuador. Climate Research, 30, 133–147. Retrieved from http://www.int-res.com/abstracts/cr/v30/n2/p133-147/

Bendix, J., Trachte, K., Cermak, J., Rollenbeck, R., & Nauß, T. (2009). Formation of Convective Clouds at the Foothills of the Tropical Eastern Andes (South Ecuador). Journal of Applied Meteorology and Climatology, 48(8), 1682–1695. doi:10.1175/2009JAMC2078.1

Bendix, J., Trache, K., Palacios, E., Rollenbeck, R., Goettlicher, D., Nauss, T., & Bendix, A. (2011). El Niño meets La Niña – anomalous rainfall patterns in the "traditional" El Niño region of southern Ecuador. Erdkunde, 65(2), 151–167. doi:10.3112/erdkunde.2011.02.04

Buytaert, W., Celleri, R., Willems, P., Bièvre, B. De, & Wyseure, G. (2006a). Spatial and temporal rainfall variability in mountainous areas: A case study from the south Ecuadorian Andes. Journal of Hydrology, 329(3-4), 413–421. doi:10.1016/j.jhydrol.2006.02.031

Buytaert, W., Deckers, & J., Wyseure, G. (2006b). Description and classification of nonallophanic Andosols in south Ecuadorian alpine grasslands (páramo). Geomorphology 73, 207–221.

Buytaert, W., Célleri, R., & Timbe, L. (2009). Predicting climate change impacts on water resources in the tropical Andes: Effects of GCM uncertainty. Geophysical Research Letters, 36(7), n/a–n/a. doi:10.1029/2008GL037048

Buytaert, W., Vuille, M., Dewulf, a., Urrutia, R., Karmalkar, a., & Célleri, R. (2010). Uncertainties in climate change projections and regional downscaling in the tropical Andes: implications for water resources management. Hydrology and Earth System Sciences, 14(7), 1247–1258. doi:10.5194/hess-14-1247-2010

Buytaert, W., Cuesta-Camacho, F., & Tobon, C. (2011). Potential impacts of climate change on the environmental services of humid tropical alpine regions. Glob. Ecol. Biogeogr. 20,19–33.

Buytaert, W., & De Bievre, B. (2012).Water for cities: the impact of climate change and demographic growth in the tropical Andes. Water Resour. Res. 48.

Campozano, L., Sánchez, E., Aviles, A., & Samaniego, E. (2014). Evaluation of infilling methods for time series of daily precipitation and temperature: The case of the Ecuadorian Andes. MASKANA, 5(1), 99–115. Retrieved from http://dspace.ucuenca.edu.ec:8080/handle/123456789/5586

Celleri, R., Willems, P., Buytaert, W., & Feyen, J. (2007). Space–time rainfall variability in the Paute basin, Ecuadorian Andes. Hydrological Processes, 21(August), 3316–3327. doi:10.1002/hyp

Coltorti, M., & Ollier, C. D. (2000). Geomorphic and tectonic evolution of the Ecuadorian Andes. Geomorphology, 32(1-2), 1–19. doi:10.1016/S0169-555X(99)00036-7

Córdova, M., Carrillo-Rojas, G., Crespo, P., Wilcox, B., & Célleri. R. (2015). Evaluation of the Penman-Monteith (FAO 56 PM) Method for Calculating Reference Evapotranspiration Using Limited Data: Application to the Wet Páramo of Southern Ecuador. Mountain Research and Development 35, 230–239.

De Bièvre, B., Alvarado, A., Timbe, L., Célleri, R., & Feyen, J. (2003). Night irrigation reduction for water saving in medium-sized systems. Journal of Irrigation and Drainage Engineering – American Society of Civil Engineers 129(2): 108-116.

Kalnay, E. (1996). The NCEP/NCAR 40-year reanalysis project. Bulletin of the American Meteorological Society, 77, 437–471. Retrieved from http://journals.ametsoc.org/doi/abs/10.1175/1520-0477(1996)077%3C0437:TNYRP%3E2.0.CO;2

Laraque, A., Ronchail, J., Cochonneau, G., Pombosa, R., & Guyot, J. L. (2007). Heterogeneous Distribution of Rainfall and Discharge Regimes in the Ecuadorian Amazon Basin. Journal of Hydrometeorology, 8(6), 1364–1381. doi:10.1175/2007JHM784.1

Lauer, W., Rafiqpoor, M., & Bendix, J. (2003). VergleichendeGeokologie der Hochgebirge der nrdlichen (Mexiko) und sdlichen (Bolivien) Randtropensowie der innerenTropen (Ecuador), Abh. der Math.-Nat. Klasse, Akad. d. Wiss. u. d. Lit. Mainz

Mejia, R., Ontaneda, G., Molinaro, D., & Rossel, F. (1996). Homogenizacion y regionalizacion de la pluviometria en la cuenca del rio Paute. Serie INSEQ. República Del Ecuador, Ministerio de Energía Y Minas, INAMHI, ORSTOM:

Quito, Ecuador, 3. Retrieved from http://www.documentation.ird.fr/hor/fdi:010006846

Mora, D. E., & Willems, P. (2011). Decadal oscillations in rainfall and air temperature in the Paute River Basin—Southern Andes of Ecuador. Theoretical and Applied Climatology, 108(1-2), 267–282. doi:10.1007/s00704-011-0527-4

Mora, D. E., Campozano, L., Cisneros, F., Wyseure, G., & Willems, P. (2014). Climate changes of hydrometeorological and hydrological extremes in the Paute basin, Ecuadorean Andes. Hydrology and Earth System Sciences, 18(2), 631–648. doi:10.5194/hess-18-631-2014

Mosquera, G., Lazo, P., Célleri, R., Wilcox, B., & Crespo, P. (2015). Runoff from tropical alpine grasslands increases with areal extent of wetlands. Catena 125: 120–128.

Ochoa, a., Pineda, L., Willems, P., & Crespo, P. (2014). Evaluation of TRMM 3B42 (TMPA) precipitation estimates and WRF retrospective precipitation simulation over the Pacific-Andean basin into Ecuador and Peru. Hydrology and Earth System Sciences Discussions, 11(1), 411–449. doi:10.5194/hessd-11-411-2014

Ochoa, A., Campozano, L., Sánchez, E., Gualán, R., & Samaniego, E. (2015). Evaluation of downscaled estimates of monthly temperature and precipitation for a Southern Ecuador case study. International Journal of Climatology, 36, 1244–1255. doi:10.1002/joc.4418

Padrón, R., Wilcox, B., Crespo, P., & Célleri, R. (2015). Rainfall in the Andean Páramo—New Insights from High-Resolution Monitoring in Southern Ecuador. Journal of Hydrometeorology 03/15. http://journals.ametsoc.org/doi/abs/10.1175/JHM-D-14-0135.1

Pourrut, P., Gómez, G., (1998). El Ecuador al cruce de varias influencias climáticas. Una situación estratégica para el estudio del fenómeno El Niño. Bulletin de l'Institut Français d'Études Andines 27, 449-457.

Poveda, G., Jaramillo, A., Gil, M., Quinceno, N., & Mantilla, R. (2001). Seasonality in ENSO-related precipitation, river discharges, soil moisture, and vegetation index in Colombia. Water Resources Research, 37(8), 2169–2178. Retrieved from http://www.sidalc.net/cgi-bin/wxis.exe/?IsisScript=CAFE.xis&method=post&formato=2&cantidad=1&expresion=mfn=008531

Rollenbeck, R., & Bendix, J. (2011). Rainfall distribution in the Andes of southern Ecuador derived from blending weather radar data and meteorological field observations. Atmospheric Research, 99(2), 277–289. doi:10.1016/j.atmosres.2010.10.018

Ronchail, J., Cochonneau, G., Molinier, M., Guyot, J.-L., De Miranda Chaves, A. G., Guimares, V., & de Oliveira, E. (2002). Interannual rainfall variability in the Amazon basin and sea-surface temperatures in the equatorial Pacific and the tropical Atlantic Oceans. International Journal of Climatology, 22(13), 1663–1686. doi:10.1002/joc.815

Thies, B., Nauss, T., & Bendix, J. (2008). Discriminating raining from non-raining cloud areas at mid-latitudes using meteosat second generation seviri night-time data, Meteorological Applications, 15 (2), 219–230, 2008.

Trachte, K., & Bendix, J. (2012). Katabatic flows and their relation to the formation of convective clouds-idealized case studies. Journal of Applied Meteorology and Climatology, 51(8), 1531–1546. doi:10.1175/JAMC-D-11-0184.1

Viviroli, D., Dürr, H., Messerli, B., Meybeck, M., and Weingartner R., (2007), Mountains of the world, water towers for humanity: Typology, mapping, and global significance, Water Resour. Res., 43, W07447, doi:10.1029/2006WR005653.

Wagemann, J., Thies, B., Rollenbeck, R., Peters, T., & Bendix, J. (2015). Regionalization of wind-speed data to analyse tree-line wind conditions in the eastern Andes of southern Ecuador. Erdkunde, 69(1), 3–19. doi:10.3112/erdkunde.2015.01.01

Wang, B. (1994). Climatic regimes of tropical convection and rainfall. Journal of Climate. Retrieved from http://journals.ametsoc.org/doi/abs/10.1175/1520-0442(1994)007%3C1109%3ACROTCA%3E2.0.CO%3B2

Wang, X. (2008a). Accounting for autocorrelation in detecting mean shifts in climate data series using the penalized maximal t or F test. Journal of Applied Meteorology and Climatology, 47(9), 2423–2444. doi:10.1175/2008JAMC1741.1

Wang, X. L. (2008b). Penalized Maximal F Test for Detecting Undocumented Mean Shift without Trend Change. Journal of Atmospheric and Oceanic Technology, 25(3), 368–384. doi:10.1175/2007JTECHA982.1

4 Comparison of Statistical Downscaling Methods for Monthly Total Precipitation: Case Study for the Paute River Basin in Southern Ecuador

This chapter is published in Advances in Meteorology, 2016, 1–13
Received: 27 October 2015 / Accepted: 27 December 2015

Comparison of statistical downscaling methods for monthly total precipitation: Case study for the Paute River basin in southern Ecuador

L. Campozano[1,2,3], D. Tenelanda[1], E. Sanchez[1,2], E. Samaniego[1,2] , J. Feyen[1]

[1] Departamento de Recursos Hídricos y Ciencias Ambientales, Universidad de Cuenca, Cuenca, Ecuador

[2] Facultad de Ingeniería, Universidad de Cuenca, Av. 12 de Abril s/n, Cuenca, Ecuador

[3] Laboratory for Climatology and Remote Sensing (LCRS), Faculty of Geography, University of Marburg, Deutschhausstr. 10, D-35032 Marburg, Germany

Corresponding author: lenin.campozano@ucuenca.edu.ec

Abstract Downscaling improves considerably the results of General Circulation Models (GCMs). However, little information is available on the performance of downscaling methods in the Andean mountain region. The paper presents the downscaling of monthly precipitation estimates of the NCEP/NCAR reanalysis 1 applying the statistical downscaling model (SDSM), artificial neural networks (ANN), and the least square support vector machines (LS-SVM) approach. Downscaled monthly precipitation estimates after bias and variance correction were compared to the median and variance of the 30-year observations of 5 climate stations in the Paute River basin in southern Ecuador, one of Ecuador's main river basins. A preliminary comparison revealed that both artificial intelligence methods, ANN and LS-SVM, performed equally. Results disclosed that ANN and LS-SVM methods depict, in general, better skills in comparison to SDSM. However, in some months SDSM estimates matched the median and variance of the observed monthly precipitation depths better. Since synoptic variables not always present local conditions, particularly in the period going from September to December, it is recommended for future studies to refine estimates of downscaling, for example by combining dynamic and statistical methods, or to select sets of synoptic predictors for specific months or seasons.

Keywords: statistical downscaling, artificial neural network, least squares support vector machine, SDSM, Andean mountain range.

4.1 Introduction

General Circulation Models (GCMs) are widely used to predict the impact of climate change on, for instance the regional precipitation trend. The resolution of these models, typically around 2°x2°, is unsuitable for climate change impact estimations at basin scale (Buytaert et al., 2010; Mora et al., 2014). Additionally, these models do not capture well the sub-grid processes, which can be very complex in mountain regions, and fail to account properly for the orographic features of those regions. Therefore, to obtain projections of the impact of climate change at basin scale, particularly in a mountain region, downscaling is a must. In general, the downscaling methods can be subdivided into two large groups: dynamical downscaling (DD) and statistical downscaling (SD) methods. On the one hand, the DD methods integrate a regional climate model (RCM) in the GCM, which enables capturing the atmospheric phenomena at a much higher resolution, in the order of tenths of kilometers. The SD techniques, on the other hand, are based on the determination of statistical relations between large-scale synoptic predictors and local observations from ground stations, which are considered to be stationary; an assumption that might not be true for future climate projections. The computational cost of these methods is low, they are relatively easy to implement, and present generally a higher accuracy than dynamical models. Particularly when the aim is not to understand the change in weather processes provoked by climate change, the generation of future projections at basin scale using SD methods might be convenient.

Several SD techniques exist and among them the **S**tatistical **D**own**S**caling **M**odel (SDSM) is probably the most widely used (Wilby et al., 2002). The SDSM approach facilitates the rapid development of multiple, low cost, single-site scenarios of daily surface weather variables, and is considered as a stochastic weather generator on a daily scale. The limited use of this technique in the Andean mountain region is perhaps the consequence of its complex topography, location in the tropical zone, and the influence of the warm and cold ENSO phases, El Niño y La Niña, respectively. All these influences add complexity to the atmospheric processes, making more difficult the representation by downscaling techniques. Artificial Neural Networks (ANN) are another SD technique commonly used, however to a limited extent in the Andes region. As stated by Coulibaly et al. (2005), the success of this technique is primarily due to its ability to map highly non-linear relations between inputs and outputs of the model. Ochoa et al. 2015 applied ANN for downscaling monthly precipitation and temperature in the Paute basin in the Andes of Ecuador. The application of ANN based SD was conducted in order to evaluate the performance on seasonality representation against DD using a regional climate model, Weather Research and Forecasting model, WRF (Skamarock et al., 2008). With respect to rainfall representation, they found that although both downscaling approaches represent qualitatively well seasonality in this highly complex terrain, ANN estimates of rainfall were more accurate than WRF estimates. This fact highlights the applicability of ANN when the understanding of the processes involved is not required. Another technique with recent application for the downscaling of GCMs is, support vector machines, SVM (Vapnik, 1995). In particular the least-squared support vector machines, LS-SVM (Suykens, 2002), downscale GCM output even better, mainly due to the reduction of the optimization problem to the resolution of a linear system reducing considerably the computational requirements. Despite SD methods presenting greater accuracy than DD methods, from a statistical point of view they possess two handicaps: bias and low variance. Normally, the quantile

mapping technique (QM) (Gudmundsson, 2012), is applied to improve the representation of the distribution of derived applications.

This paper presents a comparative evaluation of downscaled GCM estimates of monthly precipitation at the scale of a large river basin situated in the Andean mountain region in southern Ecuador, applying SDSM and two artificial intelligence (AI) techniques: artificial neural networks (ANN) and the support vector machines (SVM) approach. The downscaled results were corrected for bias and variance inflation applying the QM technique prior to the comparative analysis. For the evaluation, historic data was used.

4.2 Study area and data

The Paute River basin, tributary of the Amazon basin and 6148km^2 in size, was selected for the comparative evaluation of the downscaling methods, a basin located between the eastern and western cordillera of the Andes in Ecuador. The basin is characterized by a high spatial and temporal variation in precipitation that broadly can be classified into three rainfall regimes; respectively sub-regions with a uni-, bi- and three-modal precipitation pattern (Campozano, et al., 2016; Célleri et al., 2007). Data of 5 rainfall stations (see Table 4.1) were used of whom the geographical distribution is given in Figure 4.1. The measured monthly rainfall for the 30-year period 01-1980 to 12-2009 was used to quantify the differences in the performance of the selected downscaling methods. The dataset was split in a first set for the calibration of the methods, encompassing 75% of the total dataset, and the remaining 25% was used for the validation. The results presented herein belong all to the validation set. Quality control of the data was performed using double mass curves on the time series with gaps not exceeding 20% of the observations. The infilling of the data was accomplished using multiple linear regression with stations with higher Pearson correlation (Campozano et al., 2014).

NCEP/NCAR reanalysis 1 data (Kalnay et al., 1996) with 2.5ºx2.5º resolution was used as input. The selected synoptic predictors for the SDSM and AI models are presented in Table 4.2.

Table 4-1: Stations used for the present study.

Code	Station	Regime	Latitude (º)	Longitude (º)	Elevation (m asl)	Annual precipitation (mm)
M141	El Labrado	TM	-2.732	-79.073	3335	1286
M139	Gualaceo	BM	-2.882	-78.776	2230	820
M138	Paute	TM	-2.800	-78.763	2194	750
M045	Palmas	UM	-2.716	-78.630	2400	1341
M137	Biblián	BM	-2.709	-78.892	2640	1001

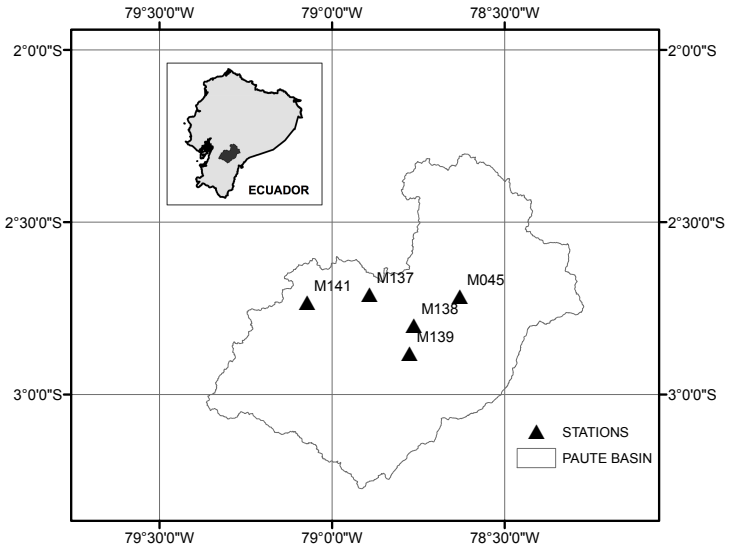

Figure 4-1: The study area Paute basin in the Andes of Ecuador.

4.3 Methods

The methodology of the present study encompasses the following steps: (i) selection of the predictors, (ii) calibration and validation of the SDSM and AI models, (iii) SDSM and AI ensemble generation, (iv) bias correction by quantile mapping, and (v) evaluation of results. SDSM can be conceived as a weather generator model, while ANN and LS-SVM are both transfer functions in statistical downscaling models. Given the analogy between ANN and LS-SVM models, the results of both formed one ensemble, which were compared to the SDSM ensemble. Notwithstanding it is well known (Pervez & Henebry, 2014) that a selection of predictors for specific months or seasons might be a good option to improve the accuracy in climate projections, in the present study only one set of predictors for the whole year was considered given that the main interest was the comparison of downscaling methods rather than the analysis of climate projections. The same predictors were used for the AI ensemble of ANN and LS-SVM models, and one set of predictors in each station for the SDSM model. A more detailed description of the tested downscaling models is given in the following paragraphs.

4.3.1 Downscaling using SDSM

SDSM is a hybrid between a stochastic weather generator and a multilinear regression method (Pervez & Henebry, 2014), forcing synoptic-scale weather variables to local meteorological variables using statistical relationships. In order to be better in agreement with the variance of the observed time series, stochastic techniques are used to artificially inflate the variance of the downscaled weather time series. The reader is referred to Wilby et al. (2002) for a detailed description of the SDSM technique, an approach widely used for the downscaling of large-scale meteorological, hydrological and environmental variables.

Partial correlation at a significance level of p=0.05 was used to select the predictors that capture best for each of the climate stations the effect of global climate. Precipitation data from the reanalysis products was evaluated as the predictor that considerably helped improving the downscaling. For the climate stations Biblián, Paute and Gualaceo, 5 predictors were identified, of whom 4 are similar: precipitation, pressure, relative humidity and the temperature 2m above the surface. For the Palmas station, the only station with a uni-modal regime, the best results were obtained using three predictors, namely precipitation, potential temperature at the 700 hPa level, and the geopotential height at the 850 hPa level. Table 4.2 provides the list of the selected predictors as a function of the downscaling technique and station.

Using the selected predictors, daily precipitation was downscaled. Given the low match with the observed time series of daily data, monthly time series were generated. At the monthly scale the precipitation time series in the study basin are continuous; months with zero precipitation are not present even during the dry months. Regarding the SDSM model, 20 versions were applied (Mahmood & Babel, 2014). Then, the median of the simulated results was calculated as the representative value for the ensemble of the SDSM model variants.

Table 4-2: Synoptic predictors.

#	Synoptic predictors	ANN/LS-SVM	SDSM				
		(all stations)	El Labrado	Gualaceo	Paute	Palmas	Biblián
1	Precipitation	*	*	*	*	*	*
2	Pressure (surface)	*		*	*		*
3	Relative humidity (surface)	*	*	*	*		*
4	Specific humidity 700 hPa	*					
5	Sea level pressure	*					
6	Temperature 2m	*	*	*	*		*
7	Potential temperature 700 hPa	*	*		*	*	
8	Zonal wind (surface)	*					
9	Omega 500 hPa	*		*			*
10	Geopotential height 200 hPa	*	*				
11	Geopotential height 500 hPa	*					
12	Geopotential height 850 hPa	*				*	

4.3.2 Downscaling using ANN

An artificial neural network (ANN) is composed of several interconnected layers of computing elements, transferring inputs to outputs subjecting at each node the incoming signal to a transfer function. ANNs are characterized by their topology, and probably the most widely-known neural network is the multilayer perceptron (MLP). The later consists of multiple layers of adaptive weights with full connectivity between inputs and hidden units, and between hidden units and outputs. The MLP is a feedforward artificial neural network mapping sets of input data onto a set of appropriate outputs. The neurons with a nonlinear activation function in the neural layers are grouped. They can

mutually but independently process portions of data. The group defines the relationships of the neurons of a neural layer with adjacent layers. For the processing of data whose properties change over time either dynamic or pseudo-dynamic networks can be used. Dynamic models feed back to the network the outputs obtained of the network, while pseudo-dynamic networks consider lagged values of the variables as input.

The neural network toolbox of Matlab (Beale et al., 2011) was used, and optimization of the neural network was pursued using the Levenberg-Marquardt method, minimizing the mean square error. The performance of a total of four ANNs were tested, respectively a model considering either one or two intermediate neural layers, and a linear or sigmoidal transfer function in the neurons (Table 4.3). For the input layer all networks had 12 neurons (equal to the number of predictors; see Table 4.2) and for the network with one hidden layer 8 neurons were used, which was determined by trial and error. In a similar way for networks with two hidden layers respectively 9 and 5 neurons were used.

Table 4-3: Artificial intelligence models.

Model	Type	Transfer Function
1	Ann	Linear & 1 hidden layer
2		Sigmoidal & 1 hidden layer
3		Linear &2 hidden layers
4		Sigmoidal & 2 hidden layers
5	LS-SVM	Linear
6		Polynomial
7		Radial basis functions

4.3.3 Downscaling using LS-SVM

Support vector machines, SVM (Vapnik, 1995), solve nonlinear classifications and estimations of functions and densities using quadratic programming. A least squares support vector machine, LS-SVM (Suykens et al., 2002), is a reformulation of a SVM replacing the solution of the convex quadratic programming problem by the solution of a set of linear equations. As explained by Suykens et al. (2002) it is possible to adopt into LS-SVM the robustness, sparseness and weightings.

Due to the fact that LS-SVM has more recent application than ANN and SDSM techniques for the downscaling of GCMs, we present here a succinct description of LS-SVM theory. For a more in deep description of LS-SVM see Suykens et al. (2002).

Lets consider $x \in \mathbb{R}^n$ and $y \in \mathbb{R}$, the LS-SVM model, mapping the x into a feature space is:

$$y = w^T \varphi(x) + b$$

The optimization problem can be stated as:

$$min_{w,e}\Gamma(w,e) = \frac{1}{2}w^T w + \gamma\frac{1}{2}\sum_{i=1}^{N} e_i^2$$

Where e and γ is the error and the regularization parameter respectively. The minimization of the cost function $\Gamma(w,e)$, is subject to the constrains:

$$y_i = w^T\varphi(x_i) + b + e_i$$

The Lagrangian of the optimization is:

$$\mathcal{L}(w,b,e,\alpha) = \Gamma(w,e) - \sum_{i=1}^{N}\alpha_i(w^T\varphi(x_i) + b + e_i - y_i)$$

Where α_i are the Lagrangian multipliers.

After considering the conditions for optimality:

$$[\partial\mathcal{L}/\partial w, \partial\mathcal{L}/\partial b, \partial\mathcal{L}/\partial e_i, \partial\mathcal{L}/\partial\alpha_i]^T = [0,0,0,0]^T$$

We obtain the matrix equation:

$$\begin{bmatrix} 0 & \bar{1} \\ \bar{1} & \Omega - \gamma^{-1}I \end{bmatrix}\begin{bmatrix} b \\ \alpha \end{bmatrix} = \begin{bmatrix} 0 \\ y \end{bmatrix}$$

Where $\Omega_{ij} = \varphi(x_i)^T\varphi(x_j)$ is the Kernel function $K(x_i, x_j)$, and I the identity matrix.

Finally the LS-SVM model for function estimation is:

$$y(x) = \sum_{i=1}^{N}\alpha_i K(x_i, x) + b$$

A Bayesian framework with three levels of inference was developed for the optimization of parameters (Suykens et al., 2002). The LS-SVMlab tool (Brabanter et al., 2011) developed in Matlab applying three Kernel tuning options (linear, polynomial and RBF) was used within the ensemble of AI methods.

4.3.4 Bias correction using the Quantile Mapping approach

First the predictors were selected, followed by the application of the multiple compositions of the SDSM model and the 7 AI models, 4 ANNs and 3 LS-SVM models (Table 4.3). The output distributions of the ensemble of SDSM models and the 7 AI models were grouped into two distinct populations. Both this populations were corrected for bias and variance inflation applying the quantile mapping technique. The QM applied to SDSM population distributions is from now on called the SDSM_QM and QM applied to ENS-AI the AI_QM.

The quantile mapping technique for bias correction and variance inflation can be regarded as a statistical transformation of the original distribution into a reference

probability distribution. It aims to find the function that maps the distribution of the model variables into the distribution of the observed variables. Basically three types of approaches exist to find the mapping function; it is adjustment i) based on theoretical distributions, ii) based on parametric transformations, and iii) based on non-parametric transformations.

After evaluation of several transformations the power parametric transformation was applied because of its good results and the parsimony of the model (Gudmunsson et al., 2012). The power parametric transformation is defined as:

$$P_0^* = b(P_m - X_0)^a$$

where P_0^* and P_m are the corrected modeled and modeled variables, and a, b, x_0 are parameters to be determined. To find the parameters a, b, x_0, the tool R QMAP was used (Gudmunsson et al., 2015). For SDSM_QM and AI_QM the parameters obtained after QM adjustment are presented in Table 4.4.

4.3.5 Criteria for model evaluation

For the qualitative assessment of the used methods of downscaling the long-term monthly mean precipitation of both ensembles, the SDSM and AI, were compared with the long-term monthly mean observed precipitation, and for the quantitative evaluation statistical metrics of the distributions of the time series of observed and modeled values for the validation period were calculated. In addition to the statistical metrics, Box-Whisker plots presenting both ensembles versus the observations were drawn. This type of graphical representation was selected throughout the study because in addition to the median, the Box-Whisker plot depicts the extreme values, respectively the minimum and maximum (the caps at the end of each box), and the outliers which fall more than 1 times the interquartile range above the third or below the first quartile (the points in the graph).

As statistical metrics the following were used:

- Pearson correlation (R): to evaluate the linear correlation.
- Mean bias (MB): to evaluate the mean (the 50th percentile) difference between modeled and observed distributions.
- The root mean squared error (RMSE): to evaluate the error between modeled and observed time series.
- The interquartile relative fraction (IRF): to evaluate the modeled variability representation relative to the observed.

$$IRF = \frac{Q_3^m - Q_1^m}{Q_3^o - Q_1^o}$$

where: IRF = the interquartile relative fraction. A value of IRF>1 represents overestimation of the variability, IRF=1 is a perfect representation of the variability, and IRF<1 is an underestimation of the variability; Q_3^m and Q_3^o = the 75th modeled and observed percentile; Q_1^m and Q_1^o = the 25th modeled and observed percentile.

- The absolute cumulative bias (ACB) was used to evaluate the bias of the 25th, 50th and 75th percentiles; or

$$ACB = |Q_1^m - Q_1^o| + |Q_2^m - Q_2^o| + |Q_3^m - Q_3^o|$$

where: ACB = the absolute cumulative bias. A value of ACB=0 is a perfect representation of the three percentiles (respectively the 25th, 50th and 75th percentile) of modeled and observed distributions, while under- or overestimation indicates a divergence of ACB from zero to positive values.

4.4 Results and discussion

4.4.1 Evaluation of SDSM and AI ensembles

4.4.1.1 Relative performance of ANN and LS-SVM models

As mentioned before, ANN and LS-SVM models were grouped into one ensemble considering both models as transfer function based models. Although previous studies (Chen et al., 2010; Tripathi et al., 2006) demonstrated the relative superior performance of SVM based downscaling methods over other approaches including ANN based methods, we compared for the first time in the region, to the best of our knowledge, an ANN ensemble against a LS-SVM ensemble to evaluate their downscaling performance. The ensembles were not bias corrected in order to evaluate their actual performance. In Table 4.5 presents the values of R, RMSE, MB, IRF, and ACB comparing ANN and LS-SVM ensembles. In El Labrado and Paute station similar results of both ensembles are obtained. However, both ensembles for Gualaceo station under represent the variability. IRF is 0.55 and 0.40 for ANN and LS-SVM respectively. Therefore LS-SVM represents 15% less variability than ANN ensemble. The MB for ANN is -2.29 mm whereas for LS-SVM is -0.21 mm, which in monthly scale is very low. The ACB metric for ANN is 33.41 mm whereas for LS-SVM is 41.70 mm, meaning that although the MB is lower for LS-SVM the bias in the 25th and 75th percentiles is higher than for the ANN ensemble. In Palmas station R is 0.25 and 0.45 respectively for the ANN and LS-SVM ensembles. IRF values of 0.45 and 0.53 for ANN and LS-SVM are obtained, indicating a greater representation in variability by the latter approach. However, MB values of -1.85 and 7.87 mean than LS-SVM present more bias in the 50th percentile than ANN. For Biblián station, MB is -18.39 mm and -7.05 mm and ACB 52.34 mm and 35.49 mm for ANN and LS-SVM ensembles respectively, meaning a strong bias for the ANN ensemble with respect to LS-SVM ensemble.

Table 4-4: Quantile Mapping parameters for artificial intelligence and SDSM ensembles.

Model	Stations	Parameters		
		a	b	x_0
AI	BIBLIAN	0.03280	1.83727	0.87053
	LABRADO	0.00820	1.98426	-8.57836
	PALMAS	0.00334	2.21628	6.04480
	GUALACEO	0.31943	1.40124	16.92140
	PAUTE	0.02791	1.94766	0.03257
SDSM	BIBLIAN	0.00986	2.08840	3.21195
	LABRADO	0.39313	1.19070	-45.84738
	PALMAS	0.00056	2.46774	-13.06023
	GUALACEO	0.00077	2.62716	-1.14051
	PAUTE	0.04141	1.80403	3.91130

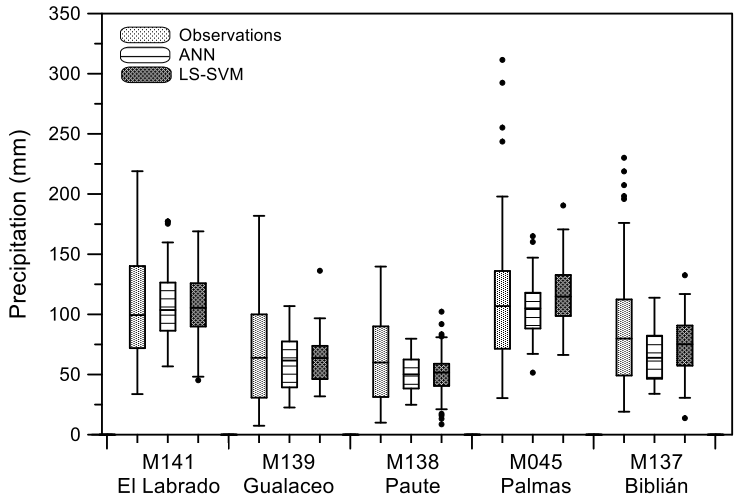

Figure 4-2: Box plots for ANN and LS-SVM ensembles evaluated in station El Labrado (M141), Gualaceo (M139), Paute (M138), Palmas (M045), and Biblián (M137).

For a qualitative evaluation of ANN and LS-SVM ensembles the Box-Whisker plots for the results during the validation period is presented in Figure 4.2. For El Labrado station both ensembles similarly represent the median, although the low variance is clearly showed, as measured by IRF in Table 4.5. For Gualaceo and Paute stations both ensembles represent less variance, with LS-SVM presenting lower values. The percentiles above 75th are strongly underestimated in both stations making evident the necessity of correction on the distribution of the ensembles. In Palmas station both ensembles under-represent the variance, and the median is rightly represented by ANN but overestimated by LS-SVM. Finally for Biblián station the variance is strongly under-estimated as well as the higher percentiles. The median is better represented by LS-SVM and under-estimated by ANN ensemble. Both methods were able to perform similarly well for the downscaling of monthly precipitation in the selected stations. In addition, comparison of the quantitative analysis based on the statistical metrics and the qualitative analysis based on Box-Whisker plots shed light on the relative performance of ANN and LS-SVM methods.

4.4.1.2 Comparison of SDSM and AI ensembles

Once the ANN and LS-SVM ensembles were evaluated, in a next step the derived SDSM and AI ensembles were compared after QM correction. Table 4.6 depicts for the 5 climate stations in the Paute River basin, of which data were used, the comparison between the SDSM and AI versus SDSM_QM and AI_QM. The evaluation between both sets is based on the statistical metrics R, RMSE, MB, ACB, and IRF. For El Labrado station SDSM_QM presents lower correlation than AI_QM with 0.38 and 0.58 values. Although SDSM_QM present a lower bias than AI_QM; the RMSE of AI_QM is a bit lower. For Gualaceo station R for AI_QM and SDSM_QM are 0.72 and 0.5. RMSE as in El Labrado station is lower for AI_QM than for SDSM_QM with 32.87 and 44.86 respectively. For Paute station also R is higher for AI_QM with 0.57 and 0.47 for SDSM_QM; although the ACB is higher for AI_QM with 15.59 and 7.77 for SDSM_QM. For Palmas there is a marked difference in R values with 0.44 for AI_QM and 0.14 for SDSM_QM, depicting for the former a lower RMSE than the latter. Also for the Biblián station is R for AI_QM higher than SDSM_QM with 0.67 and 0.45 and analogous to the Palmas station a lower RMSE of 39.87 for AI_QM compared to the RMSE for SDSM_QM, equal to 51.81.

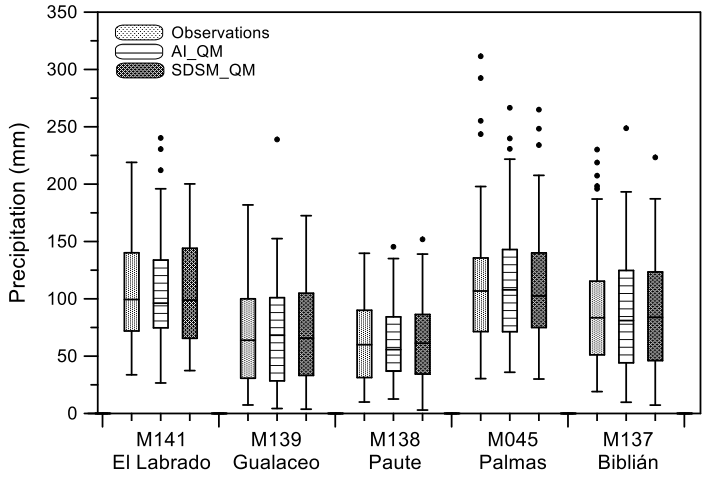

Figure 4-3: Monthly precipitation box plots for artificial intelligence and SDSM ensembles bias corrected. Results evaluated in station El Labrado (M141), Gualaceo (M139), Paute (M138), Palmas (M045), and Biblián (M137).

All other metrics in Table 4.6 present similar values. The stronger differences arise generally in the RMSE and R statistical metrics, which might be related to the fact that QM corrects only the characteristic of the distribution, as can be seen in Figure 4.3. This figure presents the monthly precipitation Box-Whisker plots for AI and SDSM ensembles bias corrected for the 5 climate stations. As can be observed the distributions are fairly alike. From the analysis for all stations AI_QM presented higher values of R than SDSM_QM. Similarly AI_QM presents better agreement with the observed data with the exception of the Paute station. This fact might point to a slightly better representation of the observed monthly precipitation distribution by AI_QM ensemble, for this specific region.

4.4.2 Evaluation of intra-annual precipitation seasonality representation

Whereas in previous section the entire distribution of downscaled estimates was evaluated, in the following the representation of seasonality is evaluated. Although the evaluation of seasonality representation might not help to quantify e.g. flooding events, however it is very important for issues related to water availability for hydroelectricity generation, drinking water availability, and agriculture. Further, the evaluation of seasonality representation is of special importance in the study region due to the low resolution of GCMs, unable to depict the precipitation regime due to meso-scale influences (Ochoa et al., 2015).

Table 4-5: Statistical metrics for ANN and LS-SVM ensembles.

Station	Metric	ANN_ENS	LSSVM_ENS
El Labrado	Pearson correlation	0.49	0.58
	IRF	0.59	0.53
	Mean-bias	4.20	6.16
	Cum_bias	31.63	37.79
	RMSE	40.73	37.63
Gualaceo	Pearson correlation	0.70	0.71
	IRF	0.55	0.40
	Mean-bias	-2.29	-0.21
	Cum_bias	33.41	41.70
	RMSE	34.82	35.33
Paute	Pearson correlation	0.55	0.54
	IRF	0.41	0.31
	Mean-bias	-9.90	-8.34
	Cum_bias	44.16	48.21
	RMSE	31.61	31.04
Palmas	Pearson correlation	0.25	0.45
	IRF	0.45	0.53
	Mean-bias	-1.85	7.87
	Cum_bias	36.99	37.81
	RMSE	52.44	47.51
Biblián	Pearson correlation	0.67	0.65
	IRF	0.57	0.54
	Mean-bias	-18.39	-7.05
	Cum_bias	52.34	35.49
	RMSE	44.75	40.97

4.4.2.1 The added value of quantile mapping

The QM correction parameters for the power parametric transformation applied to AI and SDSM ensembles are presented in Table 4.4. The comparison of the multiyear monthly mean (mymm) precipitation of the SDSM with the SDSM_QM ensemble is presented in Figure 4.4-a to e. As shown in Figure 4.4-a, SDSM applied to the El Labrado station fails to capture the observed seasonality. However, the performance, bias and variance improved considerably after applying QM. Seasonality applying SDSM to the Gualaceo (Figure 4.4-b) station is less correctly presented, and fails to capture the maximum in April and overestimates precipitation during the dry season in August. Application of QM only corrects the representation in August, but not in April. The ensemble of SDSM compositions represents well seasonality but underestimates significantly the November precipitation depth. Application of QM improves the representation of seasonality but does not improve the November estimate. The SDSM in Paute station represents seasonality well, but underestimates significantly the maximum in November. QM applied to SDSM in Paute improves the performance of seasonality, yet fails to improve the representation of the November precipitation (Figure 4.4-c) The SDSM approach calibrated to the observations of the Palmas station (Figure 4.4-d), a station with uni-modal regime (UM), depicts fairly correct seasonality notwithstanding the limited spatial extent of the UM regime and the poorly representation of the meso-scale influences in the synoptic predictors. Application of QM negatively affects the SDSM representation during the first 6 months of the year, but improves slightly the representation during the remaining period of the year. The seasonality of the Biblián station (Figure 4.4-e) is properly represented by the SDSM ensemble and so does the SDSM_QM. Only the November peak in precipitation is neither captured by SDSM nor SDSM-QM.

The comparison of mymm of the AI with the AI_QM ensembles is presented in Figure 4.4-f to j. The AI ensembles (ENS-AI) underestimates precipitation in April, overestimate in July and August and underestimate in November, although at some extend represents seasonality. QM improves the intra-annual variability, but still the November maximum is not correctly estimated. The ENS-AI in Gualaceo (Figure 4.4-g) station captures well both peaks in April and November, but underestimates precipitation in August. The estimation in August is considerably improved after correction of the bias and the inflation of the variance. In the Paute station (Figure 4.4-h) are both peaks, respectively in April and November, and the minimum in August well captured by the ENS-AI, while QM further improves the distribution of the median of the monthly precipitation. The ENS-AI represents poorly the distribution of the Palmas station (Figure 4.4-i, UM regime), even after QM application. For the Biblián station (Figure 4.4-j) the ENS-AI_QM captures the April peak one month earlier, but fails to correctly depict the magnitude of the November peak.

Table 4-6: Statistical metrics for artificial intelligence and SDSM ensembles.

Station	Metric	AI	SDSM	AI_QM	SDSM_QM
El Labrado	Pearson correlation	0.58	0.37	0.58	0.38
	IRF	0.49	1.00	0.87	1.14
	Mean-bias	4.37	-41.49	-3.24	-0.54
	Cum_bias	38.23	126.89	12.19	9.96
	RMSE	37.70	65.41	41.67	51.44
Gualaceo	Pearson correlation	0.74	0.53	0.72	0.50
	IRF	0.52	0.46	1.04	1.03
	Mean-bias	-1.01	10.28	4.33	1.85
	Cum_bias	34.02	47.50	7.35	9.01
	RMSE	33.92	38.26	32.87	44.86
Paute	Pearson correlation	0.59	0.47	0.57	0.47
	IRF	0.36	0.47	0.80	0.89
	Mean-bias	-10.46	1.14	-4.26	1.34
	Cum_bias	47.61	31.73	15.59	7.77
	RMSE	30.60	30.26	31.13	35.03
Palmas	Pearson correlation	0.44	0.16	0.44	0.14
	IRF	0.52	0.54	1.12	1.02
	Mean-bias	7.39	16.31	0.97	-3.66
	Cum_bias	38.14	56.93	8.77	12.28
	RMSE	47.45	56.09	55.73	66.62
Biblián	Pearson correlation	0.66	0.46	0.67	0.45
	IRF	0.61	0.56	1.29	1.25
	Mean-bias	-11.12	-2.87	-1.21	1.66
	Cum_bias	35.01	29.99	18.91	17.30
	RMSE	41.73	44.89	39.87	51.81

Results clearly reveal that the application of QM to the output of both modeling approaches, SDSM and ENS-AI, overall improves the representation of seasonality, as well as the representation of rainy and dry periods. However, both approaches underestimate the median value of the precipitation depth in November. This fact could indicate that the set of synoptic predictors do not include a variable that is related to an enhancement of precipitation in this period. Further studies are needed to determine the variables and related phenomena.

Table 4-7: Pearson correlations between observations and SDSM_QM and ENS-AI_QM models.

STATION	ENS-AI_QM	SDSM_QM
EL LABRADO	0.741	0.516
GUALACEO	0.946	0.672
PAUTE	0.730	0.629
PALMAS	0.788	0.593
BIBLIAN	0.691	0.532

4.4.2.2 Representation of monthly variability by downscaled results

To compare the representativeness of SDSM_QM and ENS-AI_QM, the correlation of the mymm time series with the observed values is shown in Table 4.7. For all stations ENS-AI_QM presents greater Pearson correlation coefficient than SDSM_QM. The multi-year median observed and estimated monthly precipitation depth, using respectively the SDSM_QM and ENS-AI_QM model ensembles, are presented in the Figure 4.5-a,c,e,g and i. For the graphical presentation the Box-Whisker plot type was selected, as to show in addition to the median the variation in estimates (see Figure 4.5-b,d,f,h and j).

For the El Labrado station (Figure 4.5-a,b) is the observed interquartile range higher for the period January to April, with lower values in August and September. It is worthwhile noticing that although ENS-AI_QM captures seasonality, the intra-annual variability is not captured. Even for some months SDSM_QM captures the variability better, as is the case for March. This fact suggests that an assessment for SD should be based on several models. The median and interquartile range is relatively well captured for the Gualaceo station (Figure 4.5-c,d), the variability of the months from January to September is similar for the SDSM-QM and ENS-AI_QM estimates. October and November variability is different for the two models, but the median is well represented. The variability and the median are better represented by ENS-AI_QM and slightly overestimated by SDSM_QM in the period June to August. Figure 4.5-e,f depicts the results for the Paute station, illustrating that both models relatively well represent the median and interquartile ranges in the period January to September, but fail to do so for the period October to December. This fact highlights the need to further explore the relation between the synoptic conditions and rainfall. Neither the SDSM_QM nor the ENS-AI model estimates correctly the median of the Palmas station (Figure 4.5-g,h), the only station with a uni-modal regime. Because both model approaches indistinctly overestimate or underestimate in some months it might be worthwhile examining more in detail the representation of an ensemble of both models. The interquartile range of each month is relatively well represented except in a distinct number of months, such as January, April, June, July, September and October. This could mean that in those months the influences of the meso-scale factors are not properly represented in the synoptic variables. An option for its remediation could be a methodology in which the influences of meso-scale factors are considered, e.g. dynamic downscaling, followed by the application of statistical downscaling to regional predictors. However, further studies are necessary to support the applicability of such an approach in mountain regions. For the Biblián station (Figure 4.5-i,j), the two approaches overestimate precipitation in the period January to March. ENS-AI_QM captures adequately the median from April to December, with exception of November, as was the case for the other stations. Overall, the ENS-AI_QM depicts fairly well the variability, except for October and November, whereas SDSM_QM underestimates the variability throughout the year.

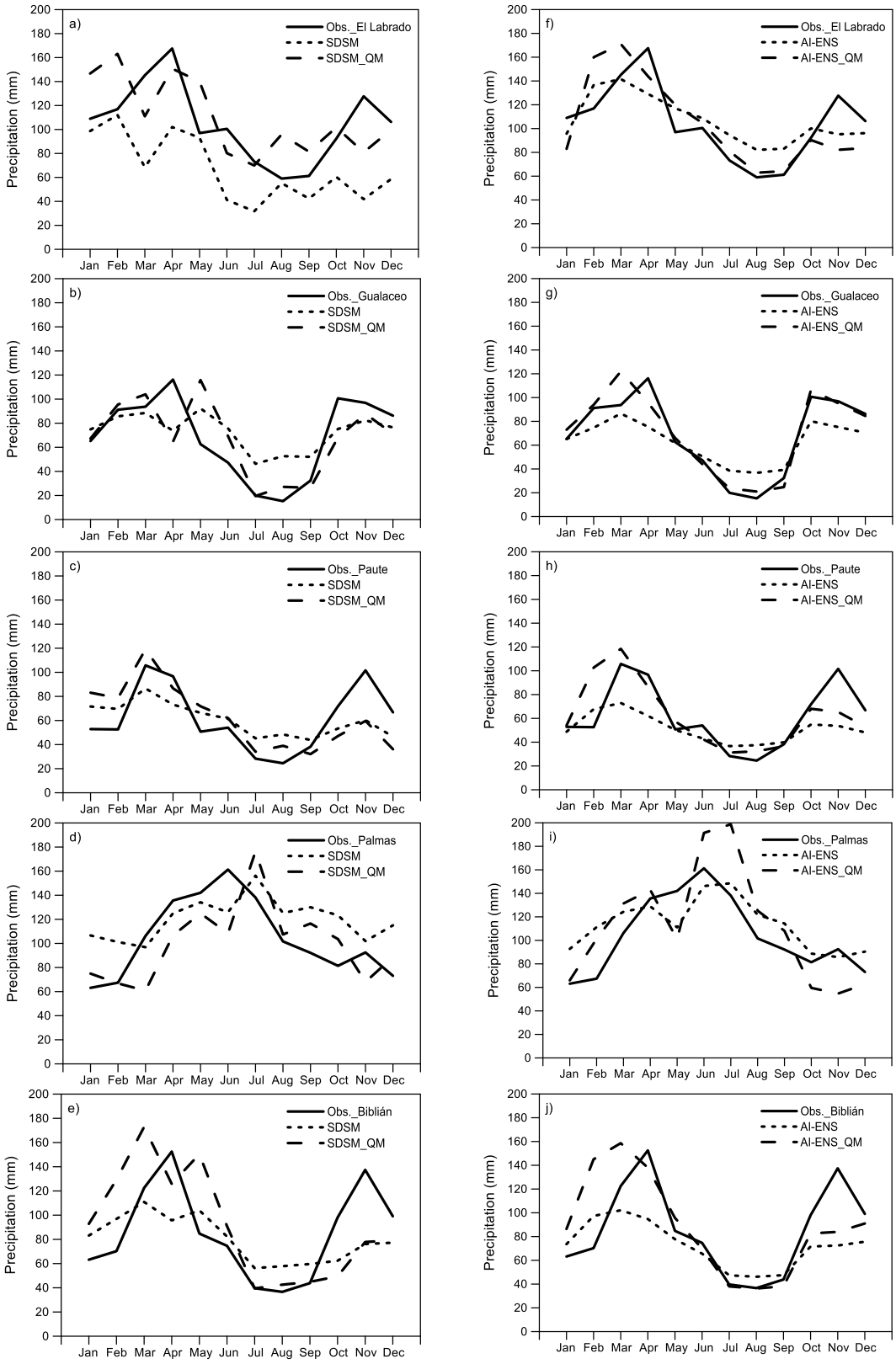

Figure 4-4: Multiyear monthly mean precipitation for SDSM ensemble and SDSM ensemble bias corrected (a-e), and multiyear monthly mean precipitation for AI-ENS and AI-ENS bias corrected (f-j).

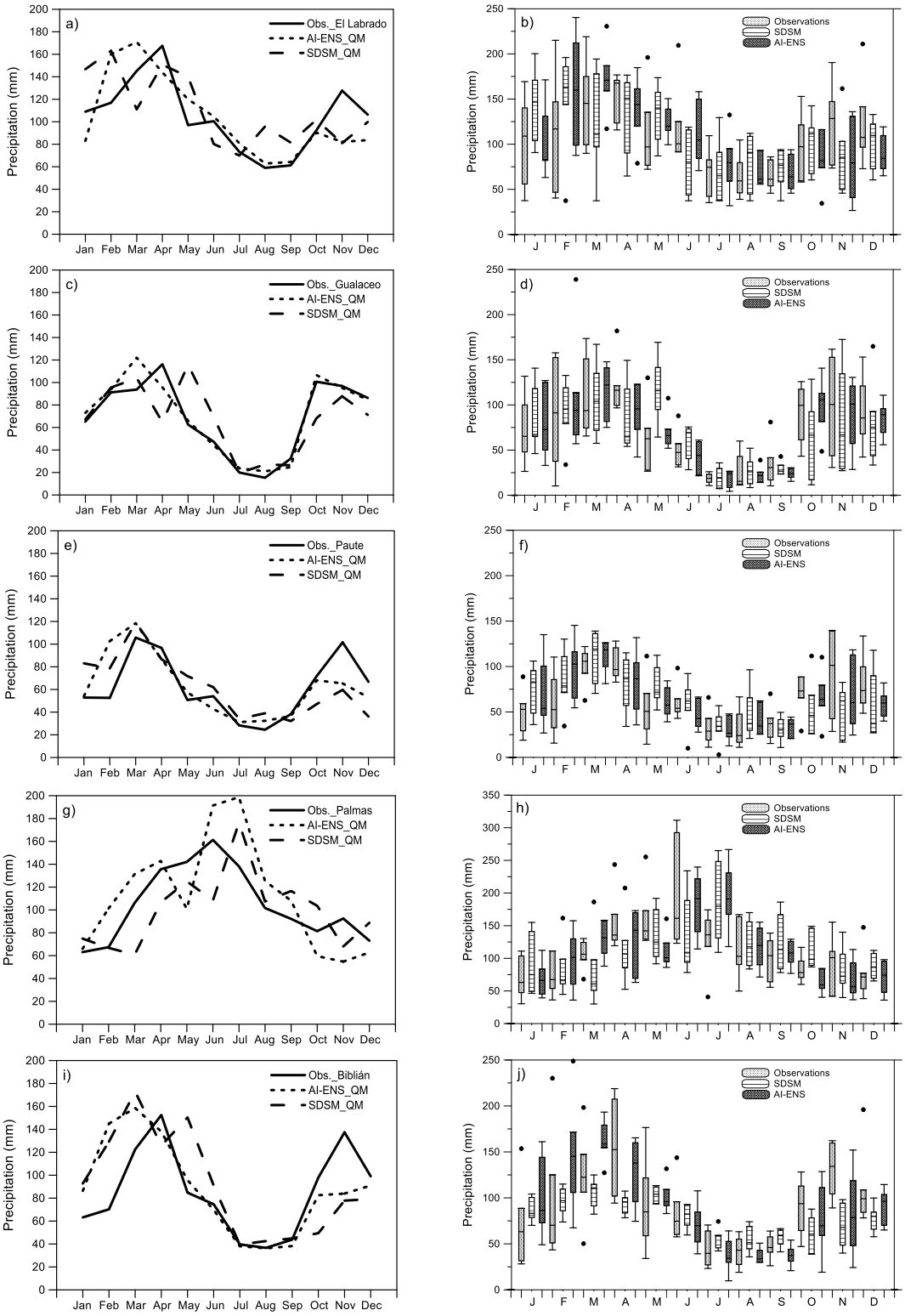

Figure 4-5: Comparison of SDSM and AI ensembles bias corrected (a, c, e, g, i), and Box-Whisker plots for SDSM and AI ensembles bias corrected, from January through December (b, d, f, h, j).

4.5 Conclusions

The evaluation of downscaling methods in mountain regions is of major importance due to the misrepresentation of climate by GCMs. The low resolution of GCMs limits the accurate prediction of the probable impacts of climate change at basin scale. In the present work, the applicability of monthly precipitation downscaling of global climate models by SDSM, and methods of artificial intelligence, as neural networks and support vector machines, was studied. Also a comparative analysis of the applied downscaling methods was conducted. Comparative analysis revealed that with respect to the downscaling of monthly precipitation neural networks and least square support vector machine models perform equally. Considering the statistical metrics, such as Pearson correlation, root mean square error, and percentiles biases, overall the AI methods showed better skills in relation to SDSM, although in some seasons and some months, the importance of considering both model approaches was necessary in order to derive robust conclusions. In general, although the representation of precipitation from January to August is adequate, especially in November both approaches failed to represent precipitation in some stations. Further analysis of the synoptic conditions for this period is therefore recommended and a methodology considering downscaling with specific predictors by month or season might be advisable. From the analysis on Palmas station, a station with important meso-scale influences, we could derive that further evaluation of a methodology of downscaling using dynamic and statistical methods in cascade, could help capture features that GCMs are not able to represent.

Acknowledgments

This work was funded by the Dirección de Investigación de la Universidad de Cuenca (DIUC) through the project "Análisis de los efectos del cambio climático en los caudales en las cuencas Andinas del Sur del Ecuador (Paute), debido a los cambios en los patrones de lluvia y temperatura", and by the Secretaria de Educación Superior, Ciencia, Tecnología e Innovación (SENESCYT) through a PhD grant for the first author. The authors would also like to thank INAMHI for providing the meteorological data.

References

Beale, M. H., Hagan, M. T., Demuth, H. B. (2014). Neural Network ToolboxTM User's Guide R 2014.

Buytaert, W., Vuille, M., Dewulf, a., Urrutia, R., Karmalkar, a., & Célleri, R. (2010). Uncertainties in climate change projections and regional downscaling in the tropical Andes: implications for water resources management. Hydrology and Earth System Sciences, 14(7), 1247–1258. doi:10.5194/hess-14-1247-2010

Campozano, L., Sánchez, E., Aviles, a, & Samaniego, E. (2014). Evaluation of infilling methods for time series of daily precipitation and temperature: The case of the Ecuadorian Andes. Maskana, 5(1), 99–115. Retrieved from http://dspace.ucuenca.edu.ec:8080/handle/123456789/5586

Campozano, L., Célleri, R., Trachte, K., Bendix, J., & Samaniego, E. (2016). Rainfall and Cloud Dynamics in the Andes : A Southern Ecuador Case Study. Advances in Meteorology, 2016, 15. doi:10.1155/2016/3192765

Celleri, R., Willems, P., Buytaert, W., & Feyen, J. (2007). Space–time rainfall variability in the Paute basin, Ecuadorian Andes. Hydrological Processes, 21(August), 3316–3327. doi:10.1002/hyp

Chen, S.-T., Yu, P.-S., & Tang, Y.-H. (2010). Statistical downscaling of daily precipitation using support vector machines and multivariate analysis. Journal of Hydrology, 385, 13–22. doi:10.1016/j.jhydrol.2010.01.021

Coulibaly, P., Dibike, Y. B., & Anctil, F. (2005). Downscaling Precipitation and Temperature with Temporal Neural Networks. Journal of Hydrometeorology, 6(4), 483–496. doi:10.1175/JHM409.1

Gudmundsson, L., Bremnes, J. B., Haugen, J. E., & Engen-Skaugen, T. (2012). Technical Note: Downscaling RCM precipitation to the station scale using statistical transformations – A comparison of methods. Hydrology and Earth System Sciences, 16(1), 3383–3390. doi:10.5194/hess-16-3383-2012

Gudmundsson, L. (2014). Package "qmap" - Statistical transformations for post-processing climate model output. Package. doi:10.5194/hess-16-3383-2012.bernexp

Kalnay, E. (1996). The NCEP/NCAR 40-year reanalysis project. Bulletin of the American Meteorological Society, 77, 437–471. Retrieved from http://journals.ametsoc.org/doi/abs/10.1175/1520-0477(1996)077%3C0437:TNYRP%3E2.0.CO;2

Mahmood, R., & Babel, M. S. (2014). Future changes in extreme temperature events using the statistical downscaling model (SDSM) in the trans-boundary region of the Jhelum river basin. Weather and Climate Extremes, 5-6, 1–11. doi:10.1016/j.wace.2014.09.001

Mora, D. E., Campozano, L., Cisneros, F., Wyseure, G., & Willems, P. (2014). Climate changes of hydrometeorological and hydrological extremes in the Paute basin, Ecuadorean Andes. Hydrology and Earth System Sciences, 18(2), 631–648. doi:10.5194/hess-18-631-2014

Ochoa, a., Campozano, L., Sánchez, E., Gualán, R., & Samaniego, E. (2015). Evaluation of downscaled estimates of monthly temperature and precipitation for a Southern Ecuador case study. International Journal of Climatology, n/a–n/a. doi:10.1002/joc.4418

Pelckmans, K., Suykens, J. A. K., (2003), LS-SVMlab toolbox user's guide. Retrieved from http://davinci.tach.ula.ve/vermig/A/tutorial1_5.pdf.

Pervez, M. S., & Henebry, G. M. (2014). Projections of the Ganges-Brahmaputra precipitation-Downscaled from GCM predictors. Journal of Hydrology, 517, 120–134. doi:10.1016/j.jhydrol.2014.05.016

Skamarock, W., Klemp, J., Dudhia, J., & Al, E. (2005). A description of the advanced research WRF version 2, (June). Retrieved from http://oai.dtic.mil/oai/oai?verb=getRecord&metadataPrefix=html&identifier=ADA487419

Suykens, JAK, Van Gestel, T., De Brabanter, J., De Moor, B., & Vandewalle, J. (2002). Least Squares Support Vector Machines, World Scientific, Singapore, 71–144.

Tripathi, S., Srinivas, V. V., & Nanjundiah, R. S. (2006). Downscaling of precipitation for climate change scenarios: A support vector machine approach. Journal of Hydrology, 330, 621–640. doi:10.1016/j.jhydrol.2006.04.030

Vapnik, V. N. (1995). The Nature of Statistical Learning Theory, Springer-Verlag, New York.

Wilby, R., Dawson, C., & Barrow, E. (2001). SDSM—a decision support tool for the assessment of regional climate change impacts. Environmental Modelling & Software, 2, 147–159. doi:10.1016/s1364-8152(01)00060-3

5 Evaluation of downscaled estimates of monthly temperature and precipitation for a Southern Ecuador case study

This chapter is published in International Journal of Climatology, 2015,36: 1244–1255.
Received: 29 January 2014 / Accepted: 22 May 2015

Evaluation of Downscaled Estimates of Monthly Temperature and Precipitation for a Southern Ecuador Case Study

A. Ochoa[1,2], L. Campozano[1,3], E. Sánchez[1,4], R. Gualán[1], E. Samaniego[1,4]

[1] Departamento de Recursos Hídricos y Ciencias Ambientales, Universidad de Cuenca, Av. Víctor Manuel Albornoz, Quinta Balzaín, Cuenca, Ecuador.

[2] Facultad de Ciencias Agropecuarias, Universidad de Cuenca, Campus Yanuncay, Cuenca, Ecuador.

[3] Laboratory for Climatology and Remote Sensing (LCRS), Faculty of Geography, University of Marburg, Deutschhausstr. 10, D-35032 Marburg, Germany.

[4] Facultad de Ingeniería, Universidad de Cuenca, Av. Víctor Manuel Albornoz, Quinta Balzaín, Cuenca, Ecuador.

Corresponding author: A. Ochoa. Email: ochoa.anaelizabeth@gmail.com. Tel/Fax: (593) 74051000 Ext 4497. Address: Av. Víctor Manuel Albornoz, Quinta Balzaín, Cuenca, Ecuador.

ABSTRACT The Downscaling of Global Climate Models (GCMs) aims at incorporating finer-scale information to their horizontal resolution in order to represent regional and local processes better. There are two main approaches to downscaling: statistical (based on data relationships between synoptic atmospheric variables and observations of local variables) and dynamical (based on the modeling of regional atmospheric processes and land surface interactions). In this study, some predictive capabilities regarding the generation of station-scale mean monthly temperature and rainfall of both a statistical (ANN-based) and a dynamical (WRF-based) downscaling approach are assessed. We have devised two versions of the statistical downscaling approach. One of them includes regional orographic variables as predictors to allow for spatial extrapolation; the other is purely local. Historical observational data, from the period 1990-1999, of two major watersheds in the Ecuadorian Southern Andes, the Jubones and Paute river basins, were used. Since, to a certain extent, the value added by downscaling techniques can be attributed to terrain information; it is worth noting that some characteristics of the selected catchments (as notorious altitude differences and the presence of qualitatively different precipitation regimes) provide a scientifically interesting location for exploring how finer-scale effects are captured. For this reason, we concentrate on the ability of downscaling techniques to reproduce seasonality. A

decade of evaluation proved that both approaches were able to qualitatively describe precipitation and temperature seasonal variations for different regimes at representative weather stations. Furthermore, the seasonality of precipitation represented by both downscaling approaches surpassed the seasonality representation of reanalysis data. However, shortcomings on the estimates were found. Specifically, dynamical downscaled precipitation estimates were prone to overestimation. Despite the fact that the considered downscaling approaches are different in nature, their ability to represent the high spatio-temporal variability in this region highlights the importance of evaluating their strengths and limitations.

Keywords: Statistical downscaling, dynamic downscaling, RCM, WRF, artificial neural network (ANNs), Ecuador.

5.1 Introduction

Climate and hydrological impact studies demand high-resolution temporal and spatial meteorological data, more in particular precipitation and temperature data. More and more, simulations of global climate models (GCMs) represent the basis of hydrologic impact studies. Although GCMs are quite skillful at large scales, they are unable to represent local climate characteristics and dynamics such as local topographical features, land surface-atmosphere interactions, and convective cloud processes (Coulibaly and Dibike, 2004). To increase the resolution of GCMs output data, both in time and space, several downscaling techniques have been developed. Fowler *et al*. (2007) considered two groups, statistical and dynamical methods.

Downscaling techniques based on artificial neural networks (ANNs) can be classified as statistical (or empirical), since they are data-driven. ANNs are well known machine-learning tools and were used in this study to derive cross-scale relationships between synoptic atmospheric (predictors) and local variables such as precipitation and temperature (predictands). Dynamical downscaling is processes-driven and can be performed by means of Regional Climate Models (RCMs). An example of an RCM is the Weather Research and Forecasting (WRF) model, selected for this study. WRF can be parallelized, is open source, and continuously updated and maintained by The National Centre for Environmental Prediction (NCEP) and The National Centre for Atmospheric Research (NCAR); which is a tremendous advantage for potential users. Dynamical downscaling not only offers higher resolution than GCMs, but also furnishes spatial information about atmospheric processes. However, a considerable handicap of dynamical downscaling in comparison to statistical techniques is its high computational demand.

With regard to statistical downscaling, one can also say that it is, in principle, of local character, in the sense that cross-scale relationships are sought between global and local surface variables at specific points in the study area. Furthermore, these relationships are supposed to be stationary (Pielke and Wilby, 2012), which is a major issue if one wishes to use this kind of techniques for climate change studies. It must be mentioned that some stationarity assumptions are also present in dynamical downscaling through the introduction of parameterized schemes (Pielke *et al*., 2012).

Early applications of RCMs were compared with GCMs or observations (Giorgi and Mearns, 1991; Giorgi *et al*., 1994); but few studies evaluated RCMs and statistical/empirical techniques against observations. Several studies indicated little

difference between statistical and dynamical downscaling results for mean monthly surface temperature and precipitation (Kidson and Thompson, 1998; Mearns *et al*., 1999; Murphy, 1999). More recently, Haylock *et al*. (2006) compared six statistical and two dynamical downscaling models for heavy precipitation and, besides the similarities between all methods, non-linear artificial neural network models proved to be the best to model inter-annual variability, although they underestimated extremes. Schmidli *et al*. (2006) found that a statistical technique was similar in performance to three RCMs in several regions of the European Alps; however they perceived that RCMs did add value in small regions. Furthermore, Hellström *et al*. (2001) found a difference between the results of two dynamical and statistical downscaled precipitation scenarios for Sweden. These authors identified a higher temporal and spatial variability of precipitation changes in the statistical downscaled scenarios than in the dynamical ones; and also the spread of the scenarios created by the statistical model was larger than that between the RCM scenarios on average. In regions of complex topography, Schmidli *et al*. (2007) obtained, for the current climate, similar bias in six statistical downscaling models and three RCMs, on the one hand, but differences with respect to inter-annual variations, on the other hand. Summarizing, dynamical and statistical downscaling approaches have their own strengths and limitations. Despite the fact that the former is conceptual and the latter empirical, their specific evaluation for applications is highly advisable for several reasons. First, they can be used as a validation tool for each other (Landsea and Knaff, 2000). Second, different applications imply different requirements. For instance, if computational cost is an issue, one could resort to a statistical method, whereas, if explaining mechanisms is the objective, dynamical downscaling appears as a better option. Finally, downscaling techniques can be combined in order to obtain more accurate predictions (Chen *et al*., 2012).

Seldom has the capability of downscaling techniques with application to the Ecuadorean Andes been tested. Buytaert *et al*. (2010) evaluated the value of an RCM with respect to a GCM, using the PRECIS model with 50 km pixel resolution. For annual precipitation, they concluded that PRECIS downscaled results added information in some cases, but in other cases they produced inappropriate results, even worse than the parent GCM (HadAM3p). With regard to temperature, they found that PRECIS produced locally better results than HadAM3p. As a general conclusion, Buytaert *et al*. (2010) stressed, given the high degree of uncertainty, the need of screening the capacity of several RCMs for the Andes region. They recommended improving the spatial resolution, and the evaluation of RCMs on seasonality description. With respect to statistical downscaling methods, just a few studies have been performed in the Andes region to the authors' knowledge (e.g. Minvielle & Garreaud, 2011; Souvignet et al., 2010; Labraga, 2009; Souvignet & Heinrich, 2011). Mora et al., 2014, applied the adjusted quantile perturbation approach to downscale climate in the Paute basin, in order to generate discharge for future scenarios. However, a prior evaluation of this statistical downscaling technique was not conducted. Consequently, assessment of the capacity of downscaling techniques in the Andes mountain region is no unnecessary luxury, since it will enable the derivation of the desired temporal and spatial resolution of temperature and precipitation, as well as other weather variables, for the purpose of model-based impact studies.

In a first step towards the understanding of the underlying processes, the representation of seasonal variations is important, and the added value of downscaling tools could greatly benefit this long-term objective. However, it is crucial to guarantee the validity of these tools. The presence of unimodal and bimodal precipitation regimes in the study area is an opportunity to evaluate if downscaled estimates do in fact add

value to the large-scale results, given that these results are not able to capture the spatial variability of climate due to meso and local scale influences. To this end, we have evaluated the predictive capability of the WRF and ANN downscaling approaches. In a preparatory stage for this evaluation, a sensitivity analysis of the WRF physical schemes and a training process of ANNs were performed. Thereafter, the downscaled monthly time series of precipitation and temperature were evaluated against observations. For the evaluation, we calculated the bias, the RMSE, and the correlation coefficient. However, our main concern was to analyze the ability of the different downscaling models to represent seasonal variations, especially with regard to the presence of qualitatively different precipitation regimes in the study area.

5.2 Materials

5.2.1 Study Area

The study region encompasses the Paute (6148 km^2) and Jubones (4353 km^2) catchments, with their outlet towards the east into the Amazon basin and towards the west into the Pacific Ocean, respectively. Catchment delineation and topography are depicted in Fig. 5.1. Both river basins are located in the Andean region of Ecuador, geographically defined by 3,8°-2,3°S to 80°-78,2°W and altitudinally ranging between 0 and 4000 m a.s.l. The importance of the study area for this research does not only come from its orographic complexity but also from its services to society. The Andean highlands are a unique natural resource system for hydropower, irrigated agriculture, fresh water for domestic and industrial uses, and ecoservices (Célleri and Feyen, 2009).

Climate is influenced by the Pacific coastal regime from the west, and the continental and tropical Atlantic air masses from the east (Vuille *et al*., 2000). Mean annual precipitation and temperature vary spatially in a significant amount: from 250 to 1500 mm and from 12°C in the highlands to 22°C in the lowlands (INAMHI, 2013). In the Paute basin, the rainfall regime can be split, according to Célleri *et al*. (2007), into four different spatial structures (two unimodal (UM) and two bimodal (BM) regimes). The two unimodal regimes, UM1 and UM2, have rainfall all year round with a pronounced rainy season in June-July. They are caused by moist advection fluxes (Laraque *et al*., 2007) coming from the central Amazon region by persistent easterlies (Bendix & Lauer, 1992), increasing orographic lifting on the east flanks of the Andes cordillera, thereby forming the Andean Occurring System (AOS). AOS is a cloud and rainfall band located along the eastern slopes of the eastern cordillera produced by the barrage effect of the Andes to the easterlies at this latitude, increasing clouds formation and rainfall. The AOS has its local influence in the lower part of the Paute basin through the Paute canyon in regions with UM regime. Regimes UM1 and UM2 were differentiated by Célleri *et al*. (2007) based on the total annual precipitation, varying between 2900 and 3400 mm yr^{-1} and 1100 and 1600 mm yr^{-1}. The two regions with unimodal rainfall regime are located on the eastern part of the basin, towards the outlet. The regions with bimodal regimes, BM1 and BM2, characterized by Célleri *et al*. (2007) as having a total annual precipitation in the range of 660 to 1100 mm yr^{-1} and 1000 to 1800 mm yr^{-1}, respectively, are located on the central and western part of the basin. BM seasonality,

with peaks in March-April and October-November, convective in nature, is the typical inter-Andean regime. The phenomenon is due to the interplay between the passage of the intertropical convergence zone (ITCZ), the solar cycle (Bendix and Lauer, 1992), and the equatorial Walker circulation. The interplay between these elements results in a strong decline in rainfall in the period June-July, typical for the dry period experienced in the region during these months (Lau and Yang, 2002). The rainfall regime in the Jubones catchment is bimodal (BM) with a heavy rainy season lasting from January to April, and the second rainfall peak from October to November is suppressed due to the South Pacific anticyclone seasonality in the lower region (Bendix and Lauer, 1992). These unique terrain characteristics and the presence of several precipitation regimes in a relatively small area make each of the studied catchments a privileged natural location for testing the skills of downscaling techniques.

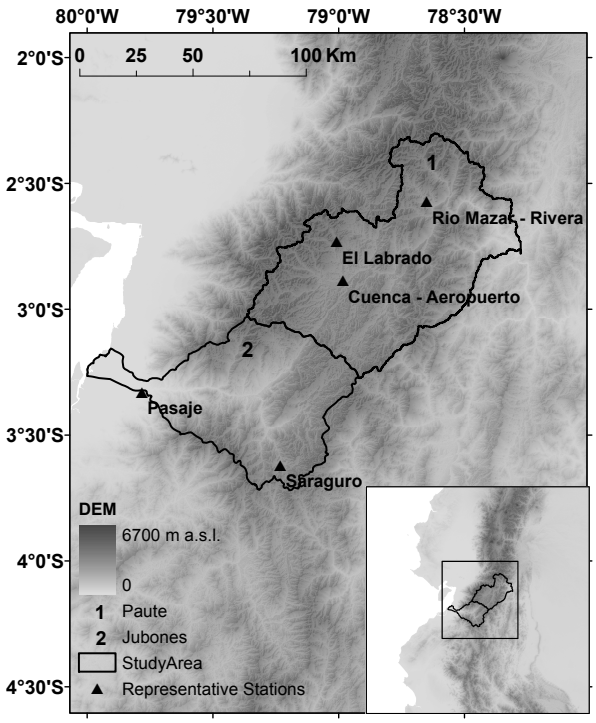

Figure 5-1: Location of the study area, WRF principal and secondary domains and meteorological stations chosen for the calibration and validation of the statistical and dynamical downscaling methods

In other respects, the effect of ENSO on precipitation at a given location in Ecuador is mainly determined by its position with respect to the western cordillera and by its elevation (Rossel *et. al.*, 1998). Regions located towards the west of the western cordillera and below 1500 masl are strongly influenced by ENSO. This effect dissipates eastward towards the higher innermost valleys, where additional climatological influences and complex precipitation processes are especially important (Rollenbeck et al 2011, Pineda et al. 2013). In the case of the Jubones basin, high elevations and sheltered canyons account for around 70% of its area, which limits ENSO influence. For inter-Andean valleys as the Paute basin, ENSO influence is almost negligible due to their high elevation and eastward oriented exposure towards the Amazon basin (Célleri

et al. 2007, Rossel *et*. *al*., 1998). Also, for the Amazon region ENSO influence is negligible (Rossel *et*. *al*., 1998), which confirms the findings of Bendix & Lauer (1992) that the Andes cordillera acts as weather divide. However, during 1982-83 and 1997-98, ENSO exceptional events affected Ecuador severely, thereby producing significant positive anomalies in precipitation countrywide. Anomalies of much lesser extent were observed during the years 1965-66, 1969-70, 1972-73, 1986-87, and 1991-92. In summary, the effect of the ENSO system in Ecuador is characterized by a high degree of uncertainty both in periodicity and in amplitude. Although ENSO influence on the studied basins is either limited or negligible most of the time, its uncertainty can distort the climate-scale representativeness of monthly averages. Since the main objective of this article is the study of climatological seasonality of precipitation, we decided to use synoptic data in periods not affected by ENSO for both the model selection and the validation of the downscaling approaches considered. This is a challenging task in itself due to the existence of complex processes in a rather complex topography.

5.2.2 Data

The National Institute of Meteorology and Hydrology of Ecuador (INAMHI) provides precipitation and temperature records in several sites within the study area. Data quality from all available stations was checked. Stations having a missing data percentage greater than 20% were not considered in the analysis. Proportionality and homogeneity of the data series were checked by using double mass plots and the R-based RHtests-V3 software package, developed by the Climate Research Division of the Meteorological Service of Canada which is available at the website of the Expert Team on Climate Change Detection, Monitoring and Indices (ETCCDMI) (Wang and Feng, 2012). While the double mass plots check for proportionality in the cumulative monthly volumes between stations, the temporal homogeneity of each station is verified applying the RHtests-V3 functions based on the penalized maximal F test, which identifies change points (shifts in the mean) in the precipitation and temperature time series (Wang, 2008a; Wang, 2008b). Although ENSO events were identified as change-points, they were not considered as shifts since they are reckoned as common climate variations in the region. Also, change-points repeatedly encountered in more than one nearby station were not interpreted as shifts assuming that they are the consequence of local modifications in the climate.

A total of 18 stations located in the study area were found to have homogeneous time series. From these stations, five were selected for temporal calibration and validation analysis, considered as accurately depicting the climate variability in both study catchments. In the Paute catchment, Rio Mazar-Rivera (M410) with a unimodal regime UM2, Cuenca-Aeropuerto (M067) with a BM1 regime, and El Labrado (M141) with a BM2 regime were chosen because of the available amount of data that those stations have, after approval by an expert (Célleri, 2013, personal communication). For the same reasons, the stations Pasaje (M040) in the Coastal region and Saraguro (M142) in the highlands, both with unimodal regime, were considered as representative for the climate variability in the lower and upper reaches of the Jubones basin. Characteristics of these 5 weather stations are listed in Table 5.1 and their location depicted in Fig. 5.1. The time series of these stations, spanning the period 1964-1999 were used for model

selection and validation of the downscaling techniques. The period 1964-1989 was chosen for model selection, and the period 1990-1999 for validation.

Table 5-1: Weather stations in the Paute and Jubones basins with weather data in the record period 1964-1999.

Code	Station name	Altitude (m a.s.l.)	Institution	% missing precipitation data
M067	Cuenca Aeropuerto	2516	DAC	0,32
M138	Paute	2289	INAMHI	7,01
M139	Gualaceo	2360	INAMHI	6,37
M141	El Labrado	3260	INAMHI	0,96
M410	Rio Mazar-Rivera	2450	INAMHI	9,24
M045	Palmas	2400	INAMHI	17,00
M040	Pasaje	40	INAMHI	5,41
M431	Sevilla de oro*	2708	INAMHI	1,20
M197	Jacarín*	2478	INAMHI	12,30
M072	Machala Aeropuerto**	4	FAE	10,00
M142	Saraguro	2525	INAMHI	0,00
M419	Girón*	2130	INAMHI	4,78
M292	Granja Sta. Inés	5	INAMHI	0,47

Legend: INAMHI: Instituto Nacional de Meteorología e Hidrología; DAC: Dirección General de Aviación Civil; INECEL: Instituto Ecuatoriano de Electrificación; FAE: Fuerza Aérea Ecuatoriana; INOCAR: Instituto Oceanográfico de la Armada. * The period for spatial cross-validation stage dates from 1996 to 2000. ** The periods for spatial cross-validation stage are 1998-2000 and 2009-2010.

Complementarily, for spatial cross-validation analysis, the Jacarín (regime BM1) and Sevilla de Oro (regime UM) stations located in the Paute basin, and Girón station located in the Jubones basin, were used to validate precipitation estimates obtained from the statistical downscaling method (refer to section 3). Meanwhile, for temperature, Paute and Machala stations in the Paute and Jubones basins, respectively, were used to validate the statistical downscaling method by spatial cross-validation (refer to section 3). Due to the high percentage of gaps in the time series of these stations, a shorter period was considered during the spatial cross-validation stage. The period for spatial cross-validation of Jacarín, Sevilla de Oro, Girón and Paute stations is from 1996 to 2000. For Machala station, the period goes from 1998 to 2000 and from 2009 to 2010 (Table 5.1).

Reanalysis data variables from NCAR/NCEP Reanalysis Project (NNRP) were used as predictors during the training and validation stages in statistical downscaling. Also NNRP data were used for the characterization of the boundary and the initial conditions for the dynamical downscaling. The National Centre for Environmental Prediction (NCEP) and The National Centre for Atmospheric Research (NCAR) maintain the NNRP dataset which has a spatial resolution of 2,5 by 2,5 degrees (approximately 209 km) with 28 sigma levels and a temporal resolution of 6 hours

(Kistler *et al*., 2001). Data is available online from 1948 to the present with more than 80 meteorological variables such as temperature, relative humidity, precipitation, etc. (NCAR *et al*., 1994). The NNRP dataset was chosen for this study since reanalysis variables come from the interpolation of observations or are at least influenced by observations assimilated in a physical based model (Kistler *et al*., 2001); therefore it is expected to allow for the best performance of a downscaling method in comparison with other datasets.

5.3 Methods

As mentioned before, downscaling methods can be grouped in two classes: statistical (SD) and dynamical (DD). Although both try to attain the same objective of incorporating finer-scale information to GCM's results, their conception is quite different, which entails different features for each method. Despite this, we have devised a methodology to obtain downscaled estimates that is intended to be as similar as possible for both approaches. First, a model selection phase was implemented. For the statistical case, several ANN models were trained: some devised to be purely local, and the other incorporating regional orographic variables (such as elevation, slope, and aspect) as predictors to explore the possibilities of obtaining spatial extrapolation capabilities from the ANN approach. With regard to dynamical downscaling, a sensitivity analysis was performed in order to compare different combinations of physical parameterizations with observations. We do not claim that the selected combination is optimal in any rigorous sense. What we try is to have some rational criterion to support the selection of a plausible combination of physical schemes, which, in our case, leads to the smallest precipitation error.

The second stage is validation. It is based on (i) temporal validation and (ii) spatial cross-validation. The former has been applied station-wise for DD and for the purely local SD. The DD model furnishes area-wide results and regional cross validation is not needed. For SD, the temporal validation consists on the comparison of the results with observations at a given station in a period different from the one used for the training stage. In contrast to temporal validation, for the spatial cross-validation of SD, the period for the training stage could be coincident with the period of validation. However, the results of simulations are compared with observations in a different station from the stations considered for training. Thus, the spatial cross-validation on SD evaluates the spatial generalization capabilities of the statistical downscaling approach. In order to assess performance for temporal validation and spatial cross-validation, the bias, root mean square error (RMSE) and the Pearson's correlation coefficient (γ) were calculated.

5.3.1 Statistical downscaling

Statistical techniques for scale reduction are based on models that relate empirically large-scale circulation variables (predictors) with regional variables observed in stations (predictands). This can, according to Dibike and Coulibaly (2007), formally be expressed as $R = F(L)$, where, R represents the predictands (i.e. precipitation and temperature), L the predictors (i.e. sea level pressure, specific humidity, geopotential heights, air temperature, relative humidity, mean wind velocity, and surface zonal

wind), and F is the transfer (cross-scale) function. The transfer functions are based on linear and nonlinear regression models to infer relationships between local predictands and large-scale predictors. Here a nonlinear technique was used. Examples of this kind of models, besides neural networks, are multiple regressions analysis, canonical correlation analysis, support vector machines, among other techniques. The authors selected neural networks for downscaling for their well-known ability to capture non-linear relationships. A typical ANN consists of a series of nodes or neurons arranged as an input layer, one or more hidden layers, and one output layer. The neurons accept a vector of inputs, which are then multiplied by a weight matrix W and summed, before further processing through an activation function f. There are no fixed rules for selecting the number of hidden layers and the number of nodes per layer. Therefore, experimentation by trial and error is still the most reliable method for delineating the optimal architecture of the network.

The model selection phase for statistical downscaling starts typically by defining the network architecture. For this work, a feed-forward network was chosen. Then, a hyperbolic tangent activation function was applied at the only hidden layer and a linear activation function at the output layer. In addition, the networks were trained using a back propagation algorithm. That is, the Mean Squared Error (MSE) between the output and the observations was back-propagated through the ANN to determine the weights for the next training iteration, until a tolerance on the MSE was reached.

5.3.2 Dynamical downscaling

As mentioned before, the Weather Research and Forecasting (WRF) model was applied as dynamical downscaling technique. It is a Regional Climate Model (RCM) simulating atmospheric processes. Since dynamical downscaling techniques are computationally demanding, the authors selected the WRF model, because the latter possesses the capacity to simulate a multitude of processes in parallel. Other elements that contributed to the selection of the WRF model are the fact that it is open source and that the model is continuously actualized and maintained by The Mesoscale and Microscale Meteorology Division of NCAR, United States. The Advanced Research WRF 3 version was used to perform the dynamical downscaling. NNRP dataset, archived in ds090.0 dataset, was used as input for the WRF model. It includes temperature, wind velocity in the x- and y-direction, relative and specific humidity, elevation, surface pressure, sea-level pressure, terrain conditions, soil moisture, sea ice, land/sea flag, and snow depth. The WRF model domains are detailed in Fig. 5.1. The nested domain covers the study area, 225 km by 225 km in size and a 15 km by 15 km resolution. This domain is placed in the main domain which is three times larger (675 km by 675 km) and it has a three times coarser resolution (45 km by 45 km) than the nested domain. The purpose of nesting the domain is to increase the resolution of the initial and boundary conditions up to 45 km by 45 km, which is much higher than the GCM resolution. The size of the bigger domain meets the recommendations made by Gill and Pyle (2011), and Moeng *et al*. (2007) leaving at least 5 cells distance from the nested domain at each side. The WRF system includes several mathematical schemes that solve the following physical processes: microphysics (MP), convective and shallow clouds (CU), surface layer (SL), land and urban surface (SF), planetary boundary layer (PBL), long wave radiation (RALW), and short wave radiation (RASW). Herewith, only a limited number of combinations among physics schemes were chosen. The first configuration SIM1 (Table 5.2) was defined according to the recommendation of Wang

et al. (2012) for regional climate modeling with a 10 to 30 km resolution. The other simulations were combined following the recommendations of Skamarock et al. (2008) who detail only schemes widely used and propose their use taking into account downscaling resolution and the fact that not all combinations of physical schemes are plausible. MP schemes recommended for a downscaling resolution greater than 10 km are Kessler (Kessler 1969), WRF Single-Moment 3-class = WSM3 (Hong et al, 2004) and WRF Single-Moment 5-class scheme = WSM5 (Hong et al, 2004); however WSM5 is similar to WSM3 but it takes supercooled water into consideration and gradual melting of snow; hence Kessler and WSM5 will be tested. CU schemes should only be used in grids bigger than 5 km and the following schemes are recommended for grids bigger than 10 km: Kain-Fritsch (KF-Eta, KF-Eta 2 and KF-Eta 3, which are small variations of KF-Eta) (Kain, 2004), Grell-Devenyi (Grell and Devenyi, 2002), and Betts-Miller-Janjic = BMJ (Janjic, 1994, 2000). SL schemes discussed in Skamarock et al. (2008) are NCAR Mesoscale Model Version 5 = MM5 which has to be combined with Yonsei University (Korea) = YSU (Hong et al., 2006) as a PBL scheme, Eta which has to be combined with Mellor-Yamada-Janjic = MYJ as a PBL scheme, and Similarity theory = PX (Pleim, 2006). Two SF schemes were chosen for parameterization: NOAH LSM and Urban canopy = Noah (Chen and Dudhia, 2001; Kusaka et al, 2001), which is the most complex and complete scheme, and also the simple Thermal scheme that was already used in Ecuadorian regions (Muñoz and Recalde, 2010). PBL schemes recommended are: YSU, MYJ and Asymmetrical Convective Model version 2 = ACM2 (Pleim, 2007) taking into account that YSU has to be combined with MM5 and MYJ with Eta scheme, thus ACM2 is combined with PX. The most complete and proven RALW schemes are Rapid Radiative Transfer Model = RRTM (Mlawer et al. 1997) and NCAR Community Atmosphere Model = CAM3 (Collins et al, 2004) while RASW recommended schemes are Goddard (Tao et al., 1989) and CAM3. Therefore, in this study, the schemes mentioned were combined as shown in Table 5.2. By finding the best scores (bias, RMSE, and Pearson's correlation coefficient) between the WRF simulations and rain gauge data, we wish to identify a plausible combination of physical schemes that leads to the smallest precipitation error in the simulated periods for the study region. Since the WRF model integrates atmospheric processes, it is recommended to use only data of ENSO neutral years, as discussed above. Therefore, two ENSO neutral years in each decade were selected for sensitivity analysis. A month prior to each simulation period was included for the model spin-up (Wei *et al*., 2002). The following periods were selected for the sensitivity analysis of the WRF model: 03/1966-04/1968, 11/1977-12/1979, and 04/1983-05/1985.

5.4 Results and discussion

5.4.1 Model selection phase for dynamical and statistical downscaling

In statistical downscaling for temporal validation, the networks were first trained with all available predictor variables from the NNRP dataset as inputs. Then, a sensitivity analysis using MSE values was conducted to identify the best performing networks. After that, a new sensitivity analysis was performed to select a smaller group

of input variables (predictors). This analysis provided a measure of the relative importance of the predictors (inputs of the neural network) by calculating how the model output varies in response to input variations. The relative sensitivity of the model to each input is calculated by dividing the standard deviation of the output by the standard deviation of the varied input. The network was then retrained with the most relevant predictor variables. In addition to the predictors selected for temporal validation, data of elevation, slope, aspect, and month switch were used as predictors for spatial cross-validation. Regarding precipitation, an ANN for each station was devised for temporal validation, on the one hand. The selected stations were Cuenca-Aeropuerto, El Labrado, Río Mazar-Rivera, Pasaje, and Saraguro. On the other hand, for spatial cross-validation, three networks were developed according to the precipitation regime of each specific region. For instance, the bi-modal region in the Paute basin, Cuenca-Aeropuerto, El Labrado, and Gualaceo stations were used for calibration and Jacarín station for validation. For the uni-modal region in the Paute basin, Río Mazar-Rivera and Palmas stations were used for calibration and Sevilla de Oro station for validation stage. Finally, for the Jubones basin, the stations Pasaje and Saraguro were used for calibration and Girón station for validation. With regard to temperature, the temporal validation was developed with one ANN for each basin, in Cuenca-aeropuerto and Saraguro for the Paute and Jubones basins, respectively. For spatial cross-validation of temperature, one ANN was developed for the Paute basin, using the stations Palmas and Cuenca-Aeropuerto for calibration and station Paute for validation; and one ANN for the Jubones basin with stations Saraguro and Granja Sta. Ines for calibration and station Machala for validation.

The model selection phase of the WRF model was based on a sensitivity analysis combining twelve parameterizations (see Table 5.2). Several schemes for the parameterization of the atmospheric microphysics, the convective and shallow cloud layer, the **surface layer**, **land**/sub-**surface**, the planetary boundary layer, and the long wave and short wave radiation were considered. The results of the combinations were compared quantitatively to the observations of the five homogeneous weather stations representing the regional climate using bias, root mean square error and Pearson's correlation coefficient, and qualitatively by comparing seasonal values. The schemes that influenced the results most were the ones that model the physics of convective and shallow clouds. Wang and Seaman (1997) and Gallus Jr. (1999), among others, also showed that the choice of the convective scheme strongly influences the simulated rainfall patterns. The scheme that produced rainfall results closest to the rain gauge data is the SIM8 simulation (Table 5.2), consisting of the combination of the Kessler scheme for microphysics, the Kain-Fritsch scheme for mimicking the convective and shallow cloud system, the Eta similarity for surface layer (Janjic, 1994), the 5-layer thermal diffusion representing the turbulence above the land surface layer, the Mellor-Yamada-Janjic Eta a local closure model for planetary boundary layer (Mellor and Yamada, 1982), and the CAM 3.0 scheme for modeling the long and shortwave radiation (Collins *et al*., 2004). Therefore, SIM8 was identified as a plausible combination of physical schemes that leads to the smallest precipitation error in the simulated periods for the study region. Table 5.3 summarizes the average bias, the RMSE and the correlation between the WRF model results and the rain gauge observations in the calibration period. The bias range of the monthly precipitation varies between 0,1 and 106 mm; the correlation coefficient is negative for the El Labrado weather station, ranging between 0,18 and 0,49 in the remaining stations (Table 5.3a). Monthly temperature bias is 8°C in

the Cuenca-Aeropuerto weather station and 3°C in the Saraguro weather station and the correlation coefficient is respectively 0,32 and 0,13 (Table 5.3b).

Table 5-2: Used parametrization schemes in the WRF model.

Simulation	MP	CU	SL	SF	PBL	RALW	RASW
SIM1	WSM 6	Kain-Fritsch	MM5	NOAH LSM and Urban canopy	YSU	CAM3	CAM3
SIM2	WSM 5	Kain-Fritsch	MM5	NOAH LSM and Urban canopy	YSU	CAM3	CAM3
SIM3	Kessler	Kain-Fritsch	MM5	NOAH LSM and Urban canopy	YSU	CAM3	CAM3
SIM4	Kessler	Kain-Fritsch	Eta	NOAH LSM and Urban canopy	MYJ	CAM3	CAM3
SIM5	Kessler	Kain-Fritsch	PX	PX	ACM2	CAM3	CAM3
SIM6	Kessler	Kain-Fritsch	Eta	NOAH LSM and Urban canopy	MYJ	RRTM	CAM3
SIM7	Kessler	Kain-Fritsch	Eta	NOAH LSM and Urban canopy	MYJ	CAM3	Goddard
SIM8	**Kessler**	**Kain-Fritsch**	**Eta**	**Thermal**	**MYJ**	**CAM3**	**CAM3**
SIM9	Kessler	BMJ	Eta	Thermal	MYJ	CAM3	CAM3
SIM10	Kessler	Grell-Devenyi	Eta	Thermal	MYJ	CAM3	CAM3
SIM11	Kessler	KF kfeta = 2	Eta	Thermal	MYJ	CAM3	CAM3
SIM12	Kessler	KF kfeta = 3	Eta	Thermal	MYJ	CAM3	CAM3

Legend: MP = microphysics, CU = convective and shallow clouds, SL = surface layer, SF = land and urban surface, PBL = planetary boundary layer, RALW = long wave radiation, RASW = short wave radiation; WSM5 = WRF Single-Moment 5-class scheme (Hong et al, 2004); WSM6 = WRF Single-Moment 6-class scheme (Hong and Lim, 2006); Kessler scheme (Kessler 1969); Kain-Fritsch scheme (KF-Eta, KF-Eta 2, KF-Eta 3) (Kain, 2004); Grell-Devenyi (Grell and Devenyi, 2002); BMJ = Betts-Miller-Janjic scheme (Janjic, 1994, 2000); MM5 = NCAR Mesoscale Model Version 5; PX = Similarity theory (PX) (Pleim, 2006); NOAH LSM and Urban canopy (Chen and Dudhia, 2001; Kusaka et al, 2001); Thermal; YSU = Yonsei University (Korea) (Hong et al., 2006) MYJ = Mellor-Yamada-Janjic PBL (Janjic, 1990, 1996, 2002); ACM2 = Asymmetrical Convective Model version 2 PBL (Pleim, 2007); CAM 3.0 = NCAR Community Atmosphere Model (Collins et al, 2004) ; RRTM = Rapid Radiative Transfer Model (Mlawer et al. 1997); Goddard (Tao et al., 1989).

Table 5-3: Bias, root mean square error (RMSE) and Pearson's correlation coefficient for precipitation (a) and temperature (b) data from 1964 to 1989 for statistical downscaling calibration period and around six years (03/1966-04/1968, 11/1977-12/1979, and 04/1983-05/1985) for dynamical downscaling model selection period.

(a)

Station	Dynamical downscaling			Statistical downscaling		
	Bias [mm]	RMSE [mm]	γ [-]	Bias [mm]	RMSE [mm]	γ [-]
Cuenca-Aeropuerto	22,07	53,69	0,18	-0,97	35,50	0,62
El Labrado	-6,60	59,69	-0,17	-0,85	40,26	0,42
Río Mazar-Rivera	0,08	43,55	0,49	2,94	44,98	0,55
Saraguro	-32,91	48,75	0,12	-2,27	37,20	0,60
Pasaje	105,78	154,76	0,45	-7,60	57,06	0,56
Average	33,49	72,09	0,21	2,93	43,00	0,55

(b)

Station	Dynamical downscaling			Statistical downscaling		
	Bias [°C]	RMSE [°C]	γ [-]	Bias [°C]	RMSE [°C]	γ [-]
Cuenca-Aeropuerto	-8,32	8,35	0,32	0,06	0,69	0,82
Saraguro	-2,82	2,86	0,13	0,02	0,57	0,55
Average	-5,57	5,61	0,23	0,04	0,63	0,69

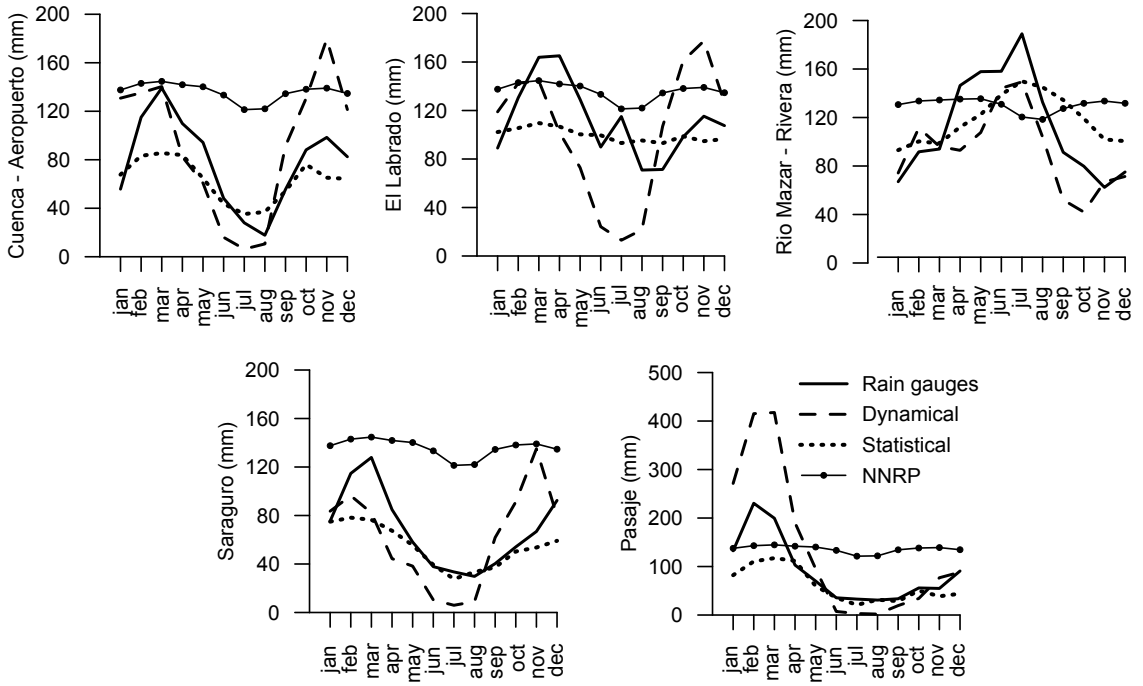

Figure 5-2: Multiyear monthly mean precipitation of the dynamical and statistical downscaling results in comparison with rain gauge data and the NNRP reanalysis dataset during the temporal validation for the period 1990-1999 for the five stations depicting the regional climate variability (Pasaje is shown with different y-axis values).

5.4.2 Predictability of monthly time series

For temporal validation stage, the multiyear monthly mean of precipitation derived by the rain gauge observations, and statistical and dynamical methods are depicted in Fig. 5.2. According to observations, the bimodal regime in the Paute catchment presents a wet season from February to May and a second but lower peak from October to December (Cuenca-Aeropuerto and El Labrado, Fig. 5.2); while the unimodal regime presents a wet season from April to August (Río Mazar-Rivera, Fig. 5.2). In the Jubones catchment, the wet season starts earlier from December to April and rainfall intensity is higher in the coastal area (Pasaje station) than in the mountain region (Saraguro station). It is shown that both statistical and dynamical methods follow the seasonal patterns of precipitation, except in El Labrado station, where only the dynamical downscaling technique is able to represent its variability. Since artificial neural networks "learn" from the provided data, it is likely that local effects on El Labrado station, related to rainfall production, are not represented by the synoptic variables on the inputs. Cuenca-Aeropuerto and El Labrado stations present bimodal regimes BM1 and BM2, respectively. The total rainfall in the dry season in both regimes differs more than 50 mm according to rain gauge measurements (Fig. 5.2). Although the WRF model captures the bimodal regime in both stations, the simulated difference in precipitation amount is not accurate. The statistical downscaling method represents well the dry season of the two bimodal regimes, with exception of El Labrado station, possibly for the reasons mentioned above. Indeed, statistical and dynamical methods are not accurate capturing precipitation amount, although the intra-annual dynamics is captured. Neural networks usually underestimate extremes probably due to their ability to extract a background signal from noisy series, tending to preserve the homogeneity of the center (Haylock *et al*., 2006). The tendency of the dynamical downscaling method to overestimate mean precipitation and underestimate dry season is shown in Fig. 5.2 and was also observed by Sunyer *et al*. (2012). These authors analyzed the performance of four different RCMs, and even the best performing RCM could not represent regional variability. The dynamical downscaling method when compared with observations presents a bias of 20 mm, a RMSE of 84 mm, and a correlation of 0.4 on average overall stations (Table 5.4a). Table 5.4a also shows that the statistical downscaling method bias is 18 mm, the RMSE is 55 mm and the correlation is around 0.5 on average overall stations.

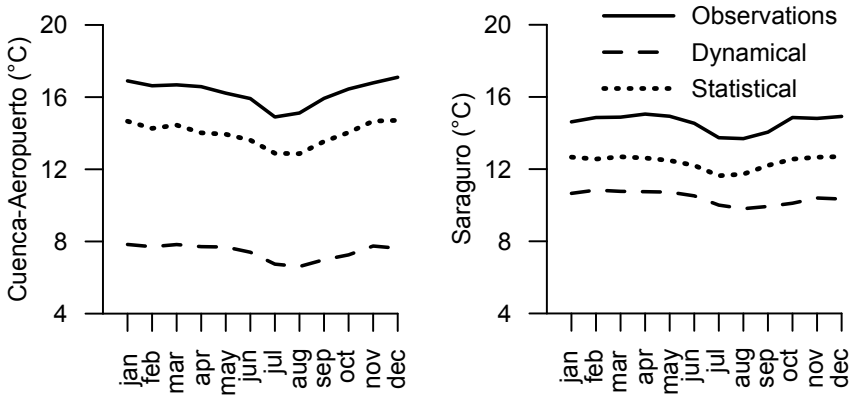

Figure 5-3: Multiyear monthly mean temperature of the dynamical and statistical downscaling results in comparison with observations during the temporal validation for the period 1990-1999.

For the spatial cross-validation stage, in Fig. 5.4, the multiyear monthly mean of precipitation is presented for Jacarín, Sevilla de Oro and Girón stations. Seasonality is well represented by statistical downscaling, and it is striking that correlation values are similar to those during the temporal validation stage. The consideration of specific ANN models by climatological regimes added to the GIS information provided for each station might account for these good results. This fact means that the ANN model for statistical downscaling have, to a certain extent, spatial generalization capabilities. On the other hand, dynamical downscaling is able to represent seasonality on Jacarín and Sevilla de Oro stations reasonably well. However, for Girón station, there is an overestimation of precipitation during the second half of the year. Although in general seasonality is well represented by DD, the amounts of precipitation are overestimated, as confirmed by high values of the bias and RMSE presented in Table 5.5a. This fact could be largely explained by an overestimation of the convective component of rainfall of WRF model during the equinoxes (Bendix & Lauer, 1992).

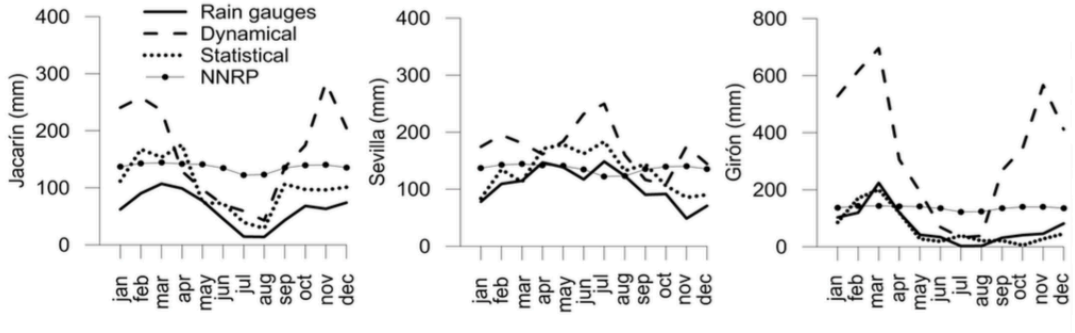

Figure 5-4: Multiyear monthly mean precipitation of dynamical and statistical downscaling results in comparison with rain gauge data and NNRP reanalysis dataset during the spatial cross-validation period 1996-2000 for three stations of the study area (Girón is shown with different y axis values)

With regard to temperature seasonality, it is qualitatively well represented by both downscaling methods during temporal validation and spatial cross-validation (Fig. 5.3&5.5), confirming the findings by Buytaert *et al*. (2010). Due to strong gradients of elevation in the Ecuadorian region, there is a strong spatial variability in temperature compared to the seasonal variation. For instance, the annual mean temperature in Cuenca-Aeropuerto station is around 17°C, in Saraguro 15°C, in Machala station is around 25°C. However, seasonal temperature variations are minimal, around 3°C. Country-wide during July and August there is a small dip-in that was correctly seized by both downscaling methods (Fig. 5.3&5.5). Quantitatively, the dynamical downscaling method presents a 6 ºC bias and RMSE, and a 0.6 correlation in the temporal validation (Table 5.4b), while the spatial cross-validation analysis results in a 4 ºC bias and RMSE and a 0.7 correlation coefficient (Table 5.5b). The statistical downscaling bias and RMSE are lower for the temporal validation (2 ºC) than for spatial cross-validation (7 ºC), while the correlation coefficient is similar in both analysis (0.7) (Table 5.4b&5.5b). The SD method is able to represent even small differences in temperature among stations. DD method results are highly biased presenting lower mean monthly temperatures for all stations.

Table 5-4: Bias, root mean square error (RMSE) and Pearson's correlation coefficient for the dynamical and statistical downscaling results compared to precipitation (a) and temperature (b) data for temporal validation during the period 1990-1999.

(a)

Station	Dynamical downscaling			Statistical downscaling		
	Bias [mm]	RMSE [mm]	γ [-]	Bias [mm]	RMSE [mm]	γ [-]
Cuenca-Aeropuerto	31,57	72,87	0,41	-30,02	41,28	0,60
El Labrado	-8,95	84,62	0,16	-13,11	51,90	0,33
Río Mazar-Rivera	-16,20	63,86	0,43	5,76	52,83	0,42
Saraguro	-5,00	54,61	0,39	-13,07	40,21	0,57
Pasaje	40,42	143,40	0,63	-30,02	89,59	0,52
Average	20,43	83,87	0,40	18,40	55,16	0,49

(b)

Station	Dynamical downscaling			Statistical downscaling		
	Bias [°C]	RMSE [°C]	γ [-]	Bias [°C]	RMSE [°C]	γ [-]
Cuenca-Aeropuerto	-8,84	8,86	0,71	-2,33	2,37	0,86
Saraguro	-4,21	4,28	0,43	-2,20	2,30	0,58
Average	6,53	6,57	0,57	2,27	2,34	0,72

Table 5-5: Bias, root mean square error (RMSE) and Pearson's correlation coefficient for the dynamical and statistical downscaling results compared to precipitation (a) and temperature (b) data for spatial cross-validation during the period 1996 - 2000.

(a)

Station	Statistical Downscaling			Dynamical Downscaling		
	Bias [mm]	RMSE [mm]	ã [-]	Bias [mm]	RMSE [mm]	ã [-]
Jacarín	38,82	59,29	0,60	127,70	189,96	0,49
Sevilla	25,51	63,15	0,32	75,35	125,45	0,17
Girón	-5,35	58,77	0,67	313,39	427,64	0,68
Average	23,23	60,40	0,53	172,15	247,68	0,45

(b)

Station	Statistical Downscaling			Dynamical Downscaling		
	Bias [°C]	RMSE [°C]	ã [-]	Bias [°C]	RMSE [°C]	ã [-]
Paute	-2,37	2,44	0,80	-9,67	9,70	0,71
Machala	-5,58	5,77	0,57	-4,80	4,90	0,81
Average	3,98	4,11	0,69	7,24	7,30	0,76

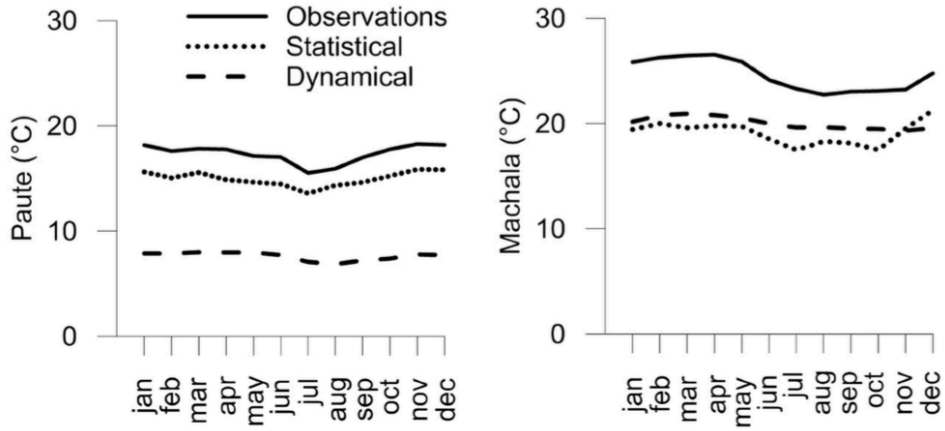

Figure 5-5: Multiyear monthly mean temperature of dynamical and statistical downscaling results in comparison with observations during the spatial cross-validation period 1996-2000.

To evaluate de added value of downscaling techniques with respect to NNRP reanalysis data, Figs. 5.2&5.4 show the multiyear monthly mean precipitation from the NNRP reanalysis dataset plotted together with the downscaled estimates. Due to the coarse resolution of the NNRP data, all stations, except Río Mazar-Rivera and Sevilla de Oro stations, are located in the same grid. Therefore, the precipitation on these stations is estimated as a bimodal regime, lacking seasonal variability representation and agreement with observations. Although Río Mazar-Rivera and Sevilla de Oro stations are located in a neighboring pixel, neither was the seasonality at these stations represented properly by the reanalysis data. Similar results were found in a climate change study using dynamical downscaling by Mannig *et al*. (2013), concluding that simulations are closer to observational data than reanalysis data. The fact that the unimodal and bimodal regimes are captured qualitatively by both tested downscaling techniques suggests that these methods, when compared to NNRP data, improve not only the grid size resolution but also have a better representation of local climate variability. Therefore, it is important to evaluate the strengths and limitations of SD and DD for specific applications, as in the case of the present study, to the southern Andes of Ecuador, a region characterized by complex interactions between orographic features and several large-scale circulation influences.

5.5 Conclusions

In this study, some predictive capabilities regarding the generation of station-scale mean monthly temperature and rainfall of both a statistical (ANN-based) and a dynamical (WRF-based) downscaling approach were assessed. Since, to a certain extent, the value added by downscaling techniques can be attributed to terrain information, it is worth noting that some characteristics of the selected catchments (the Paute and the Jubones catchments, in the south Andes of Ecuador), as notorious altitude differences and the presence of qualitatively different precipitation regimes, provide a scientifically interesting situation for exploring how finer-scale effects are captured. Therefore, we concentrate on the ability of downscaling techniques to reproduce

seasonality as a first step towards the understanding of the underlying processes. A decade of evaluation proved that both approaches were able to qualitatively describe precipitation and temperature seasonal variations for different regimes in representative weather stations. Further, the seasonality of precipitation represented by both downscaling approaches surpassed the seasonality representation of NNRP reanalysis data, fitting observations better. However, shortcomings on amount estimations, especially for precipitation, were found. Specifically, dynamical downscaled estimates were prone to overestimation.

Despite the fact that the SD and DD are empirical and conceptual in nature, both approaches added value in representing seasonality in precipitation and temperature in a region of complex topography as the Andes of South Ecuador, a region characterized by complex interactions between orographic features and several large-scale circulation influences. Given that GCMs are validated against reanalysis data, these facts highlight the value of considering downscaling techniques in the local representation of present and future climate. Furthermore, the evaluation of strengths and limitations for the specific application of each approach is highly advisable for several reasons, as mentioned in the Introduction. First, they can be used as a validation tool for each other; for instance, because SD might constrain unrealistically the cross-scale relationships intended to model future climate. Second, different applications entail different requirements. For instance, if computational cost is an issue, one could resort to a statistical method, whereas, if explaining mechanisms is the objective, dynamical downscaling appears as a better option. Finally, it is important to keep in mind that downscaling techniques can be combined in order to obtain more accurate and useful predictions (Chen *et al*., 2012), given that blending the best features of each one is feasible for specific applications.

Acknowledgments

The authors gratefully acknowledge the financial support given by the National Institution of Higher Education, Science, Technology and Innovation-SENESCYT through the PIC-11-728 project and Ecuador's state power generation holding company CELEC. Furthermore, the authors like to express gratitude to the National Institute of Meteorology and Hydrology (INAMHI) for having provided weather observations, rainfall and temperature data. Finally, we thank Professor Rolando Célleri for his expert advice when choosing representative stations for this study.

References

Bendix J, Lauer W. 1992. Die niederschlagsjahreszeiten in Ecuador und ihre klimadynamische interpretation. *Erdkunde* 46: 118-134.

Bendix, J., Trache, K., Palacios, E., Rollenbeck, R., Goettlicher, D., Nauss, T., & Bendix, A. (2011). El Niño meets La Niña – anomalous rainfall patterns in the “traditional” El Niño region of southern Ecuador. *Erdkunde*, *65*(2), 151–167. doi:10.3112/erdkunde.2011.02.04

Bureau of Meteorology. 2012. El Niño - Detailed Australian analysis. Retrieved from *http://www.bom.gov.au/climate/enso/enlist/* [May 11, 2012].

Buytaert W, Vuille M, Dewulf A, Urrutia R, Karmalkar A, Célleri R. 2010. Uncertainties in climate change projections and regional downscaling in the tropical Andes: implications for water resources management. *Hydrology and Earth System Sciences* 14(7): 1247–1258. DOI:10.5194/hess-14-1247-2010.

Célleri R, Feyen J. 2009. The hydrology of tropical Andean ecosystems: Importance, knowledge status, and perspectives. *Mt. Res. Dev.* 29: 350-355.

Célleri R, Willems P, Buytaert W, Feyen J. 2007. Space-time variability of rainfall in the Paute River basin of South Ecuador. *Hydrol. Process.* 21: 3316-3327.

Chen F, Dudhia J. 2001. Coupling an advanced land-surface/ hydrology model with the Penn State/ NCAR MM5 modeling system. Part I: Model description and implementation. *Mon. Wea. Rev.* 129: 569–585.

Chen J, Brissette FP, Leconte R. 2012. Coupling statistical and dynamical methods for spatial downscaling of precipitation. Climatic Change 114(3-4): 509–526. DOI: 10.1007/s10584-012-0452-2.

Collins WD, Rasch PJ, Boville BA, Hack JJ, McCaa JR, Williamson DL, Kiehl JT, Briegleb B, Bitz C, Lin S-J, Zhang M, Dai Y. 2004. Description of the NCAR Community Atmosphere Model (CAM 3.0). National Center for Atmospheric Research, Climate and Global Dynamics Division, Boulder, CO, 226 pp.

Coulibaly P, Dibike YB. 2004. Downscaling of global climate model outputs for flood frequency analysis in the Saguenay river system. Project No. S02-15-01, Final Report, 85 pp. Retrieved from *http://www.hydrology.mcmaster.ca/documents/CCAF_Final_ Report.pdf* [July 12, 2013].

Dibike YB, Coulibaly P. 2006. Temporal neural networks for downscaling climate variability and extremes. *Neural Networks* 19(2): 135-44.

Fowler HJ, Blenkinsop S, Tebaldi C. 2007. Linking climate change modelling to impacts studies: Recent advances in downscaling techniques for hydrological modelling. *Int. J. Climatology* 27: 1547-1578.

Gallus Jr, William A. 1999. Eta simulations of three extreme precipitation events: Sensitivity to resolution and convective parameterization. *Wea. Forecasting* 14(3): 405-426.

Gill D, Pyle M. 2011. Nesting in WRF. NCEP, NOAA, National Weather Service, 40 pp. Retrieved from *http://www.mmm.ucar.edu/wrf/users/tutorial/201107/WRFNesting.ppt.pdf* [October 15, 2012].

Giorgi F, Brodeur CS, Bates G. 1994. Regional climate change scenarios over the United States produced with a nested regional climate model. *J. Climate* 7(3): 375-399.

Giorgi F, Hewitson B, Arritt R, Bates B, Benestad R, Boer G, Buishand A, Castro M, Chen D, Cramer W, Crane R, Crossley JF, Dehn M, Dethloff K, Dippner J, Emori S, Francisco R, Fyfe J, Gerstengarbe FW, Gutowski W, Gyalistras D, Hantel M, Hassell DC, Heimann D, Jack C, Jacobeit J, Kato H, Katz R, Kauker F, Knutson T, Lal M, Landsea C, Laprise R, Leung LR, Lynch AH, May W, Mcgregor JL, Miller NL, Murphy J, Ribalaygua J, Rinke A, Rummukainen M, Semazzi F, Walsh K, Werner P, Widmann M, Wilby R, Wild M, Xue Y. 2001. Regional Climate Information - Evaluation and Projections, 56 pp. Retrieved from *http://www.grida.no/climate/ipcc_tar /wg1/pdf/TAR-10.PDF* [May 11, 2012].

Giorgi F, Mearns L. 1991. Approaches to the simulation of regional climate change: A review. *Rev. Geophys*. 29(2): 191-216.

Grell GA, Devenyi D. 2002: A generalized approach to parameterizing convection combining ensemble and data assimilation techniques. *Geophys. Res. Lett,* 29(14): Article 1693.

Haylock MR, Cawley GC, Harpham C, Wilby RL, Goodess CM. 2006. Downscaling heavy precipitation over the United Kingdom: A comparison of dynamical and statistical methods and their future scenarios. *Int. J. Climatology* 26: 1397-1415.

Hellström C, Chen D, Achberger C, Räisänen J. 2001. Comparison of climate change scenarios for Sweden based on statistical and dynamical downscaling of monthly precipitation. *Climate Res*. 19(1): 45-55.

Hong S-Y, Dudhia J, Chen S-H. 2004: A revised approach to ice microphysical processes for the bulk parameterization of clouds and precipitation. *Mon. Wea. Rev*. 132: 103-120.

Hong S-Y, Noh Y, Dudhia J. 2006: A new vertical diffusion package with an explicit treatment of entrainment processes. *Mon. Wea. Rev*. 134: 2318–2341.

INAMHI (Instituto Nacional de Meteorología e Hidrología del Ecuador). 2013. Mapas Climáticos del Ecuador. Retrieved from *http://www.inamhi.gob.ec/index.php/paute* [May 6, 2013].

COAPS (Center for Ocean-Atmospheric Prediction Studies), Florida State University (FSU). JMA SST ENSO Index. Retrieved from *http://coaps.fsu.edu/jma* [November 2, 2012].

Janjic ZI. 1990: The step-mountain coordinate: physical package, *Mon. Wea. Rev.* 118: 1429–1443.

Janjic ZI. 1994. The step-mountain Eta coordinate model: Further developments of convection, viscous sublayer, and turbulence closure schemes. *Mon. Wea. Rev.* 122: 927–945.

Janjic ZI. 1996: The surface layer in the NCEP Eta Model, Eleventh Conference on Numerical Weather Prediction, Norfolk, VA, 19–23 August; *Amer. Meteor. Soc. Boston, MA,* 354–355.

Janjic ZI. 2000: Comments on "Development and Evaluation of a Convection Scheme for Use in Climate Models", *J. Atmos. Sci.* 57: 3686.

Janjic ZI. 2002: Nonsingular Implementation of the Mellor–Yamada Level 2.5 Scheme in the NCEP Meso model, NCEP Office Note 437, 61 pp.

Kain JS. 2004: The Kain–Fritsch convective parameterization: An Update. *J. Appl. Meteor.* 43: 170–181.

Kessler E. 1969. On the distribution and continuity of water substance in atmospheric circulation. *Amer. Meteor. Soc.*32, 84 pp.

Kidson JW, Thompson CS. 1998. A comparison of statistical and model-based downscaling techniques for estimating local climate variations. *J. Climate* 11: 735-753.

Kistler R, Kalnay E, Collins W, Saha S, White G, Woollen J, Chelliah M, Ebisuzaki W, Kanamitsu M, Kousky V, Van Den Dool H, Jenne R, Fiorino M. 2001. The NCEP-NCAR 50-year reanalysis: Monthly means CD-ROM and documentation. *Bull. Am. Meteorol. Soc*. 82: 247-267.

Kusaka H, Kondo H, Kikegawa Y, Kimura F. 2001: A simple single-layer urban canopy model for atmospheric models: Comparison with multi-layer and slab models. *Bound.-Layer Meteor.* 101: 329–358.

Labraga JC, 2009: Statistical downscaling estimation of recent rainfall trends in the eastern slope of the Andes mountain range in Argentina. *Theoretical and Applied Climatology*. 99(3-4): 287–302.

Landsea CW, Knaff JA. 2000. How Much Skill Was There in Forecasting the Very Strong 1997–98 El Niño? Bulletin of the American Meteorological Society 81(9): 2107–2119. DOI: 10.1175/1520-0477(2000)081<2107:HMSWTI>2.3.CO;2.

Laraque A, Ronchail J, Cochonneau G, Pombosa R, Guyot JL. 2007. Heterogeneous distribution of rainfall and discharge regimes in the Ecuadorian Amazon Basin. *J. Hydrometeorol*. *8*(6): 1364-1381.

Lau K-M, Yang S. 2002. Walker circulation. *M. Shankar*, 6 pp. DOI:10.1006/rwas.2002.0450.

Mannig B, Müller M, Starke E, Merkenschlager C, Mao W, Zhi X, Podzune R, Jacob D, Paeth H. 2013. Dynamical downscaling of climate change in Central Asia. *Global and Planetary Change* 110: 26-39.

Mearns LO, Bogardi I, Giorgi F, Matyasovszky I, Palecki M. 1999. Comparison of climate change scenarios generated from regional climate model experiments and statistical downscaling. *J. Geophys. Res*. 104: 6603-6621.

Mellor GL, Yamada T. 1982: Development of a turbulence closure model for geophysical fluid problems. *Rev. Geophys.* 20: 851-875.

Minvielle M, Garreaud RD. 2011. Projecting Rainfall Changes over the South American Altiplano. *Journal of Climate.* 24(17): 4577–4583.

Mlawer EJ, Taubman SJ, Brown PD, Iacono MJ, Clough SA. 1997: Radiative transfer for inhomogeneous atmosphere: RRTM, a validated correlated-k model for the longwave. *J. Geophys. Res.* 102(D14): 16663–16682.

Moeng C-H, Dudhia J, Klemp J, Sullivan P. 2007. Examining two-way grid nesting for large eddy simulation of the PBL using the WRF Model. *Mon. Weather Rev*. 135(6): 2295-2311.

Mora DE, Campozano L, Cisneros F, Wyseure G, Willems P. 2014. Climate changes of hydrometeorological and hydrological extremes in the Paute basin, Ecuadorean Andes. *Hydrology and Earth System Sciences.* 18(2): 631–648. DOI:10.5194/hess-18-631-2014.

Murphy J. 1999. An evaluation of statistical and dynamical techniques for downscaling local climate. *J. Climate* 12: 2256-2284.

Murphy J. 2000. Predictions of climate change over Europe using statistical and dynamical downscaling techniques. *Int. J. Climatol*. 20: 489-501.

Pielke RA, Wilby RL. 2012. Regional climate downscaling: What's the point? *Eos, Transactions American Geophysical Union* 93(5): 52. DOI: 10.1029/2012EO050008.

Pleim JE. 2006: A simple, efficient solution of flux-profile relationships in the atmospheric surface layer. *J. Appl. Meteor. and Clim*. 45: 341–347.

Pleim JE. 2007: A combined local and non-local closure model for the atmospheric boundary layer. Part 1: Model description and testing*, J. Appl. Meteor. and Clim.* 46: 1383–1395.

Rollenbeck R, Bendix J. 2011. Rainfall distribution in the Andes of southern Ecuador derived from blending weather radar data and meteorological field observations. Atmos. Res. 99(2): 277-289.

Rossel F, Mejía R, Ontaneda G, Pombosa R, Roura J, Le Goulven P, Cadier E. 1998. Régionalisation de l'influence du El Niño sur les précipitations de l'Equateur. Bull. Inst. Fr. Etudes Andin. 27(3): 643-654.

Skamarock WC, Klemp JB, Dudhia J, Gill DO, Barker DM, Duda MG, Huang X, Wang W, Powers JG. 2008. A Description of the Advanced Research WRF Version 3. National Center for Atmospheric Research Bouder, Colorado, USA.

Schmidli J, Frei C, Vidale PL. 2006. Downscaling from GCM precipitation: A benchmark for dynamical and statistical downscaling methods. Int. J. Climatology 26(5): 679-689.

Schmidli J, Goodess CM, Frei C, Haylock MR, Hundecha Y, Ribalaygua J, Schmith T. 2007. Statistical and dynamical downscaling of precipitation: An evaluation and comparison of scenarios for the European Alps. J. Geophys. Res. 112(D4): 1-20.

Souvignet M, Gaese H, Ribbe L, Kretschmer N, Oyarzun R. 2010. Statistical downscaling of precipitation and temperature in north-central Chile: an assessment of possible climate change impacts in an arid Andean watershed, Hydrol. Sci. J. 55(1): 41–57. DOI:10.1080/02626660903526045, 2010.

Souvignet M, Heinrich J. Statistical downscaling in the arid central Andes: uncertainty analysis of multi-model simulated temperature and precipitation, Theor. Appl. Climatol. 106(1-2): 229–244. DOI:10.1007/s00704-011-0430-z, 2011.

Sunyer MA, Madsen H, Ang PH. 2012. A comparison of different regional climate models and statistical downscaling methods for extreme rainfall estimation under climate change. *Atmos. Res*. 103: 119-128.

Tao W-K, Simpson J, McCumber M. 1989: An ice-water saturation adjustment. *Mon. Wea. Rev*. 117: 231–235.

Vuille M, Bradley RS, Keimig F. 2000. Climate variability in the Andes of Ecuador and its relation to tropical Pacific and Atlantic sea surface temperature anomalies. *J. Climate* 13: 2520-2535.

Wang W, Bruyère C, Duda M, Dudhia J, Gill D. 2013. ARW Version 3 Modelling System's User Guide 384. National Center for Atmospheric Research, Mesoscale & Microscale Meteorology Division, 411 pp. Retrieved from http://www.mmm.ucar.edu/wrf/users/docs/user_guide_V3/ ARWUsersGuideV3.pdf [October 15, 2012].

Wang W, Seaman NL. 1997. A comparison study of convective parameterization schemes in a mesoscale model. *Mon. Weather Rev*. 125: 252-278.

Wang XL, Feng Y. 2012. Software for data homogenization: RHtestsV3, RHtests_dlyPrcp. Climate Research Division, Science and Technology Branch, Environment Canada.

Retrieved from *http://cccma.seos.uvic.ca/ETCCDMI/software.shtml* [April 14, 2012].

Wang XL. 2008a. Accounting for autocorrelation in detecting mean shifts in climate data series using the penalized maximal t or F Test. *J. Appl. Meteorol. Clim*. 47: 2423-2444.

Wang XL. 2008b. Penalized maximal F-test for detecting undocumented mean-shifts without trend-change. *J. Atmos. Oceanic Tech.*. 25(3): 368-384. DOI:10.1175/2007/JTECHA982.1.

Wei H, Gutowski W, Vorosmarty C, Fekete B. 2002. Calibration and validation of a regional climate model for Pan-Arctic hydrologic simulation. *J. Climate* 15(22): 3222-3236.

Wilby R, Wigley T. 1997. Downscaling general circulation model output: A review of methods and limitations. *Prog. Phys. Geog*. 21(4): 530-548.

6 Climate changes of hydrometeorological and hydrological extremes in the Paute basin

This chapter is published in Hydrology and Earth System Sciences, 2014, 18(2), 631–648.
Received: 30 April 2013 / Accepted: 6 January 2014

Climate changes of hydrometeorological and hydrological extremes in the Paute basin, Ecuadorean Andes

D. E. Mora[1,2], L. Campozano[5,6], F. Cisneros[2], G. Wyseure[4], and P. Willems[1,3]

[1]KU Leuven, Hydraulics Divison, Kasteelpark Arenberg 40, 3001 Leuven, Belgium

[2]Universidad de Cuenca, PROMAS, Av. 12 de abril, Cuenca, Ecuador

[3]Vrije Universiteit Brussel, Department of Hydrology & Hydraulic Engineering, Pleinlaan 2, 1050 Brussels, Belgium

[4]Katholieke Universiteit Leuven, Soil and Water Management Divison, Celestijnenlaan 200E, 3001 Leuven, Belgium

[5]Universidad de Cuenca, Dpto. RR HH y CC Ambientales, Av. 12 de abril, Cuenca, Ecuador

[6]LCRS, Fac. of Geography, University of Marburg, Marburg, Germany

Correspondence to: D. E. Mora (diego.mora@ucuenca.edu.ec)

Received: 30 April 2013 – Published in Hydrol. Earth Syst. Sci. Discuss.: 24 May 2013
Revised: 12 December 2013 – Accepted: 6 January 2014 – Published: 19 February 2014

Abstract. Investigation was made on the climate change signal for hydrometeorological and hydrological variables along the Paute River basin, in the southern Ecuador Andes. An adjusted quantile perturbation approach was used for climate downscaling, and the impact of climate change on runoff was studied for two nested catchments within the basin. The analysis was done making use of long daily series of seven representative rainfall and temperature sites along the study area and considering climate change signals of global and regional climate models for IPCC SRES scenarios A1B, A2 and B1. The determination of runoff was carried out using a lumped conceptual rainfall–runoff model. The study found that the range of changes in

temperature is homogeneous for almost the entire region with an average annual increase of approximately +2.0 C. However, the warmest periods of the year show lower changes than the colder periods. For rainfall, downscaled results project increases in the mean annual rainfall depth and the extreme daily rainfall intensities along the basin for all sites and all scenarios. Higher changes in extreme rainfall intensities are for the wetter region. These lead to changes in catchment runoff flows, with increasing high peak flows and decreasing low peak flows. The changes in high peak flows are related to the changes in rainfall extremes, whereas the decreases in the low peak flows are due to the increase in temperature and potential evapotranspiration together with the reduction in the number of wet days.

6.1 Introduction

The impact of climate change on hydrological systems is receiving higher attention during the last decades due to its consequences on water resources, especially related to droughts and floods (Nijssen et al., 2001; Hirabayashi et al., 2008; Urrutia and Vuille, 2009; Dirmeyer et al., 2012). Changes in rainfall are strongly related to changes in runoff and therefore with water availability (Bradly et al., 2006). Changes in temperature, humidity, and atmospheric pressure are related to changes in evapotranspiration, which is also an important input of the hydrological system. In addition, rainfall intensity is a primary weathering agent for rocks and soils increasing the transport of sediments and dissolved solids to water bodies. Furthermore, hydrological processes at the land surface influence the natural environment at a range of spatial and temporal scales through their impacts on biological activity and water chemistry (Beldring et al., 2008). This is also the case for the Paute River basin in Ecuador, where future climate change might severely impact hydrological and ecological conditions. Especially the water availability is a concern (Ontaneda et al., 2002), due to changes in temperature and humidity and high variability in rainfall extreme events (Parry et al., 2007).

A common methodology to quantify climate change signals makes use of general circulation model or global climate model (GCM) results. These results might, however, be too coarse to provide regional and local details, and should not be used directly for hydrological modeling, especially for regions with a high spatial and temporal variability in climate variables. This is the case of the Paute River basin in the tropical Andes in southern Ecuador (Célleri et al., 2007; Mora and Willems, 2012). One solution is the use of regional climate model (RCM) results, which provides finer-scale information. However, Buytaert et al. (2010) state that for some tropical regions and scales of aggregation, RCM simulations, especially for precipitation, do not necessarily give better results compared with GCM simulations. In addition, Cloke et al. (2013) conclude that the inability of some RCMs to produce realistic precipitation to be used in local climate impact studies for flooding, even in present conditions, is a serious issue. Two available RCM were considered in this study: the Precis Hadley and the Precis Echam (see Table 6.1).

To solve this problem, different statistical downscaling techniques, with different strengths and weaknesses (Fowler et al., 2007) were developed in order to obtain a higher spatial resolution (Giorgi et al., 2001; Hewitson and Crane, 1996). The

application of these downscaling techniques to climate variables as rainfall and temperature may account for the mesoscale hydro-climatologic processes for areas of complex topography. In the study of Maraun et al. (2010), a perfect prognosis statistical downscaling, model output statistics and weather generators were reviewed as an improvement of the representation of rainfall space–time variability. The main uncertainties arise for the representation of extreme precipitation, subdaily precipitation and full precipitation fields on fine scales. Within the statistical downscaling techniques, the delta change or perturbation techniques are developed to translate large-scale GCM/RCM outputs onto a finer resolution based on change factors (Prudhomme et al., 2002; Willems et al., 2012). The change factors consider the differences between control and future GCM/RCM simulations and are applied to observed series.

Taking this state of the art into account, this paper aims to estimate future scenario projections for temperature, rainfall and discharge within the Paute River basin for 2045– 2065. This is done with the application of an adjusted change factor-based statistical downscaling method, the quantile perturbation approach (QPA). The effect of changes in temperature and rainfall are used to estimate changes in discharge for two catchments in the basin. Following sections describe the study area, the data, the adjusted QPA and the evaluation of the approach. This is followed by a section that presents and discusses the climate change impact results. The final section summarizes this study with some concluding remarks.

6.2 Methodology

6.2.1 Study area

The basin of the Paute River is located in the inter-Andean depression separating the western and Cordillera Real in southern Ecuador (Coltorti and Ollier, 2000). With an área of 5066 km^2 and elevation range from 1840 to 4680 m a.s.l., the basin has a vital hydropower plant complex at its downstream end. The upper part of the basin is located only 62 km from the Pacific coast line at its western point. The downstream part of the basin ends in a scattered region between the Andes and the Amazon (Fig. 6.1). For the discharge analysis, two subcatchments within the Paute River basin are analyzed. The catchment of Tomebamba in Monay (To Mo) is located in the western headwaters of the Paute River basin. It has an extension of 1265 km^2 and an elevation range between 2500 and 4680 m a.s.l. The city of Cuenca is located within this catchment with nearly 350 000 inhabitants (the third largest city). The catchments consist mainly of tropical alpine grasslands (páramo) and native forests, agriculture and urban areas. Within the catchment of To Mo, the subcatchment of Matadero in Sayausi (Ma Sa) is located, with an area of 300 km^2 that covers mainly páramo and native forest land use.

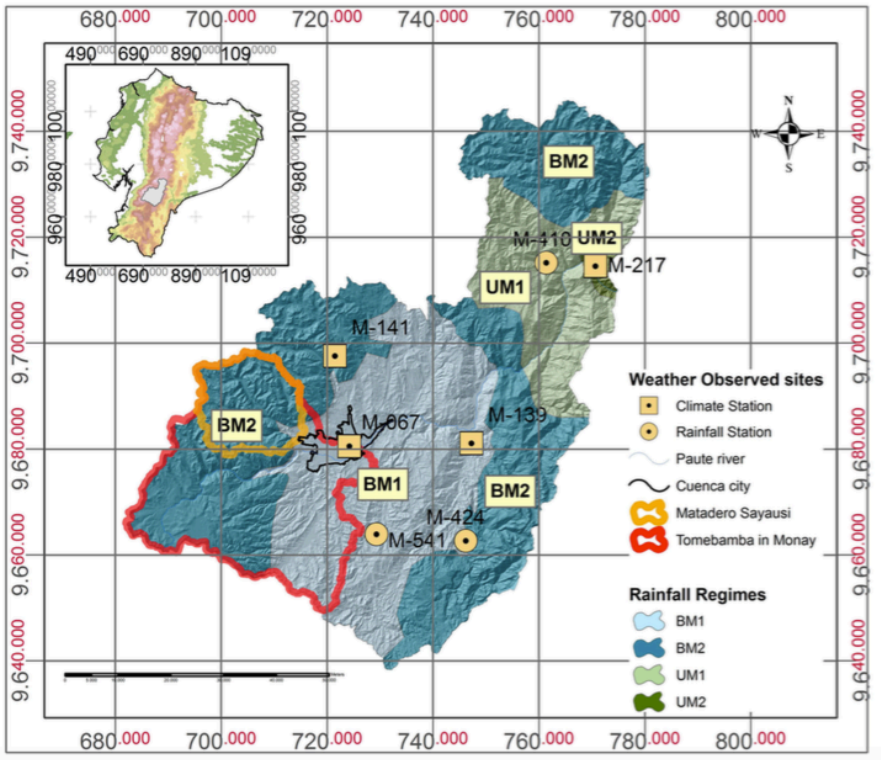

Figure 6-1: Rainfall regimes in the Paute River basin (spatial regions BM1, BM2, UM1 and UM2).

6.2.2 Database

The Paute River basin is one of the most monitored basins in Ecuador. It has rainfall and temperature observation records since 1963 due to its importance in hydropower energy production. For this research, 7 sites located in different rainfall regime regions and at varying elevations were selected. The available data series start near 1962–1964 and continue till 1992–1993 with daily series for rainfall and monthly series for mean temperature. The names and characteristics of these sites are shown in Table 6.1. The available GCM-RCM control and scenario simulations covering Ecuador, which were considered in this study, are shown in Table 6.1. The control runs are available with daily simulation results for the historical period 1961–1990 and the future scenario simulation results for 2045–2065. The simulated future greenhouse gas emissions were based on the IPCC Special Report on Emission Scenario (SRES) for the A1B, A2 and B1 scenarios (Nakicenovic et al., 2000; Solomon et al., 2007).

Table 6-1: GCM/RCM runs for the Ecuadorean region (top), and observed rainfall/temperature sites (bottom).

Model run	Center	Country
1. cccr_bcm2_0	Bjerknes Centre for Climate Research	Norway
2. cccma cgcm3_1	Canadian Centre for Climate Modelling and Analysis	Canada
3. cccma_cgcm3 1 t63		
4. crm_cm3		
5. csiro_mk3_0	Australia's Commonwealth Scientific and Industrial Research Organization	Australia
6. csiro_mk3_5		
7. gfdl_cm2_0	Geophysical Fluid Dynamics Laboratory	USA
8. gfdl_cm2_1		
9. giss_aom	Goddard Institute for Space Studies	USA
10. giss_model_e_r		
11. iap_fgoals1_0_g	Institute of Atmospheric Physics	China
12. ingv_echam4	National Institute of Geophysics and Volcanology	Italy
13. inmcm3_0	Institute for Numerical Mathematics	Russia
14. ipsl_cm4	Institute Pierre Simon Laplace	France
15. miroc3_2_hires	Meteorological Research Institute, Japan	Japan
16. miroc3_2_medres		
17. miub_echo_g	Meteorological Institute, University of Bonn	Germany
18. mpi_echam5	Max-Planck Institute for Meteorology	Germany
19. mri_cgcm2_3_2a	National Institute for Environmental Studies	Japan
20. ncar_ccsm3_0	National Centre for Atmospheric Research	USA
21. ncar_pcm1		
22. Precis Hadley	Hadley Center	UK
23. Precis Echam	Hadley Center/Max-Planck Institute for Meteorology	UK/Germany

Site	Name	Elevation	Region
M410	Rio Mazar-Rivera	2600	UM1
M217	Penas Coloradas	2000	UM2
M139	Gualaceo	2360	BM1
M067	Cuenca Aeropuerto	2516	BM1
M424	Sigsig INAMHI	2600	BM2
M141	El Labrado	3260	BM2
M541	Cochapamba–Quingeo	2760	BM1

6.2.3 Perturbation or delta approach

The perturbation approach is the most common method to transfer the signal of climate change from a climate system level represented by climate models to the hydrological system level represented by hydrological models (Middelkoop et al., 2001; Andréasson et al., 2004; Nguyen et al., 2007; Olsson et al., 2012; Willems et al., 2012). This method is applied to the most relevant climate variables in hydrology, notably rainfall, temperature and ET_0. In its most simple form, monthly perturbation factors (PF), Eqs. (1) and (2), are determined and applied to the input series of hydrological models:

$$T_{F,daily} = T_{ob,daily} + (T_{CMF,monthly} - T_{CM20th,monthly}) \quad (1)$$

$$P_{F,daily} = P_{ob,daily} * (P_{CMF,monthly} / T_{CM20th,monthly}) \quad (2)$$

where T_{ob} and P_{ob} are the observed temperature and rainfall values in the series, T_{CM20th} and P_{CM20th} the 20th century climate model control run results, T_{CMF} and P_{CMF} the projected future climate model results and T_F and P_F the projected future results after perturbation.

However, some of the disadvantages of this method include the assumption of no shift in the shape and type of changes. Extremes are indeed modified by the same factor as the other events. In addition, the assumption of no change in the number or the frequency of events is another disadvantage (Harrold and Jones, 2003).

The adjusted perturbation approach considers a climate change signal on both the number of wet or dry days and on the rainfall intensity. The change in the rainfall intensity is calculated in a quantile-based way, making use of a quantile mapping technique (Nguyen et al., 2008; Ntegeka and Willems, 2008; Willems and Vrac, 2011) hence with the PF depending on the exceedance probability. The method is applied with a relative PF or an absolute shift in the rainfall intensity, depending on whether relative or absolute changes are applied.

The change in wet day frequency is calculated as the ratio of the number of wet days for the scenario period (2045– 2065) over the number of wet days for the control period (1961–1990) considering that a wet day is any day with rainfall depth above a certain daily rainfall intensity threshold (wd_th). The PF on the wet day frequency (PF_{wf}) is > 1 when the scenario series have more wet days than the control series and PF_{wf} is < 1 when dry days should be added (or wet days should be removed) from the observed series.

Once the PF_{wf} is obtained, the PF on the wet day rainfall intensity (PF_{ri}) is determined in a quantile-based way by comparing ranked daily extremes from the control period vs. the scenario period. Instead of using a unique PF for all events, the rainfall intensity PF is obtained dependent on the empirical exceedance probability of the intensity (see Fig. 6.2). However, the application of a relative intensity PF on observed values close to zero will produce signal changes near to zero even if the PF is high, or vice versa, small absolute changes between scenario and control values might lead to excessive PF when the control value is close to zero. Therefore the inclusion of an absolute change applied

to rainfall intensities α under a threshold exceedance probability is considered in the adapted methodology. For high rainfall intensities corresponding to exceedance probabilities below p(α), a relative rainfall intensity PF is applied. For rainfall intensities corresponding to exceedance probabilities above p(α) the rainfall intensity change is derived by calculation of a weighted average of the relative and absolute rainfall intensity changes. The weighting factor varies linearly between p(α) and p(0), where p(0) is the exceedance probability of the ranked rainfall intensities equal to the wet day threshold on the observed series (see Fig. 6.3). In case $PF_{wf} > 1$, wet days need to be added to the observed series to obtain perturbed series. The intensities of these days are taken from the absolute change in rainfall intensity corresponding to exceedance probabilities above p(0). For the addition of the different wet/dry days, the wet/dry spells are first identified in the observed series and ranked per month according to rainfall volume and duration of the different spells. In the case new days need to be added, the first wet day will be added at the end of the highest/longer rainfall volume/duration wet spell. A second day will be added at the end of the second highest/longer spell and so on. In case that a dry day is added, a wet day rainfall intensity will be changed to zero at the end of the lowest/shorter rainfall spell. In case the number of new wet or dry days is higher than the number of wet or dry spells, the addition of new days will start again in the ranked spells.

This method solves the above mentioned problem related to the application of a relative PF to low rainfall intensities and allows to determine the rainfall intensity values of the additional wet days.

6.2.4 Rainfall–runoff model

The downscaled future series of rainfall and evapotranspiration were used for the study of the climate change impact on river discharges based on a calibrated lumped conceptual model with emphasis on the peak flows. The model has been implemented using the generalized lumped conceptual and parsimonious model-structure identification and calibration (VHM) approach of Willems (2000, 2014) and Willems et al. (2014). The model was previously calibrated and validated for the To Mo and Ma Sa catchments (Célleri et al., 2010), and previously applied for hydrological climate change or variability impact analysis by Taye et al. (2011), Liu et al. (2011), Van Steenbergen and Willems (2012) and Taye and Willems (2013).

The equations of Penman–Monteith (Penman, 1948; Monteith, 1965) were used to estimate future evapotranspiration (ET_0) series considering the future temperature series previously described. For the calculation of ET_0, future series of maximum, mean and minimum air temperature were applied. Future catchment rainfall and ET_0 were estimated with the downscaled climate model output series at each site and lumped at catchment scale by interpolation using the inverse distance squared method. However, attention must be paid to the moment of using the estimated future ET_0 series. The Penman–Monteith equation involves other parameters than temperature, which were not taken into account in this research and therefore were kept constant. Future series of solar radiation, humidity and wind speed, among others, may have an influence on the future ET_0 as well. According to Vuille et al. (2003), humidity and convective cloud cover tend to increase in the region. This might have an impact on the future ET_0, increasing discharge peaks and reducing the frequency of low flows.

6.2.5 Impact indicators

In order to evaluate the impact of the different climate scenario projections on temperature, rainfall and runoff, few statistics are used as impact indicators. These indicators summarize the changes between historical and future conditions. To evidence the influence of the downscaling technique, the indicators are first calculated based on the GCM-RCM results, considering changes between the future and the control period series. Subsequently, the high climate variability along the study area, for both temperature and rainfall, are described in function of these indicators. Finally, the impact indicators based on the GCM-RCM outputs are compared against the impact indicators derived from the downscaled series. This comparison is for the future projections based on the SRES scenario A2, as results from one RCM is also available for this scenario. Based on the analysis of the indicators, the influence of the local site specific properties, the statistical downscaling technique and the interaction with the changes projected by the climate model simulations is studied.

The impact indicators considered in this study focus on the change in annual and monthly mean values, in the frequency of wet–dry days, and in annual and daily values at different quantiles. The change in the frequency accounts the change in the number of wet days. A wet day is any daily rainfall depth higher than or equal to 0.5 mm. The changes at different quantiles allow identifying the dependency of the changes with the probability of no exceedance (p.n.e.). For rainfall, quantiles are considered for 100, 99, 97, 95 and 90 p.n.e. This allows the changes to be analyzed for extremes.

For temperature, the quantiles are considered for 100, 75, 50, 25 and 0 p.n.e. also called quartiles (Max, Q_3 , Q_2 , Q_1 , Min). These impact indicators are calculated at each site for the ensemble of all GCM-RCM control and scenario run combinations and for the three future scenarios A1B, A2 and B1. Figure 6.4 shows, as an example, the impact indicators for rainfall change for scenario A2 at site M067. In the results and discussion section, results of the ensemble models are averaged.

6.3 Results and discussion

This section reports on the change in the downscaled series for temperature and rainfall at the seven sites previously described, and the change in runoff for the To Mo and Ma Sa catchments.

6.3.1 Spatio-temporal patterns from the observed series

The observed series of rainfall and temperature show the presence of high spatial and temporal variability within the region for both variables. Table 6.2 shows some properties of temperature and rainfall at the observed sites. The spatial variability in temperature is explained by its correlation to elevation. Sites at higher elevations present lower temperatures than sites at lower elevations. The temperature gradient is ca. 0.6 C per 100 m increase in elevation. Figure 6.5 shows the spatio-temporal patterns in monthly averages within the Paute River basin based on the sites. There is a small temporal variability in temperature throughout the year. Warmer months are found during DJF and colder months during JJA. The seasonal distribution of temperature is similar at all sites, but with different magnitudes. The same is valid for the distribution of quantiles.

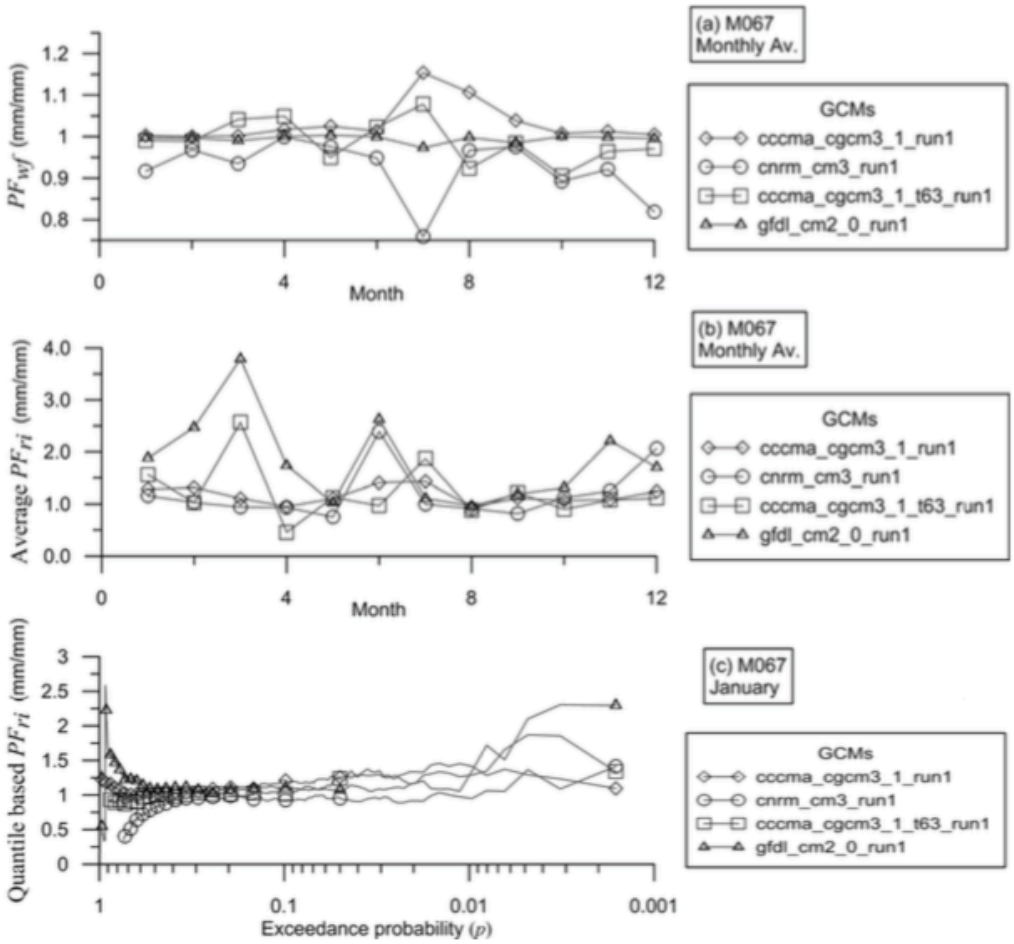

Figure 6-2:(a) Perturbation factor of the wet day frequency PF_{wf}, (b) perturbation factor of the rainfall intensity PF_{ri} averaged for each month and (c) quantile-based PF_{ri} for January in site M067 for the four selected GCM runs.

To explain the variability in rainfall, Célleri et al. (2007) and Mora et al. (2012) classified the basin in four rainfall regime regions according to the annual rainfall distribution (see Fig. 6.1). Two rainfall regimes show a bimodal rainfall distribution, BM1 and BM2. BM1 is highly marked with two wet seasons during May-March-April (MMA) and September-October-November (SON), and two dry seasons during June-July-August (JJA) and December-January-February (DJF) and with annual rainfall depths between 700 and 900 mm (Fig. 6.5). Region BM2 presents a less notable bimodal annual distribution, but in similar to BM1. The annual rainfall depth for the BM2 region is about 1000 mm. This region corresponds to the upstream part of the Paute basin, having páramo soils. The bimodal annual cycle is determined by the displacement of the intertropical convergence zone (ITCZ). In addition, rainfall regimes BM1 and BM2 are influenced by Pacific Ocean airstreams and the anticyclone from the south. The first one is a west–east direction current with two main rainy periods during February and March and other less intense rainy periods in October and November. The El Niño phenomena have a major impact on this current. The anticyclone from the south is present during the south winter (JJA) and prevents precipitation in the southern part

of the basin. The more uniform annual rainfall distribution for region BM2 is influenced by raising of coastal moisture along western Andes slopes.

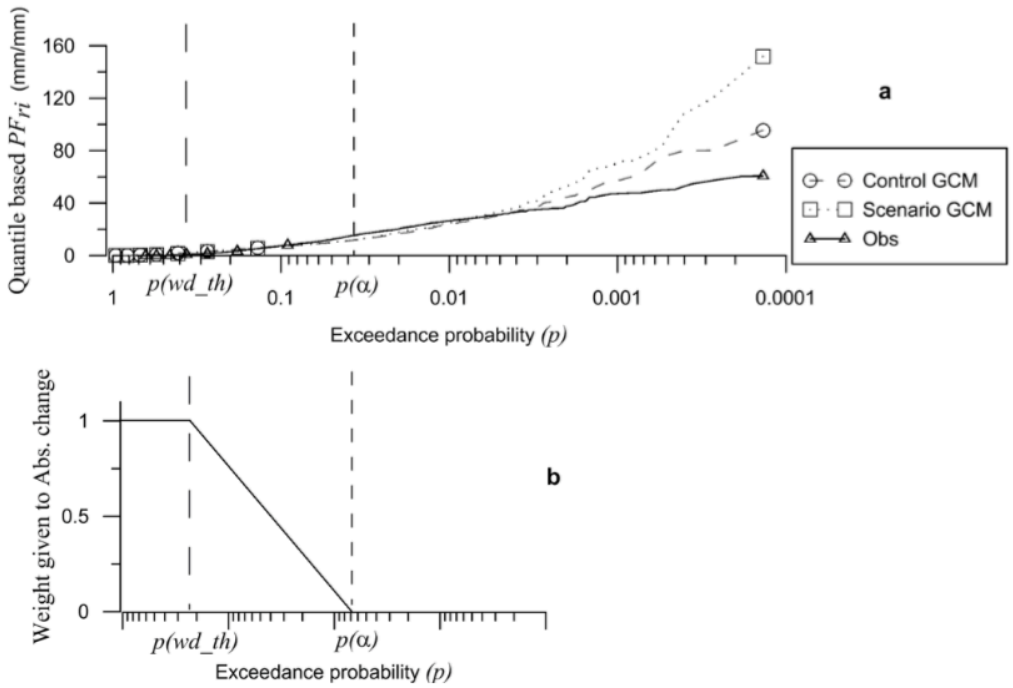

Figure 6-3:(a) Illustration of the second adjustment to the QPA including an exceedance probability threshold value p(α) for site M067 and GCM run cnrm_cm3_run1; (b) relative weight given to absolute change (vs. relative change).

Regions UM1 and UM2 are located in the downstream eastern part of the basin (Fig. 6.1). These regions are close to the tropical forest influence and to the easterly continental low level jet during austral winter (JJA), (Garreaud, 2009). This results in high annual rainfall depths of ca. 1300 mm for UM1 and 3000 mm for UM2. The annual distribution shows a single wetter season during JJA.

Table 6.1 shows that the ratio of the number of wet days over the total number of days is 0.4 for sites located at BM1 (M067, M139), 0.6 for sites at UM1 (M410), 0.8 for sites at UM2 (M217) and 0.85 for BM2 (site M141). This means that region BM2 has the highest number of wet days in the basin, even more wet days than regions UM1 and UM2 that are influenced by the tropical forest. As annual and monthly magnitudes vary from site to site, variability is also high for extreme events. High rainfall intensities (quantile Q_{100}) of about 100 mm day^{-1} are found in site M217 (UM2). For sites located in regions BM1 and BM2, Q_{100} quantile have daily intensities up to about 60 mm day^{-1}. The rainfall distribution shows that high intensities occur at Q_{100} and Q_{99}. For all sites the rainfall intensity at Q_{100} is about two times than at Q_{99} , and reduces strongly towards Q_{95} . Sites M141 and M217 have the highest extreme intensities. Regions UM1 and UM2 are influenced by the Amazon airstream, which is a current that enters the basin from the east–west and is related to periods of higher rainfall between March and October.

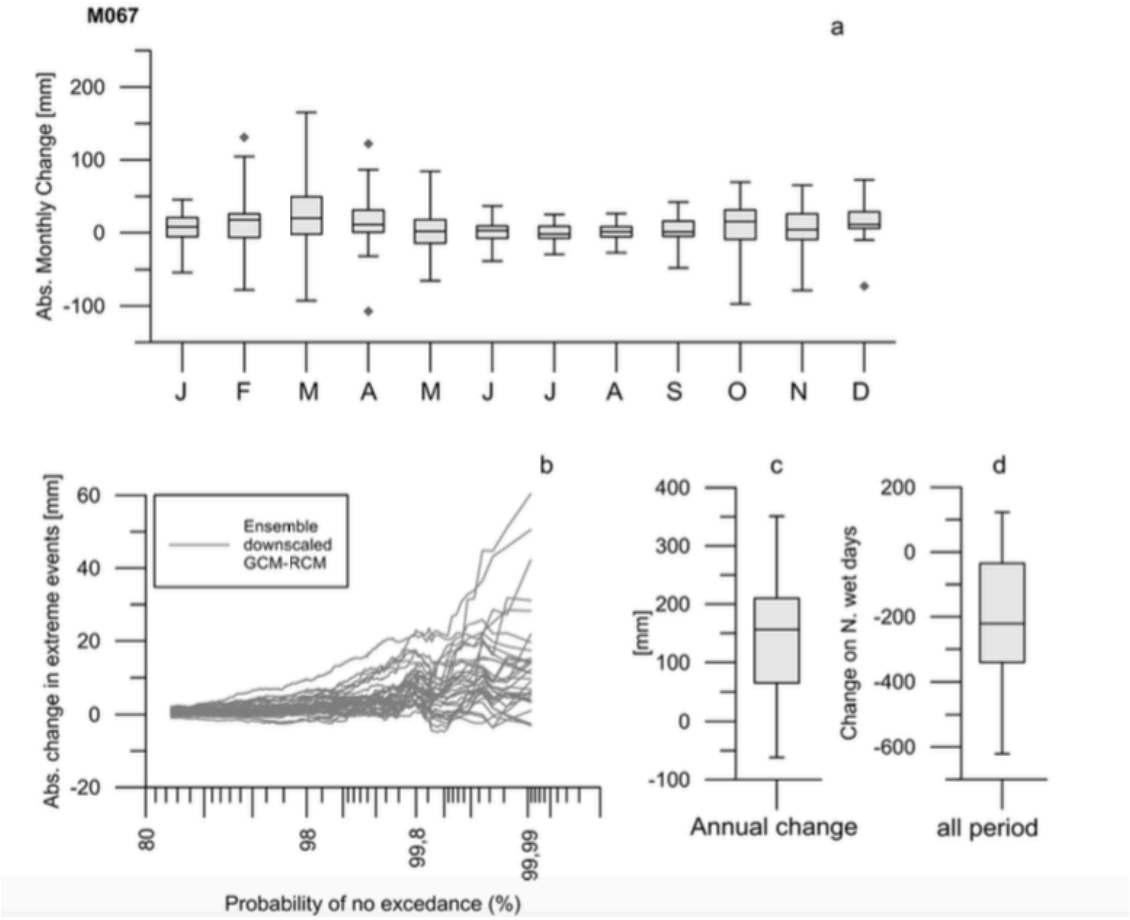

Figure 6-4: Example of the impact indicators for downscaled rainfall change in site M065 (scenario A2). (a) Change of monthly rainfall depths, (b) change of rainfall depths at extreme quantiles, (c) change of annual rainfall depths and (d) change in the number of wet days.

6.3.2 Impact indicators from the GCM-RCM series

The different impact indicators were first calculated for the changes resulting directly from the climate model simulations, hence without the influence of statistical downscaling.

Table 6.3 shows that all sites in the basin have a similar change in mean annual temperature. This change is approximately +2.0 C on average for all GCM simulations. Results from individual GCM simulations may, however, differ from that average; they range between +1.1 and +2.9 C. However, note that the change is the same for sites M067 and M541 and for M141 and M410 because they share the same pixel for most of the GCMs. The different GCM simulations also report similar annual average temperatures for all sites (23 C). This is opposed to the spatial temperature variations we reported in Sect. 3.1. Due to the coarse resolution of the GCMs, the spatial variability because induced by the topographical variations is indeed not accounted for. This is different for the RCMs, where different pixels cover the spatial variability hence is better described by these regional models. However, when the simulation results are evaluated for the RCM Precis_echam model (not shown), the projected changes are approximately the same (+2.6 C) for all sites. This change is about the same as for the Echam GCM (+2.5 C). It shows that the changes (not the absolute values) are primarily

controlled by the GCM in which the RCM is nested. A similar conclusion was formulated by Wood et al. (2004), ho stated that a dynamical downscaling step does not lead to large improvement in retrospective hydrological simulation relative to the direct use of the GCM output. However, climate dynamics are intrinsically more detailed in RCMs and we believe that the use of RCM outputs should be considered in further research.

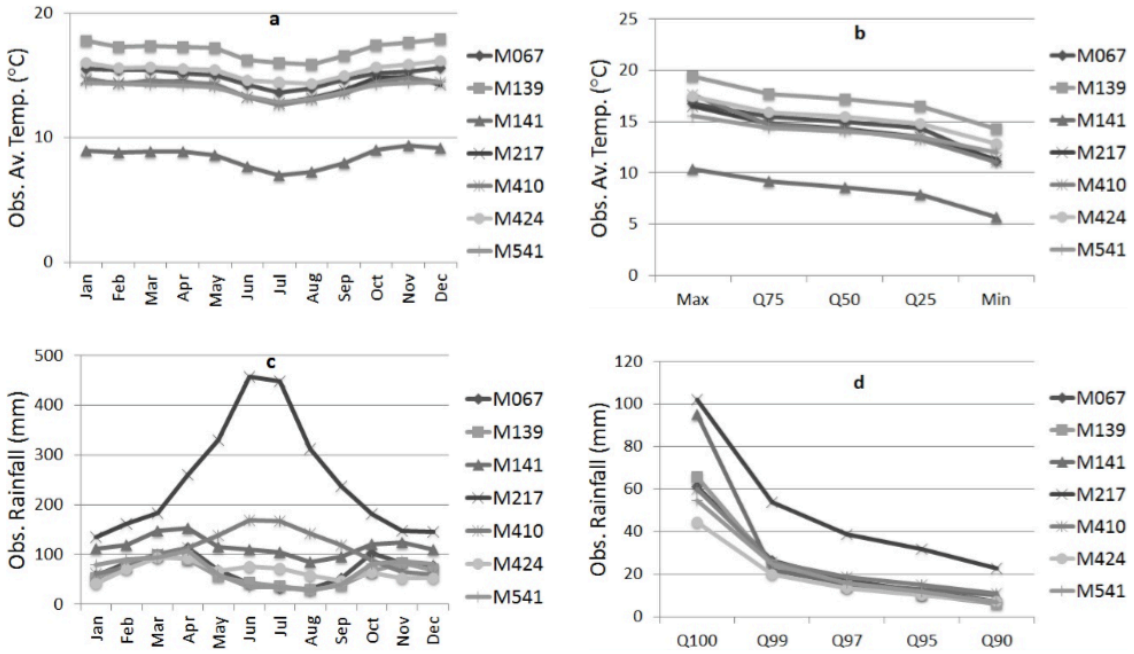

Figure 6-5: Temperature and rainfall properties at observed sites (1960 – 1990). (a) Monthly average temperature distribution, (b) monthly temperature for different quantiles, (c) monthly rainfall depth distribution, (d) daily rainfall depths for different quantiles.

Temporal analysis of the monthly temperature (Fig. 6.6) shows higher changes in the monthly temperatures for the colder months June-July-August (JJA) (on average +2.3 C) and lower changes for the warmer months December-January-February (DJF) (on average +1.9 C). The changes for different quantiles show that most GCMs predict higher changes at higher temperatures. For the highest temperature monthly quantiles the changes are about +2 C, whereas for the lowest monthly quantiles the temperature changes are about +1.6 C in all sites. The temporal distribution of temperature is similar for all sites, not only for the temporal changes but also for the absolutes temperature magnitudes. This again differs from the observed series, where higher spatial differences are noted (see Sect. 3.1).

Table 6-2: Observed mean annual temperature and rainfall, quantiles of monthly temperature, quantiles of daily rainfall depths, and number of wet/dry days at the observed sites during the control period (1960 – 1990).

Temperature (C)		Quantiles				
Site	Year	Max	Q3	Q2	Q1	Min
M067	14.9	16.8	15.5	15	14.4	11.1
M139	17.1	19.4	17.7	17.2	16.5	14.3
M141	8.4	10.4	9.2	8.6	7.9	5.7
M217	14.1	16.5	14.8	14.3	13.5	11.3
M410	14	17.6	14.7	14.2	13.3	11.1
M424	15.3	17.5	15.9	15.5	14.8	12.9
M541	13.9	15.6	14.4	14	13.5	12

Rainfall (mm)		Frequency			Quantiles				
Site	Year	Nwet days	Ndry days	Ratio Nw /Ntot	Q100	Q99	Q97	Q95	Q90
M067	840	2800	4505	0.4	61.1	26.5	17.2	12.2	7.4
M139	736	2693	4612	0.4	65.7	24.2	14.5	10.7	6.2
M141	1392	6296	1009	0.9	95.3	22	15.6	13.2	10
M217	2997	5823	1482	0.8	101.9	53.9	38.8	31.8	22.6
M410	1296	4161	3144	0.6	60	25.6	18.8	15.1	10.8
M424	784	2951	4354	0.4	44.5	20	13.4	10.2	7.1
M541	813	2969	4336	0.4	54.6	24.7	15.7	11.9	6.8

Results for rainfall change (Table 6.3 and Fig. 6.6) are similar to those for temperature. The high rainfall variability is not described by the GCMs. The control and scenario series give similar annual rainfall depths for all sites. These result in a homogeneous annual rainfall change of about 102 mm on average for all GCM simulations. The annual rainfall change for individual GCM simulations ranges between 203 and 327 mm. In contrast to the case of temperature, annual rainfall depth changes projected by the RCM Precis_echam differ much from site to site (not shown). This is different from the spatially homogenous changes in the results of the Echam GCM, in which the RCM is nested, about (+72 mm) for all sites. However, it is seen that the annual rainfall depths projected by the RCM during the control period differ strongly from the observed depths. The RCM projects increases in annual rainfall depths between +175 and +650 mm for sites located in the BM1 and BM2 rainfall regions and +1285 mm for region UM1. However, for site M410 located in region UM2, the model predicts a change of 1450 mm. More details about the performance of GCMs compared with observed series for this study area can be found in Mora et al. (2012).

Table 6-3: Impact indicators for temperature and rainfall output series of GCM-RCMs without downscaling for 2045 – 2065, scenario A2.

Temperature	Annual	Abs. Change	Abs. changes quantiles [C]				
	mean	on annual mean					
Site	[C]	[C]	Max	Q3	Q2	Q1	Min
M067	22.5	2	2	2	2	2	1.6
M139	22.4	2.1	2.2	2.1	2.1	2.1	1.8
M141	22.6	2	2.3	2	2	2	1.7
M217	22.6	2	2.3	2	2	2	1.7
M410	22.5	2	2.3	2	2	2	1.7
M424	22.5	1.9	2	2	2	2	1.5
M541	22.5	2	2	2	2	2	1.6

Rainfall	Annual	Abs(rel) change	Frequency			Abs. changes in quantiles [mm]				
	mean	annual mean	Nwet	Ndry	Ratio					
Site	[mm]	[mm] ([%]) days	days	Nw /Ntot		Q100	Q99	Q97	Q95	Q90
M067	2030	104 (5.4)	5210	2095	0.7	11	2.6	1.5	1	0.8
M139	2030	104 (5.4)	5232	2073	0.7	11	2.6	1.5	1	0.8
M141	2135	104 (5.0)	5649	1656	0.8	9.9	2.6	1.4	0.9	0.6
M217	2135	101 (5.0)	5649	1656	0.8	9.9	2.6	1.4	0.9	0.6
M410	2135	101 (5.0)	5650	1655	0.8	9.9	2.6	1.4	0.9	0.6
M424	2030	102 (5.4)	5232	2073	0.7	11	2.6	1.5	1	0.8
M541	2030	104 (5.4)	5232	2073	0.7	11	2.6	1.5	1	0.8

The change in monthly rainfall depths is similar for all sites. The GCMs project nearly no change (ca. +5 mm) during JJA and negative changes (ca. 45 mm) for SON at all sites. The change in the frequency of events shows for all sites an increase in the number of wet days. This increase is similar for all sites. The ratio of the number of wet days over the total number of days is about 0.7. The RCM presents different ratios depending on the site, although these values again differ from the observed ones. Sites located in the eastern region (M424, M410, M217, M139) are projected with a higher increase in the number of wet days (ratio ≈ 0.9), independent of the rainfall regime region. In contrast, sites located in the western part of the basin (M067, M141, M541) have a lower increase in the number of wet days (ratio ≈ 0.55). Changes in extreme daily rainfall quantiles are spatially homogeneous for most GCM simulations with relatively low changes (about +10mm day^{-1}). No significant changes are projected at the 99% quantile (about +2.5 mm day^{-1}). The spatial pattern of changes in quantiles again differs from the pattern of the observed quantiles. There is no need to have both patterns the same, because changes are controlled by large-scale circulation whereas absolute rainfall values are more affected by local (topographical) conditions. However, also the absolute rainfall results differ much from the observed values, and some changes are

inconsistent with the observations. The RCM-based change in annual rainfall depth of 1450 mm at site M410 is for instance higher than the observed annual rainfall depth of 1300 mm at that site. That climate models are less reliable in the simulation of precipitation than temperature has been reported by many researchers (Parry et al., 2007; Buytaert et al., 2010). This does, however, not mean that the climate model results for precipitation cannot be trusted. The change signal from both, GCM and RCM simulations, are mainly greenhouse gas scenario driven. Transferring this signal to the local-scale changes is one of the aims of statistical downscaling. Converting the coarse spatial-scale precipitation from GCM-RCMs to the local scale by making use of local observations is proposed with the present downscaling technique. These local observations are expected to intrinsically reflect the effect of local, mainly topography driven, small-scale conditions.

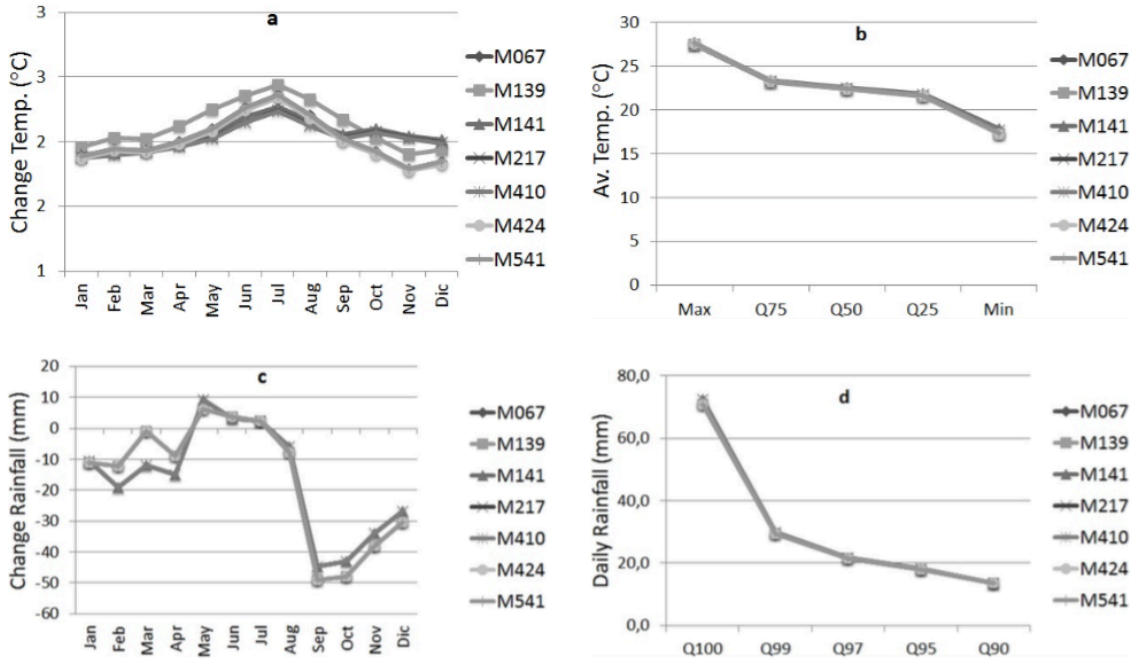

Figure 6-6:Temperature and rainfall properties obtained from the average of ensemble GCM-RCM simulations (2045 – 2065). (a) Monthly average temperature distribution, (b) monthly temperature for different quantiles, (c) monthly rainfall depth distribution, (d) daily rainfall depth for different quantiles.

6.3.3 Impact indicators from the downscaled series

The same impact indicators but applied to the downscaled observed versus the observed series are shown in Tables 6.4 and 6.5 and Fig. 6.7.

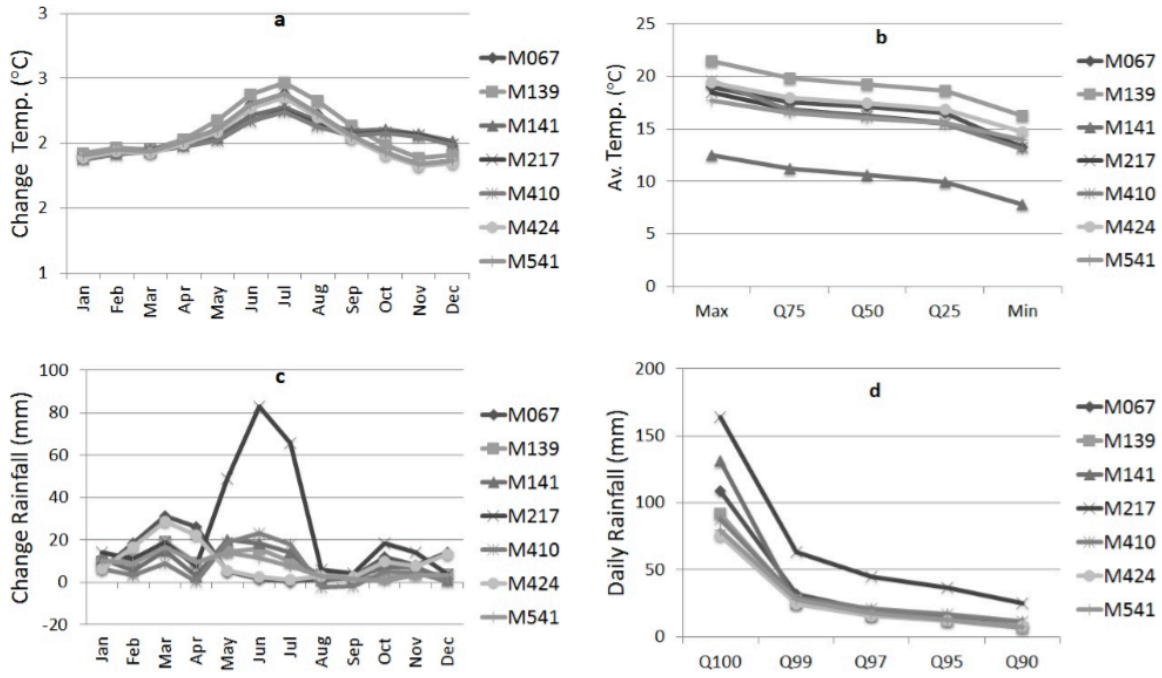

Figure 6-7: Temperature and rainfall properties obtained from the average of ensemble downscaled series (2045 – 2065). (a) Monthly average temperature distribution, (b) monthly temperature for different quantiles, (c) monthly rainfall depth distribution, (d) daily rainfall depth for different quantiles.

Similar to the changes obtained directly from the climate models, the changes in downscaled mean annual temperature show a spatially uniform value of about +2.0 C on average for all sites. The individual GCM simulations give changes that range between +0.4 and +2.9 C. Also based on the RCM model results, no strong spatial variation in these changes is found. Moreover, the temporal variations in mean monthly temperature changes after statistical downscaling are similar to those obtained from the climate model outputs. They show higher changes of about +2.3 C during colder months (JJA), and lower changes of about +1.9 C for DJF. The monthly temperature quantile distribution, however, differs from site to site. This is in contrast to the temperature quantile distributions projected by the climate models. In addition, the monthly quantile distributions of downscaled temperature are close to those derived from the observed series, whereas the climate model outputs show a less uniform temperature distribution. It is expected that this is due to the influence of the topographical variations on the local temperature dynamics. Because this influence is reflected in the observed series, it is also transferred to the statistically downscaled series, as opposed to the non-downscaled series. However, the change in temperature quantiles is again approximately the same (+2.0 C) for all sites. This is due to the fact that the changes in temperature are mainly controlled by the changes in the large-scale circulation (GCM outputs), as discussed before in Sect. 3.2.

Table 6-4: Impact indicators for temperature and rainfall downscaled output series for 2045 – 2065, scenario A2.

Temperature	Annual mean	Abs. Change on annual mean	Abs. changes quantiles [C]				
Site	[C]	[C]	Max	Q3	Q2	Q1	Min
M067	17	2	2.1	2.1	2.1	2.1	2.2
M139	19.2	2.1	2	2.1	2	2.1	2
M141	10.5	2.1	2.1	2	2	2	2.1
M217	16.2	2	1.9	2	2	2.1	2
M410	16.1	2	1.9	2	1.9	2.2	2
M424	17.4	2	2	2	2	2	1.8
M541	16	2	2.1	2.1	2	2	1.9

Rainfall	Annual mean	Abs(rel) change annual mean	Frequency			Abs. changes in quantiles [mm]				
Site	[mm]	[mm] ([%]) days	Nwet days	Ndry Nw /Ntot	Ratio	Q100	Q99	Q97	Q95	Q90
M067	967	127 (15.1)	2518	4787	0.3	48.1	5.4	2.4	2	0.7
M139	841	105 (14.3)	2448	4857	0.3	25.9	2.7	1.6	1.2	0.7
M141	1497	105 (7.5)	5747	1558	0.8	35.9	3.1	2	1.4	0.7
M217	3292	295 (9.8)	5444	1861	0.7	62.2	9.5	5.9	4.7	2.8
M410	1381	84 (6.5)	3779	3526	0.5	27.7	3.4	2.1	1.7	0.9
M424	903	120 (15.3)	2688	4617	0.4	30.9	4.6	2.3	1.8	0.7
M541	902	79 (9.8)	2664	4641	0.4	25.2	2.9	1.6	1.1	0.7

When the downscaled series of temperature are compared among the different scenarios, no significant differences are found between scenario A1B and A2 and annual average temperature changes remain approximately constant (+2.0 C) for the different sites. However, annual average temperature changes projected for scenario B1 indicate a low increase compared to the other scenarios (+0.5 C). This will have an effect on the runoff changes, as discussed in the next section. Changes in the temperature quantile distributions are similar (ca. +2.0 C for scenarios A1B and A2, and ca. +0.5 C for scenario B1). All scenarios project higher changes for colder months and lower changes for warmer months.

Table 6-5: Impact indicators for temperature and rainfall downscaled output series for 2045 – 2065, scenarios A1B and B1.

Temperature		Annual mean	Abs. Change on annual mean	Abs. changes quantiles [C]				
Sc.	Site	[C]	[C]	Max	Q3	Q2	Q1	Min
A1B	M067	16.9	2.0	2.2	2.1	2.0	2.0	2.1
A1B	M139	19.1	2.0	2.0	2.1	2.0	2.0	1.9
A1B	M141	10.5	2.0	2.1	2.0	2.0	1.9	2.1
A1B	M217	16.1	2.0	2.0	2.0	2.0	2.0	1.9
A1B	M410	16.1	2.0	2.0	2.0	1.9	2.1	1.9
A1B	M424	17.4	2.0	2.0	2.1	2.0	2.0	1.9
A1B	M541	15.9	2.0	2.2	2.1	2.0	2.0	1.9
B1	M067	15.6	0.7	1.8	0.7	0.6	0.6	0.8
B1	M139	17.5	0.4	0.4	0.5	0.4	0.4	0.3
B1	M141	8.9	0.5	0.6	0.4	0.4	0.4	0.6
B1	M217	14.6	0.5	0.4	0.4	0.5	0.5	0.6
B1	M410	14.5	0.5	0.4	0.4	0.4	0.6	0.4
B1	M424	15.8	0.5	0.5	0.5	0.4	0.5	0.4
B1	M541	14.3	0.4	0.5	0.4	0.4	0.4	0.4

Rainfall		Annual mean	Abs(rel) change annual mean	Abs. changes in quantiles [mm]				
Sc.	Site	[mm]	[mm] ([%]) days	Q100	Q99	Q97	Q95	Q90
A1B	M067	923	82 (9.8)	30.3	2.5	1.1	1.1	0.6
A1B	M139	817	81 (11.0)	19.9	2.4	1.2	0.9	0.6
A1B	M141	1498	106 (7.6)	22.0	2.9	2.1	1.4	0.8
A1B	M217	3249	252 (8.4)	50.2	10.9	5.4	3.8	2.3
A1B	M410	1415	119 (9.2)	19.2	4.0	2.2	1.8	1.0
A1B	M424	874	91 (11.6)	27.4	3.8	1.9	1.5	0.6
A1B	M541	891	78 (9.6)	18.4	2.2	1.5	1.0	0.6
B1	M067	921	81 (9.6)	27.9	2.6	1.3	1.5	0.7
B1	M139	796	61 (7.6)	18.6	1.4	0.8	0.6	0.5
B1	M141	1463	71 (4.9)	17.5	1.7	1.2	0.8	0.4
B1	M217	3245	248 (7.6)	53.5	11.0	6.6	4.4	2.3
B1	M410	1370	73 (5.4)	15.0	1.9	1.2	1.3	0.6
B1	M424	847	64 (7.5)	22.2	1.9	1.3	1.3	0.6
B1	M541	870	57 (6.6)	19.5	1.4	1.0	0.6	0.5

For rainfall, the effect of the statistical downscaling is more evident than for temperature. The projected annual rainfall depths differ from site to site. In addition the changes are less homogenous as was the case for the direct results of the climate models. For instance, sites M541 and M217 project positive changes in annual rainfall depths of +79 and +295 mm, respectively. In contrast to the climate model outputs,

the downscaled rainfall series show heterogeneous changes in monthly rainfall depths, following the patterns found at observed series (Sect. 3.1). The spatio-temporal patterns of the rainfall changes follow the bimodal or unimodal distributions, with higher changes are projected for wetter months and lower changes (decreasing depths in some cases) for drier months. The frequencies of wet/dry days differ from those projected by the climate model outputs. The ratio of the number of wet days over the total number of days is 0.35 at sites M067, M139 (BM1), 0.5 at site M410 (UM1), 0.75 at site M217 (UM2) and 0.8 at site M141 (BM2). This is similar to the frequencies obtained from the observed series. Also the quantile distributions derived from the downscaled series are closer to the quantile distributions derived from the observed series. This is the result of the intrinsic climate bias involved in the selected QPA statistical downscaling method. When rainfall changes are analyzed, extreme quantile changes are also different than those projected by the climate model outputs. Higher changes are projected at higher intensities. The 100 % quantiles project the highest changes. These changes vary in magnitude depending on the location (i.e. +62 mm for site M217 and +25 mm for site M541). The 99 % quantiles, in contrast to those obtained from the direct output of GCM/RCMs, still show significant changes.

Table 6-6: Absolute (relative) change in annual runoff quantiles for the To Mo and Ma Sa catchments, all scenarios.

Change in runoff depth [mm /day] ([%])						
Scenario	Site	Min	Q1	Average	Q3	Max
A1B	To Mo	-0.05 (-38)	-0.01 (-0.4)	0.12 (7.7)	0.19 (9.4)	3.19 (45)
A2	To Mo	-0.07 (-50)	-0.02 (-2.2)	0.17 (10.5)	0.27 (13.7)	4.84 (68)
B1	To Mo	-0.05 (-34)	0.01 (1.2)	0.13 (8.6)	0.21 (10.6)	2.89 (41)
A1B	Ma Sa	-0.12(-39)	0.07 (3.7)	0.34 (11.9)	0.50 (14.3)	4.23 (34)
A2	Ma Sa	-0.16 (-51)	0.03 (1.3)	0.34 (12.0)	0.53 (15.2)	5.33 (43)
B1	Ma Sa	-0.13 (-41)	0.03 (1.4)	0.21 (7.4)	0.31 (8.8)	2.91 (24)

The rainfall increase depends on the scenario and the site. The highest absolute increase is projected for site M217 (ca. +250 mm) for all scenarios, whereas site M541 shows the lowest increase (< +80 mm) for all scenarios. The temporal pattern of changes in the different scenarios is similar. There is a higher rainfall increase for wet periods and a lower increase for the dry periods. However, when relative changes in rainfall are analyzed, higher changes occur in sites located in the middle part of the basin, that is, sites M067, M139 and M424 with relative changes of ca. 10, 15 and 8 % for scenarios A1B, A2 and B1, respectively (see Fig. 6.8). When the frequency of wet/dry days is compared to those obtained from the observed series, a reduction in the number of wet days is found for all sites and for all scenarios. The projected increase in annual and monthly rainfall depths thus is due to increasing rainfall intensities for the remaining wet days. Scenario A2 is the scenario that shows the higher reduction in the number of wet events and the higher increase in annual and monthly rainfall depths versus the other scenarios.

The changes in quantiles indicate that the more extreme events are affected by higher rainfall increases. Sites M217, M424 and M067 show the highest increases in the rainfall extremes for all scenarios. Also site M141 presents high rainfall intensity changes but only for scenario A2. This scenario A2 shows for all sites the highest

changes in rainfall extremes in comparison with the other scenarios.

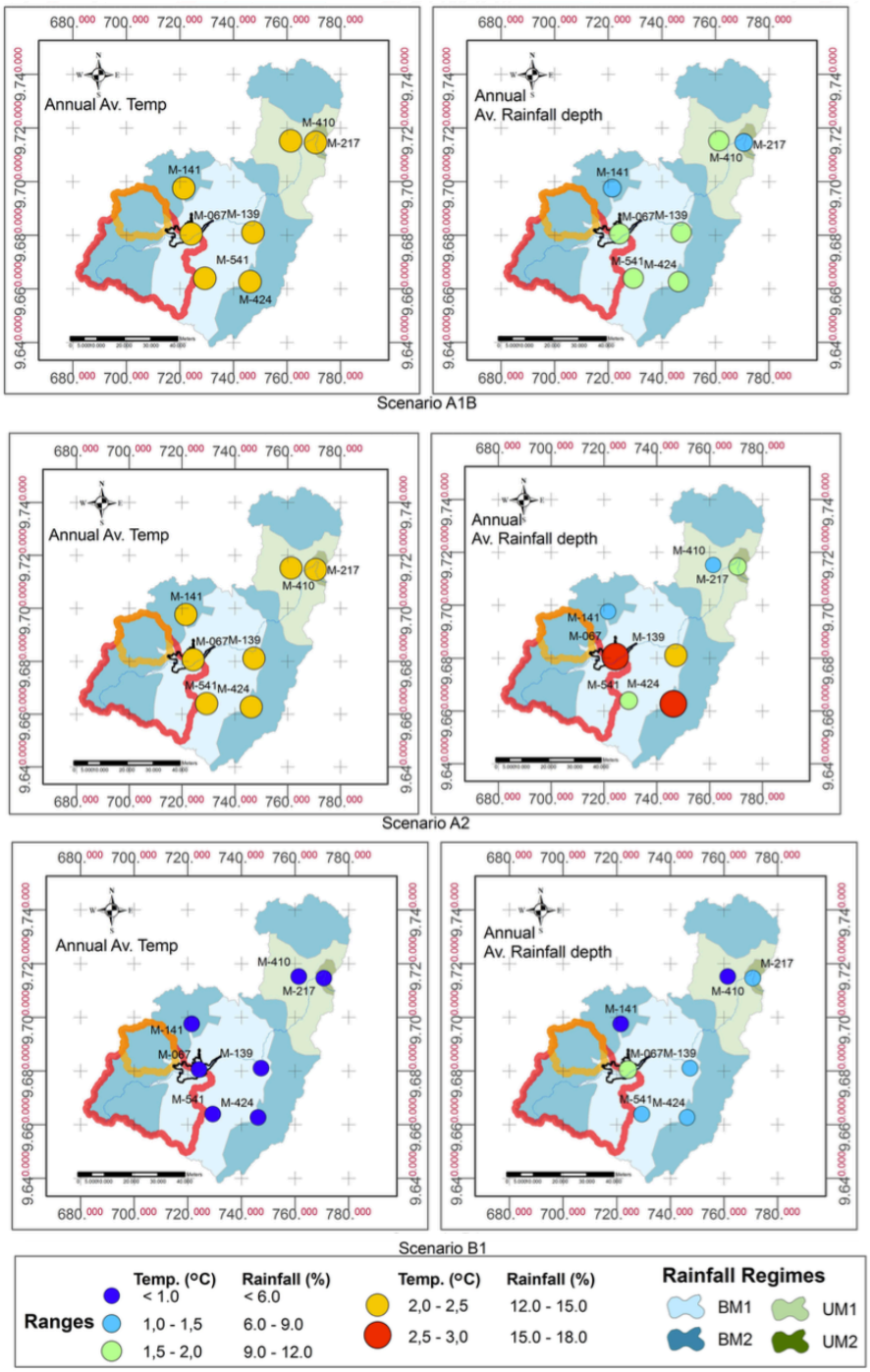

Figure 6-8: Map of average change for annual temperature and annual rainfall depth (2045 – 2065, all scenarios).

6.3.4 Impacts on runoff

Changes in runoff discharges are analyzed based on the same types of impact indicators than for rainfall and temperature. First, the conversion of discharges in runoff depth was made. When annual averaged runoff is analyzed, Ma Sa shows a higher increase (ca. +0.30 mm day^{-1}) than To Mo (ca. +0.14 mm day^{-1}). These absolute changes correspond to relative changes of ca. 8% for To Mo and ca. 10% for Ma Sa (see Fig. 6.9). When runoff is analyzed at different quantiles, high daily runoff extremes indicates that for the To Mo catchment increases are about +3.6 mm day^{-1} and for Ma Sa about +4.2 mm day^{-1}. Low quantile daily runoff is about 0.06 and 0.15 mm day^{-1} for the To Mo and Ma Sa respectively. These suggest that higher changes are projected for the Ma Sa catchment. However, relative changes in high quantile indicate higher changes for the To Mo catchment, that is, 68% for To Mo and 43% for Ma Sa for scenario A2 (see Table 6.6). This difference might be due to the lower runoff in the To Mo catchment compared with to the Ma Sa catchment. When interpreting these impact results on runoff, it is worth mentioning that the runoff results have higher uncertainty for the To Mo catchment.

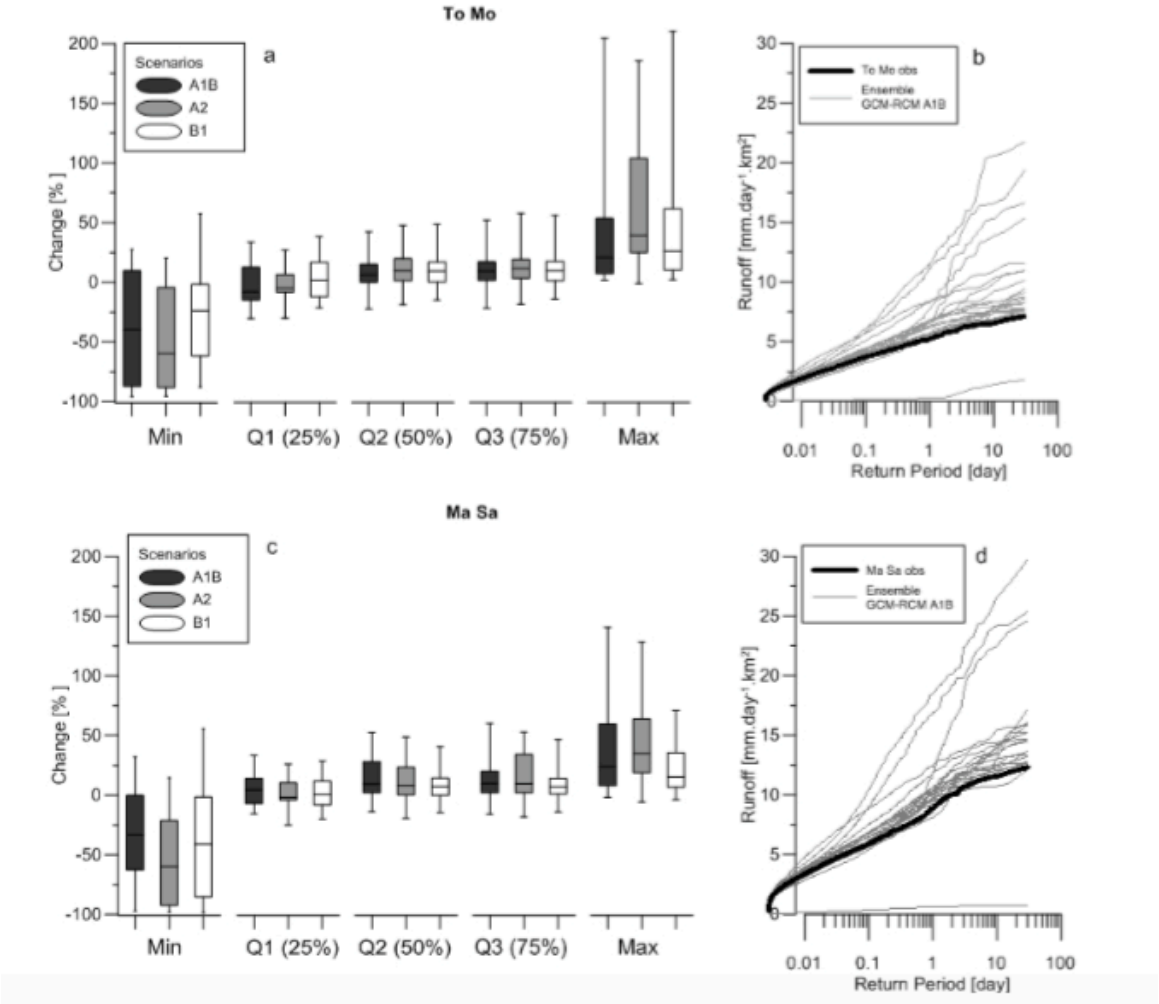

Figure 6-9: Projected changes in daily runoff for To Mo and Ma Sa catchments (2045 – 2065). (a) and (c) relative changes in runoff quantiles (all scenarios), (b) and (d) extreme runoff vs. return period (scenario A1B).

The changes in runoff are obviously related to the changes in rainfall and temperature. The increase in high runoff extremes is mainly controlled by the increase in rainfall extremes. Consequently, as for rainfall, higher changes in runoff are observed for extremes (higher quantiles). In contrast, the negative changes in low runoff events are due to the increase in temperature and to the low increase in rainfall for some scenarios. Higher changes in temperature are presumed to produce higher evapotranspiration causing a decrease in low runoff flows. In addition, the reduction in the number of wet days contributes to the decrease in runoff. This is shown for the low runoff flows in the To Mo catchment for scenario A1B, in which daily runoff below quartile Q_3 shows lesser increase despite the fact that the rainfall increase is lower for scenario B1. However, in catchment Ma Sa, the effect of low changes in temperature is not reflected in the runoff. This might be explained by the more uniform rainfall distribution in that catchment due to which changes in runoff are also more uniformly distributed.

6.4 Conclusions

This study brings new knowledge about the impact of climate change in the tropical Andean basin of the Paute River, which is strongly related to the high heterogeneity of the region. This knowledge might be useful to determine the climate change impacts on water resources.

Within the analysis of the GCM-RCM outputs, the RCM- based temperature changes are mainly driven by the large-scale circulation models in which the RCM is nested. This is different for the RCM projected rainfall changes, which show that topographical or other local dynamics control the climate projections. However, rainfall patterns are not similar to those identified in the observed series and inconsistent changes are projected. This brings some discussion on the accuracy of RCM outputs and its direct use, although we believe that the inclusion of RCM outputs should be considered for statistical downscaling together with the GCM outputs. RCMs indeed intrinsically involve climate dynamics acting at spatial scales smaller than the coarse GCM resolution.

The comparison between climate model outputs and downscaled series for scenario A2 shows that the local variation in temperature and rainfall are properly identified and transferred to the downscaled series with the advanced QPA downscaling technique. This, however, requires good quality observed data with a temporal resolution that is sufficient to derive the local patterns which might influence the results. In this study, this was the monthly resolution for temperature and the daily resolution for rainfall.

As other statistical downscaling techniques, the present methodology has some limitations. First, the method does account for (and transfer) the local properties that control the spatial variability in the meteorological variables from the observed series, but future changes in these properties are not taken into account. As explained before, we (and several other authors) expect that the properties (such as local topography) are not subject to future changes. This, however, needs further investigation (e.g. based on high resolution RCMs). Second, although the method applied for addressing the wet/dry day changes is systematic, it still is a rather crude method based on assumptions regarding the clustering of wet spells, which needs further investigation.

Nevertheless, the proposed downscaling technique is considered to be a potential option to assess local climate impacts. Cloke et al. (2013) also encourage the use of statistical downscaling techniques above the direct use of RCMs. However, these techniques must be used together with multiple evidence streams considering grand ensembles of GCM/RCM. In addition, other downscaling techniques can be compared with the proposed technique. In this way, this sensitivity of the downscaled impact results to the assumptions underlying statistical downscaling can be tested. One interesting analysis would be the comparison between statistical downscaling methods that make direct use of the rainfall results of climate models and statistical downscaling techniques that take advantage of observed relationships between rainfall and large-scale circulation.

From the downscaled results it was learned that the changes in annual averaged temperature are homogeneous for almost the entire region with an increase of about +2.0 C. Despite the fact that the temperature variability between sites was properly identified and transferred by the downscaling technique, no difference in the changes was found related to the spatial scale. However, this homogeneity may be due to the monthly temporal resolution of the observed data. Therefore, higher resolution (i.e. daily) temperature series need to be explored in future research.

Despite the stable annual temperature average, the temperature changes differ at temporal scale. The warmest period of the year would experience lower changes than the colder ones, and the coldest period of the year would have higher changes. This finding disagrees with the idea that warmer months will become warmer and that colder months will become colder. Another insight gained from the temperature impact assessment is that scenario B1 brings the lowest temperature increase, whereas scenarios A1B and scenario A2 show similar changes in temperature. This differs from other temperature impact results around the world, where scenario A2 projects the highest temperatures among other scenarios.

For rainfall, the changes are more heterogeneous than the changes projected for temperature. The downscaled results project an annual rainfall depth increase along the basin for all sites and for all scenarios. No site and no scenario indicate decrease in annual rainfall depths. However, the frequency of wet days reduces. This suggests that the annual rainfall depth increase is due an increase in the remaining wet day intensities, as was confirmed by quantile analysis. Higher rainfall increases are indeed projected for more extreme rainfall intensity events.

Absolute changes in runoff are higher for the Ma Sa catchment than for the To Mo catchment, both higher increases in high runoff flows and stronger decreases in the low runoff flows. The increase in high runoff extremes can be linked to the fact that the Ma Sa catchment is more wet than the To Mo catchment. The changes in extreme rainfall intensities are indeed also higher in the wetter regions (i.e. sites M217, M141). Therefore, changes in high runoff extremes are mainly related to the changes of rainfall extremes for both catchments, whereas the decrease in low runoff flows are linked to the increase in temperature together with the reduction in the number of wet days. However, this conclusion should be taken with care, as climate change might influence other hydrological catchment characteristics that were not taken into account in this study. This is the case for parameters involved in the estimation of evapotranspiration. In this research, future variables of solar radiation, humidity and wind speed were kept constant, overestimating the ET_0 values. Other hydrological parameters not taken into account are the ones related to the soil properties of the páramo tropical alpine region,

which involves a high water retention capacity that is highly dependent on cold temperatures (Buytaert et al., 2011).

The climate change found in this study for temperature, rainfall and runoff might bring consequences to the hydrological processes and related water management needs; hence, this will need further investigation as well.

Acknowledgements. The research was feasible thanks to a grant of the Selective Bilateral Agreement of the KU Leuven, Belgium, and its cooperation with the Universidad de Cuenca, Ecuador. The research was made within the frame of the VLIR-IUC project Integrated Water Quality Management. Special thanks go to the staff of the Hydraulics Division of KU Leuven and to PROMAS – U. Cuenca for the support in research activities and data access, and to Rolando Celleri for his support in the application of the VHM model.

Edited by: F. Pappenberger

References

Andréasson, J., Bergström, S., Carlsson, B., Graham, L. P., and Lindström, G.: Hydrological Change – Climate Change Impact Simulations for Sweden, Ambio, 33, 228–234, 2004.

Beldring, S., Engen-Skaugen, T., Førland, E. J., and Roald, L. A.: Climate change impacts on hydrological processes in Norway based on two methods for transferring regional climate model results to meteorological station sites, Tellus A, 60, 439–450, 2008.

Buytaert, W., Vuille, M., Dewulf, A., Urrutia, R., Karmalkar, A., and Célleri, R.: Uncertainties in climate change projections and regional downscaling in the tropical Andes: implications for water resources management, Hydrol. Earth Syst. Sci., 14, 1247– 1258, doi:10.5194/hess-14-1247-2010, 2010.

Buytaert, W., Cuesta-Camacho, F., and Tobón, C.: Potential impacts of climate change on the environmental services of humid tropical alpine regions, Global Ecol. Biogeogr., 20, 19–33, 2011.

Célleri, R., Willems, P., Buytaert, W., and Feyen, J.: Space–time rainfall variability in the Paute basin, Ecuadorian Andes, Hydrol. Process., 21, 3316–3327, 2007.

Célleri, R., Willems, P., and Feyen, J.: Evaluation of a data-based hydrological model for simulating the runoff of medium sized Andean basins, Maskana Vol. 1, U. Cuenca, Cuenca, Ecuador, 61–77, 2010.

Cloke, H. L., Wetterhall, F., He, Y., Freer, J. E., and Pappenberger, F.: Modelling climate impact on floods with ensemble climate projections. Q. J. Roy. Meteorol. Soc., 139, 282–297, doi:10.1002/qj.1998, 2013.

Coltorti, M. and Ollier, C.: Geomorphic and tectonic evolution of the Ecuadorian Andes, Geomorphology, 32, 1–19, 2000.

Dirmeyer, P. A., Cash, B. A., Kinter, J. L., Stan, C., Jung, T., Marx, L., Towers, P., Wedi, N., Adams, J. M., Altshuler, E. L., Huang, B., Jin, E. K., and Manganello, J.: Evidence for Enhanced Land– Atmosphere Feedback in a Warming Climate, J. Hydrometeorol., 13, 981–995, 2012.

Fowler, H. J., Blenkinsop, S., and Tebaldi, C.: Linking climate change modelling to impacts studies: recent advances in downscaling techniques for hydrological modelling, Int. J. Climatol., 27, 1547–1578, 2007.

Garreaud, R. D.: The Andes climate and weather, Adv. Geosci., 22, 3–11, doi:10.5194/adgeo-22-3-2009, 2009.

Giorgi, F., Christensen, J., Hulme, M., von Storch, H., Whetton, P., Jones, R., Mearns, L., Fu, C., Arritt, R., Bates, B., Benestad, R., Boer, G., Buishand, A., Castro, M., Chen, D., Cramer, W., Crane, R., Crossly, J., Dehn, M., Dethloff, K., Dippner, J., Emori, S., Francisco, R., Fyfe, J., Gerstengarbe, F., Gutowski, W., Gyalistras, D., Hanssen-Bauer, I., Hantel, M., Hassell, D., Heimann, D., Jack, C., Jacobeit, J., Kato, H., Katz, R., Kauker, F., Knutson, T., Lal, M., Landsea, C., Laprise, R., Leung, L., Lynch, A., May, W., McGregor, J., Miller, N., Murphy, J., Ribalaygua, J., Rinke, A., Rummukainen, M., Semazzi, F., Walsh, K., Werner, P., Widmann, M., Wilby, R., Wild, M., and Xue, Y.: Regional Climate Information Evaluation and Projections, Climate Change 2001: The Scientific Basis, in: Contribution of Working Group to the Third Assessment Report of the Intergouvernmental Panel on Climate Change, edited by: Houghton, J. T., Ding, Y., Griggs, D. J., Noguer, M., van der Linden, P. J., Dai, X., Maskell, K., and Johnson, C. A., http://epic.awi.de/4973/, Cambridge University Press, Cambridge, UK and New York, USA, 2001.

Harrold, T. I. and Jones, R.: Downscaling of GCM rainfall: A refinement of the perturbation method, in: EGS-AGU-EUG Joint Assembly, Presented at the EGS-AGU-EUG Joint Assembly, 6– 11 April, Nice, France, p. 1338, 2003.

Hewitson, B. and Crane, R.: Climate downscaling: techniques and application, Clim. Res., 07, 85–95, 1996.

Hirabayashi, Y., Kanae, S., Emori, S., Oki, T., and Kimoto, M.: Global projections of changing risks of floods and droughts in a changing climate, Hydrolog. Sci. J., 53, 754–772, 2008.

Liu, T., Willems, P., Pan, X. L., Bao, An. M., Chen, X., Veroustraete, F., and Dong, Q. H.: Climate change impact on water resource extremes in a headwater region of the

Tarim basin in China, Hydrol. Earth Syst. Sci., 15, 3511–3527, doi:10.5194/hess-15-3511- 2011, 2011.

Maraun, D., Wetterhall, F., Ireson, A. M., Chandler, R. E., Kendon, E. J., Widmann, M., Brienen, S., Rust, H. W., Sauter, T., Themeßl, M., Venema, V. K. C., Chun, K. P., Goodess, C. M., Jones, R. G., Onof, C., Vrac, M., and Thiele-Eich, I.: Precipitation downscaling under climate change: Recent developments to bridge the gap between dynamical models and the end user, Rev. Geophys., 48, RG3003, doi:10.1029/2009RG000314, 2010.

Middelkoop, H., Daamen, K., Gellens, D., Grabs, W., Kwadijk, J. C. J., Lang, H., Parmet, B. W. A. H., Schädler, B., Schulla, J., and Wilke, K.: Impact of Climate Change on Hydrological Regimes and Water Resources Management in the Rhine Basin, Climatic Change, 49, 105–128, 2001.

Monteith, J.: Evaporation and environment, Presented at the Symp. Soc. Exp. Biol, Rothamsted Experimental Station, Harpenden, UK, p. 4, 1965.

Mora, D. E. and Willems, P.: Decadal oscillations in rainfall and air temperature in the Paute River Basin–Southern Andes of Ecuador, Theor. Appl. Climatol., 108, 267–282, 2012.

Mora, D. E., Liu, T., Cisneros, F., Wyseure, G., and Willems, P.: Statistical Analysis on the Performance of Global and Regional Climate Models for the Paute River Basin in the South-Ecuadorian Andes, Proceedings of 10th International Conference on Hydroinformatics, Hamburg, Germany, 2012.

Nakicenovic, N., Alcamo, J., Davis, G., de Vries, B., Fenhann, J., Gaffin, S., Gregory, K., Grubler, A., Jung, T. Y., Kram, T., La Rovere, E. L., Michaelis, L., Mori, S., Morita, T., Pepper, W., Pitcher, H. M., Price, L., Riahi, K., Roehrl, A., Rogner, H.-H., Sankovski, A., Schlesinger, M., Shukla, P., Smith, S. J., Swart, R., van Rooijen, S., Victor, N., and Dadi, Z.: Special Report on Emissions Scenarios: A Special Report of Working Group III of the Intergovernmental Panel on Climate Change (No. PNNL- SA-39650), Pacific Northwest National Laboratory, Richland, WA, USA, Environmental Molecular Sciences Laboratory, USA, 2000.

Nguyen, V. T. V., Desramaut, N., and Nguyen, T. D.: Estimation of urban design storms in consideration of GCM-based climate change scenarios, Proceedings International Conference on "Water and Urban Development Paradigms: Towards an Integration of Engineering, Design and Management Approaches", 15– 17 September, Leuven, Belgium, 347–356, 2008.

Nguyen, V.-T.-V., Nguyen, T.-D., and Cung, A.: A statistical approach to downscaling of sub-daily extreme rainfall processes for climate-related impact studies in urban areas, Presented at the Sustainable and Safe Water Supplies, International Water Association, International Symposium, Hong Kong, China, 183–192, 2007.

Nijssen, B., O'Donnell, G., Hamlet, A., and Lettenmaier, D.: Hydrologic Sensitivity of Global Rivers to Climate Change, Climatic Change, 50, 143–175, 2001.

Ntegeka, V. and Willems, P.: Trends and multidecadal oscillations in rainfall extremes, based on a more than 100-year time series of 10 min rainfall intensities at Uccle, Belgium, Water Resour. Res., 44, W07402, doi:10.1029/2007WR006471, 2008.

Olsson, J., Willén, U., and Kawamura, A.: Downscaling extreme short-term regional climate model precipitation for urban hydrological applications, Hydrol. Res., 43, 341–351, 2012.

Ontaneda, G., Garcia, G., and Arteaga, A.: Evidencias del cambio climdtico en Ecuador, Proyecto ECU/99/G31 Cambio Climatico, Fase 2, Comite Nacional sobre el Clima GEF-PNUD, Ministerio del Ambiente, Quito, Ecuador, 2002.

Parry, M. L., Canziani, O. F., Palutikof, J. P., van der Linden, P. J., and Hanson, C. E.: Climate Change 2007: Impacts, Adaptation and Vulnerability: Working Group II Contribution to the Fourth Assessment Report of the Intergovernmental Panel on Climate Change, Vol. 4, Cambridge University Press, UK, 976– 986, 2007.

Penman, H. L.: Natural Evaporation from Open Water, Bare Soil and Grass, P. Roy. Soc. Lond., 193, 120–145, 1948.

Prudhomme, C., Reynard, N., and Crooks, S.: Downscaling of global climate models for flood frequency analysis: Where are we now?, Hydrol. Process., 16, 1137–1150, 2002.

Solomon, S., Qin, D., Manning, M., Chen, Z., Marquis, M., Averyt, K., Tignor, M., and Miller, H.: The physical science basis, Contribution of working group I to the Fourth Assessment Report of the Intergovernmental Panel of Climate Change, Cambridge University Press, UK, 235–337, 2007.

Taye, M. T. and Willems, P. : Identifying sources of temporal variability in hydrological extremes of the upper Blue Nile basin, J. Hydrol., 499, 61–70, 2013.

Taye, M. T., Ntegeka, V., Ogiramoi, N. P., and Willems, P.: Assessment of climate change impact on hydrological extremes in two source regions of the Nile River Basin, Hydrol. Earth Syst. Sci., 15, 209–222, doi:10.5194/hess-15-209-2011, 2011.

Urrutia, R. and Vuille, M.: Climate change projections for the tropical Andes using a regional climate model: Temperature and precipitation simulations for the end of the 21st century, J. Geophys. Res., 114, D02108, doi:10.1029/2008JD011021, 2009.

Van Steenbergen, N. and Willems, P.: Method for testing the accuracy of rainfall–runoff models in predicting peak flow changes due to rainfall changes, in a climate changing context, J. Hydrol., 414–415, 425–434, 2012.

Vuille, M., Bradley, R. S., Werner, M., and Keimig, F.: 20th entury climate change in the tropical Andes: observations and model results, Climatic Change, 59, 75–99, 2003.

Willems, P.: Probabilistic immission modelling of receiving surface waters, PhD Thesis, KU Leuven, Leuven, Belgium, 2000.

Willems P.: Parsimonious rainfall–runoff model construction supported by time series processing and validation of hydrological extremes – Part 1: Step-wise modelstructure identification and calibration approach, J. Hydrol., 510, 578–590, 2014.

Willems, P. and Vrac, M.: Statistical precipitation downscaling for small-scale hydrological impact investigations of climate change, J. Hydrol., 402, 193–205, 2011.

Willems, P., Olsson, J., and Arnbjerg-Nielsen, K.: Impacts of Climate Change on Rainfall Extremes and Urban Drainage Systems, IWA Publishing, London, UK, 239 pp., 2012.

Willems, P., Mora, D. E., Vansteenkiste, Th., Teferi Taye, M., and Van Steenbergen, N.: Parsimonious rainfall–runoff model construction supported by time series processing and validation of hydrological extremes – Part 2: Intercomparison of models and calibration approaches, J. Hydrol., 510, 591–609, 2014.

Wood, A. W., Leung, L. R., Sridhar, V., and Lettenmaier, D. P.: Hydrologic implications of dynamical and statistical approaches to downscaling climate model outputs, Climatic Change, 62, 189– 216, 2004.

7 Summary and Outlook

7.1 Summary

The main objective of this research is to study the downscaling of precipitation at basin scale in the Paute river basin, which is located in the tropical Andes of Southern Ecuador. The main assumption is that, by incorporating orographic information in the downscaling of precipitation, improved estimates of precipitation can be achieved. Such research is important, both from a scientific perspective as well as for water resource management and planning assessment for this developing country.

The main results of the WPs are as follows:

1- In the first place, the spatio-temporal dynamics of precipitation and clouds, as well as the potential cross-scale generation processes of rainfall in the Paute basin were investigated with the aim of evaluating the influence of both the orography and the synoptic climate signals on the climate of the basin. To convey such investigations, the regionalization of precipitation regimes is necessary prior to the study of the diverse orographic and synoptic borne influences on the precipitation regimes. Previous studies conducted the regionalization of precipitation regimes by correlation among a scarce group of stations and delineation by expert knowledge. In this work for the first time precipitation models were used to regionalize precipitation regimes in the PB at high resolution (e.g. 1km). Precipitation models using satellite cloud products and GIS data revealed the spatial extension of three regimes: a tri-modal (TM) regime, mainly present across the basin; a bi-modal (BM) regime, typical for sheltered valleys; and a uni-modal (UM) regime, characteristic of the windward slopes of the eastern cordillera. These results show an important application of clouds products to derive precipitation products at basin scale, which may be useful especially in remote regions of complex orography. The synoptic analysis of 600 hPa omega vertical velocity show that the ITCZ plays an important role in enhancing convection throughout the year. However, during boreal summer, the strengthening of the Walker Circulation produce subsidence, accounting for the dry season of the inter-Andean regions. On the hand the analysis on 600 hPa zonal wind and specific humidity showed that during boreal summer, the easterlies bringing moist air from the Amazon, which enhances the precipitation amounts on the eastward oriented slopes. From these results, we can derive the processes involved in generating precipitation during the rainy seasons. This is a novel finding from the present study. For instance, during April-May and October-November, precipitation is of convective nature, whereas, during boreal summer low advective shallow cap clouds mainly cause precipitation in UM regions, e.g. from 1000 to 3000 m asl on the eastern flanks of the Andes and along transition zones between UM and BM regimes. As a main result of these findings a conceptual model of rainfall was proposed for the PB, which could also be applied along the tropical region of the Andes.

2- Subsequently, the evaluation of the performance of statistical downscaling methods applied to monthly precipitation in the Andes of Ecuador was conducted. With the aim of capturing the complex atmospheric processes occurring in mountain regions, non-lineal methods for downscaling were used for this study. To the best knowledge of the author, no previous studies have evaluated statistical techniques such as, SDSM, and methods of artificial intelligence, as neural networks and support vector machines, on the tropical Andes. A comparative analysis of the applied downscaling methods was conducted. Using statistical metrics, such as Pearson correlation, root mean square error, and percentiles biases to evaluate artificial intelligence against the well-established SDSM approach, the former showed better skills in relation to the latter. The intercomparison of artificial intelligence methods with respect to the downscaling of monthly precipitation, showed that neural networks and least square support vector machine models perform equally. However, in some stations, and some months, it was important to consider both model approaches AI and SDSM, in order to derive robust conclusions. Good performance of the statistical downscaling techniques was obtained along the year. However shortcomings especially in November rainfall depths were found in some stations. These results could also be influenced by the set of predictors used on each case. For instance, AI methods keep the original set of predictor variables. Whereas, SDSM evaluates the most significant set of variables using partial correlation, and then uses them to calibrate the models. This could derive in discarding important variables, which may have non-linear relations with the predictant. The analysis of the predictors used by SDSM for all stations, shows that Palmas station, the only UM station which has important meso-scale influences, kept only 3 variables from 12 variables in the original set, whereas BM and TM stations kept at least 5 variables. Thus a methodology considering downscaling with specific predictors by month or season might be advisable.

3- Once some statistical approaches were evaluated, the predictive capabilities regarding the generation of station-scale mean monthly temperature and rainfall of both a dynamical (WRF-based) and a statistical (ANN-based) downscaling approach was assessed. Because to some extent the added value of dynamical downscaling can be attributed to terrain information, WRF model was run at high resolution, e.g. 15 km in the PB. To the best knowledge of the author it is the first time that WRF model is applied at high resolution in the Andes and an exhaustive sensibility analysis of sub-grid parameterizations is conducted. To evaluate the added value of regional modeling we chose two basins with complex orography, e.g. Paute and Jubones, which present high altitudinal gradients and diverse precipitation regimens. From a decade of evaluation it was unveiled that both approaches were able to qualitatively describe precipitation and temperature seasonal variations for different regimes in representative weather stations. However shortcomings in the estimation of monthly rainfall depths were found. For instance, despite the fact that an exhaustive sensitivity analysis was conducted to choose the adequate set of microphysical parameters for WRF, its results showed consistent overestimation. This finding is in agreement with other studies around the world. It is important to highlight that downscaling results from both approaches surpassed the precipitation seasonality representation of NNRP reanalysis data. In fact, NNRP show a bi-modal regime over the entire region. However both downscaling approaches

could capture the uni-modal regime, which is due to the meso-scale influence of the Andes. This is particularly important for the regional modeling approach because it implies that the processes, which modify the synoptic signal, are captured. A limitation was found in the representation of the transition regime between uni and bi modal regimens, e.g. three-modal regime. It was not captured neither by statistical nor the dynamical techniques. With respect to the regional modeling approach this shortcoming may indicate that even higher resolution is necessary in order to capture local modifications to the synoptic signal of precipitation. On the other hand for statistical methods the consideration of predictors at higher resolution, which account for local atmospheric influences, may be necessary. Thus the statistical downscaling of dynamically downscaled fields could be an option. This fact may encourage the evaluation of a methodology of downscaling using dynamic and statistical methods in cascade, which could help capture meso-scale and local climatic features.

4- Finally, the statistical downscaling of GCMs and RCMs (Precis Hadley and Precis Echam) was conducted to generate projections of precipitation and temperature in the Paute basin. Due to computational limitations, the projections of climate (e.g. from 2045 to 2065), with the regional climate model PRECIS on 50km resolution was used. Thus, for the first time in the PB, the added value of combining both the dynamical and the statistical downscaling approaches at daily scale was evaluated. The statistical downscaling approach, e.g. the adjusted quantile perturbation method, was used to downscale GCMs as well as PRECIS results. The projections were calculated for the A2, A1B, and B2 SRES future scenarios from 2045 to 2065. For A2 scenario, increases of +2°C are projected across the entire basin, whereas for precipitation the projected changes varies from +175 to +650 mm/year, and for others negative trends in the order of the observed precipitation depths. Such results call the attention about the reliability of the projected values of precipitation, although similar values for temperature have been reported previously. Projected statistically downscaled temperature changes based on RCMs reflected more spatial variability than direct RCM based changes. However, the range of values remained similar, showing that RCM-based temperature changes are driven by the GCMs in which RCMs are nested. In a similar way, the changes projected from GCMs are similar to the statistically downscaled values, despite the fact that, the latter showed more spatial variability. However, for precipitation, RCM outputs present local gradients that are not similar to observations, and inconsistent changes are projected. On the other hand, the precipitation changes from the statistically downscaled results either from GCMs and RCMs showed similar variations. This brings some discussion on the accuracy of RCM outputs and its direct use. It is important to acknowledge that the limited performance of the RCMs used in this study, e.g. Precis Hadley and Precis ECHAM, may be related to (i) the resolution, ca. 50km, which may not reflect the complex orography of the Paute basin, and (ii) the lack of a specific sensitivity analysis of the parameterizations, causing that sub-grid effects may be affecting the results.

Thus the following aspects are the main contributions of the present work:

- The determination of the orographic and synoptic factors generating uni, bi, and three modal precipitation regimes in the PB, which may also explain the dynamics of precipitation along the tropical Andes. As a result a conceptual model of rainfall for mountain regions with complex orography as the PB was presented.
- The development of high-resolution precipitation models based on cloud products, which were used for the regionalization of precipitation regimes in the PB. This could have important applications in remote regions of complex orography.
- The novel application in the Andes of Ecuador, of several non-linear statistical downscaling approaches as SDSM, artificial neural networks and support vector machines. It was shown that such techniques can capture meso-scale climatic influences, however shortcomings on the representation of local modification of the climatic signal were found.
- The development of an exhaustive sensitivity analysis of sub-grid parameterization in the PB prior to the evaluation of high-resolution regional climate modeling, e.g. WRF 15km in the Tropical Andes. It was determined that RCM-WRF is able to capture meso-scale modifications of the synoptic signal, however strong over-estimation of precipitation amounts were found.
- The evaluation of the added value of applying both, the dynamical and statistical downscaling approaches in cascade (e.g. PRECIS and perturbation factor respectively), proved to present improved estimates of precipitation in the PB.

7.2 Outlook

The findings from the present investigation encourage further research related to the downscaling of global climate models in mountain regions.

In the downscaling of GCMs several uncertainties are involved, as was previously mentioned in section 1. Thus research efforts might be oriented towards the reduction of the diverse sources of uncertainty. For instance, to date there is a lack of studies evaluating the representation of the synoptic conditions either from GCMs or reanalysis data on this region, and furthermore their correspondence. Such investigations are of major importance for downscaling due to the fact that reanalysis data is used for the calibration of statistical models, or for the sensitivity analysis in dynamical approaches. However GCMs drive the future projections of climate, thus the evaluation of both inputs should be conducted. Nevertheless, the evaluation of GCMs and reanalysis data requires an improvement of the understanding of atmospheric processes. However, for a deeper understanding of such processes, the improvement of observational networks, in spatio-temporal representation, is required.

Uncertainty is also inherent to the methods used for the downscaling of climate variables. Thus efforts should be oriented towards a more comprehensive evaluation of methods. For instance, successful applications of weather typing approaches have been studied especially in developed countries, however to date limited studies have been conducted on this region, e.g. Pineda, & Willems, (2015). Also, specifically applied in statistical approaches, the interpolation of point estimates is conducted as a final step to

produce downscaled grids. In regions with complex orography as the Andes such process may introduce further uncertainties, which are amplified by scarce monitoring networks in a region with strong climatic gradients. Thus the application of adequate geoestatistical methods for the interpolation of downscaled climatic fields in complex terrain should be further studied. For the present study two RCMs, e.g. Precis and WRF, were used. However in order to make more robust assessments of climate change, despite the fact that high computational power is required, more efforts towards the generation of ensembles of downscaled estimates are necessary.

Another aspect, which is central to the assessment of climate change impact at basin scale, is the study of climate extremes. Such evaluation in regions where the GCMs representation of climate still limited is even more important. The representation of extremes can be achieved either by extreme climate indicators thresholds, or by the evaluation of extreme percentiles. However, the investigation related to the downscaling of extremes in complex terrain is not a trivial matter. For instance, methodological aspects, as, e.g. the downscaling of fields, and further calculation of extremes, or the calculation of extremes followed by the interpolation of fields, still in discussion.

References

Chen J, Brissette FP, Leconte R. 2012. Coupling statistical and dynamical methods for spatial downscaling of precipitation. Climatic Change 114(3-4): 509–526. DOI: 10.1007/s10584-012-0452-2.

Pineda, L. E., & Willems, P. (2015). Multisite downscaling of seasonal predictions to daily rainfall characteristics over Pacific-Andean River Basins in Ecuador and Peru using a non-homogeneous hidden Markov model. Journal of Hydrometeorology, (November), 151016095329004. doi:10.1175/JHM-D-15-0040.1

8 Zusammenfassung

Das Hauptziel der vorliegenden Studie ist die Erforschung des Downscaling von Niederschlägen auf die Einzugsgebietskala des Paute Flusses, welcher sich in den tropischen Anden im südlichen Ecuador befindet. Die Hauptannahme ist, dass durch die Berücksichtigung orographischer Informationen beim Downscaling von Niederschlägen eine Verbesserung der Niederschlagsprognosen ermöglicht wird. Eine solche Forschung ist sowohl aus wissenschaftlicher Sicht, als auch für das Management von Wasserressourcen sowie der raumplanerischen Beurteilung in dem Entwicklungsland wichtig.

Die Hauptresultate der WPs sind die Folgenden:
1- Zunächst wurden die raumzeitlichen Dynamiken von Niederschlag und Wolken, als auch mögliche skalenübergreifende Prozesse der Niederschlagsentstehung in dem Paute Becken (PB) untersucht um den Einfluss orographischer und synoptischer Klimasignale auf das Klima des Becken auszuwerten. Hierfür ist zunächst eine Regionalisierung der Niederschlagsregime notwendig um anschließend verschiedene orographische und synoptische Einflüsse auf die Niederschlagsregime zu untersuchen. Vorangehende Studien erreichten die Regionalisierung von Niederschlagsregimen mittels Korrelationen aus einer kleinen Gruppe von Messstationen und der Beurteilung durch Expertenwissen. In dieser Arbeit wurden zum ersten Mal Niederschlagsmodelle benutzt, um Niederschlagsregime im PB in hoher Auflösung (1 km) zu regionalisieren. Diese Niederschlagsmodelle, basierend auf satellitengestützten Wolkenprodukten und GIS Daten, zeigten die räumliche Ausdehnung von drei Regimen: Ein trimodales Regime (TM) hauptsächlich über dem Becken; ein bimodales Regime (BM) typisch für geschützte Täler; und ein unimodales Regime (UM) typisch für windexponierte Hänge der östlichen Cordillera. Die Ergebnisse zeigen die Bedeutung von Wolkenprodukten wenn Niederschlagprodukte auf Skala von Einzugsgebieten abgeleitet werden sollen, was vor allem in weit abgelegene Regionen mit komplexer Geländeoberfläche nützlich sein kann. Die synoptische Analyse der 600 hPa Omega Vertikalgeschwindigkeit zeigt, dass die innertropische Konvergenzzone (ITCZ) das ganze Jahr über die Konvektion verstärkt. Eine Abmilderung durch die ausgeprägte Walkerzirkulation während des borealen Sommers ist verantwortlich für die Trockenzeit in den interandinen Regionen. Die Analyse von 600 hPA zonalem Wind und spezifischer Luftfeuchtigkeit zeigte, dass während des borealem Sommers die Ostwindzone feuchte Luftmassen vom Amazonas bringen, wodurch die Niederschlagsmengen an ostexponierten Hängen steigen. Aus diesen Erkenntnissen können Prozesse abgeleitet werden welche die Niederschlagsentstehung während der Regenzeit bestimmen. Dies ist eine neue Erkenntnis der vorliegenden Studie. So sind beispielsweise, von April bis Mai und Oktober bis November, Niederschläge konvektivem Ursprungs, wohingegen während des borealen Sommers die Niederschläge hauptsächlich advektiv, mittels „shallow cap“ Wolken, in die UM Regionen gelangen, so z.B. von 1000 bis 3000 m ü. NN an der Ostflanke der Anden und entlang der Übergänge von UM zu BM Regimen. Als ein Hauptergebnis dieser Erkenntnisse wurde ein konzeptionelles Regenmodell für das PB vorgeschlagen, welches ebenso auf andere tropische Regionen entlang der Anden angewendet werden kann.

2- Anschließend, wurde die Anwendbarkeit von statistischen Downscaling Methoden auf die monatlichen Niederschläge in den Anden von Ecuador ausgewertet. Um die in

den Anden vorkommenden, komplexen Prozesse der Atmosphäre zu erfassen, wurden nicht lineare Methoden des Downscalings in dieser Studie verwendet. Nach Wissensstand des Autors haben keine der bisherigen Studien statistische Techniken, beispielsweise SDSM, oder Methoden der künstlichen Intelligenz, wie neuronale Netzwerke und Support Vector Machines (SVM) für die tropischen Anden angewendet. Eine vergleichende Analyse der angewandten Downscaling Methoden wurde durchgeführt. Mit der Verwendung von statistischen Kennzahlen, wie beispielsweise dem Pearsons Korrelationskoeffizient, der Wurzel der mittleren Fehlerquadratsumme und der Perzentil Bias wurden die Ansätze der künstlichen Intelligenz (artificial intelligence – AI) mit dem etablierten SDSM Ansatz verglichen; wobei Erstgenannte besser abschnitten als Letzterer. Der Vergleich der Methoden der AI beim Downscalings der monatlichen Niederschlagsmengen zeigte, dass sich neuronale Netze und least square SVM-Modelle gleichermaßen anwenden lassen. Es war jedoch für manche Messstationen und in manchen Monaten wichtig beide Modelansätze, AI und SDSM, zu berücksichtigen um aussagekräftige Schlussfolgerungen zu gewinnen. Über das Jahr hinweg wurde ein gutes Funktionieren der statistischen Downscaling Techniken festgestellt. Jedoch wurden vor allem bei den Niederschlagsmengen im November für manche Stationen Fehler festgestellt. Diese Ergebnisse könnten von der Festlegung der Prädiktoren, die für jeden Fall verwendet worden, beeinflusst worden sein. So behalten zum Beispiel AI Methoden ihre ursprünglich festgelegten Variablen bei. Demgegenüber berechnet SDSM mit Hilfe von partiellen Korrelationen die signifikanteste Zusammenstellung von Variablen aus und benutzt diese, um die Modelle zu kalibrieren. Dies kann dazu führen, dass wichtige Variablen verworfen werden, welche eventuell nicht-lineare Zusammenhänge mit dem Prädiktoren haben. Die von SDSM für alle Stationen benutzte Analyse von Prädiktoren zeigt, dass Palmas Station, die einzige UM Station mit wichtigen mesoskaligen Einflüssen, lediglich drei der zwölf Variablen der ursprünglichen Zusammenstellung beibehält, wohingegen die BM und TM Stationen mindestens fünf Variablen beibehalten. Folglich könnte eine Methodik welche ein Downscaling mit monatlich oder jahreszeitlich spezifischen Prädiktoren verwendet empfehlenswert sein.

3- Nach der Auswertung einiger statistischer Ansätze, wurden die Voraussagemöglichkeiten hinsichtlich der Erzeugung von stationsskalierten mittleren monatlichen Temperaturen und Niederschlägen, sowohl von dynamischen (WRF-basiert) als auch statistischen (ANN-basiert) Downscaling Ansätzen beurteilt.Da die hinzugefügten Werte des dynamischen Downscalings zu gewissem Grad Geländeinformationen zugeschrieben werden können, wurden die WRF Modelle mit hoher Auflösung (15 km) für das PB gerechnet werden konnten. Nach Wissenstand des Autors ist es das erste Mal, dass das WRF Model mit hoher Auflösung in den Anden angewendet und eine vollständige Sensibilitätsanalyse der sub-grid Parametrisierung durchgeführt wurde. Um die hinzugefügten Werte der regionalen Modellierung auszuwerten, haben wir zwei Becken mit komplexer Geländeformung ausgesucht, Paute und Jubones, welche große Höhendifferenzen und verschieden Niederschlagsregime aufweisen. Jahrzehntelange Auswertungen zeigten, dass beide Ansätze anwendbar waren um die saisonalen Niederschlags- und Temperaturschwankungen für verschiedene Regime in repräsentativen Wetterstationen zu beschreiben. Es wurden jedoch Fehler in der Schätzung der monatlichen Regenfälle gefunden. So zeigten beispielsweise die Ergebnisse einer vollständigen Sensibilitätsanalyse trotz einer angemessenen Zusammenstellung von mikrophysikalischen Parametern der WRF, eine stetig überhöhte Schätzung. Diese Erkenntnis stimmt mit anderen Studien aus der

ganzen Welt überein. Es ist wichtig hervorzuheben, dass die Ergebnisse des Downscalings beider Ansätze die Darstellung der jahreszeitlichen Niederschläge der neu analysierten NNRP Daten übertreffen. Im Grunde zeigt NNRP ein bi-modales Regime für die ganze Region. Beide Downscalingansätze konnten jedoch ein uni-modales Regime erfassen, welches dem meso-skaligem Einfluss der Anden zuzuschreiben ist. Dies ist speziell für die regionalen Modellierungsansätze wichtig, da hier Prozesse welche die synoptischen Signale verändern, erfasst wurden. Eine Beschränkung war in der Darstellung des Übergangs von uni- zum bimodalen Regime, dem tri-modeln System zu finden. Dieses konnte weder von statistischen noch dynamische Techniken erfasst werden. Im Kontext des regionalen Modelansatzes kann dieser Mangel darauf hinweisen, dass eine weiter erhöhte Auflösung notwendig ist, um lokale Änderungen im synoptischen Signal des Niederschlags zu erfassen. Für die statistische Verfahren scheint die Berücksichtigung von Prädiktoren, die lokale atmosphärische Einflüsse bedingen, mit höherer Auflösung erforderlich zu sein. So könnte das statistische Downscaling von dynamisch ge-downscalten Feldern eine Option sein. Diese Ergebnisse ermutigen zur Auswertung einer Methodologie des Downscalings durch das Nutzen von dynamischen und statistischen Verfahren in Kaskade, welche beitragen könnten mesoskalige und lokale klimatische Merkmale zu erfassen.

4- Schließlich wurde das statistische Downscaling von GCMs und RCMs (Precis Hadley und Precis Echam) durchgeführt um Vorhersagen von Temperatur und Niederschlägen im PB zu erzeugen. Limitiert durch die Rechnerleistung wurden die Vorhersagen des Klimas von dem regionalen Klimamodell PRECIS mit 50 km Auflösung benutzt. Somit wurde das erste mal im PB, der zusätzliche Wert resultierend aus der Kombination von dynamischen und statistischen Downscaling Ansätzem auf täglicher Basis ausgewertet. Der statistische Downscaling Ansatz, namentlich „adjusted quantile perturbation method“, wurde für das Downscaling der GCMs sowie der PRECIS Ergebnisse verwendet. Die Vorhersagen wurden für das A2, A1B und das B2 SRES Zukunftsszenario für 2045 bis 2065 gerechnet. Für das A2 Szenario, ist eine Erwärmung von 2 °C für das gesamte Becken vorhergesagt , wobei die Vorhersagen für den Niederschlag variieren von einer Zunahme von 175 bis 650 mm/Jahr und teilweise sogar negative Trends für die Niederschlagsmengen beobachtet werden. Solche Ergebnisse rufen zur Vorsicht auf über die Zuverlässigkeit der projizierten Niederschlagswerte, obwohl für die Temperatur ähnliche Werte bereits früher aufgezeichnet wurden. Projizierte, statistisch gedownscalte Temperaturänderungen basierend auf RCMs, spiegelten mehr räumliche Variabilität als die direkte RCM basierte Werte wieder. Jedoch blieb der Wertebereich ähnlich, was zeigt, dass RCM-basierte Temperaturänderungen durch die GCMs gesteuert werden, in denen RCMs eingebunden sind. In ähnlicher Weise sind die von den GCMs vorhergesagten Veränderungen ähnlich zu den statistisch gedownscalten Werten, ausser das Letztere eine höhere räumlichere Variabilität aufweisen. Für den Niederschlag zeigen die RCM Ergebnisse jedoch lokale Gradienten, die den Beobachtungen nicht ähnlich sind, zudem werden inkonsistente Änderungen projiziert. Andererseits zeigten die Niederschlagsänderungen von den statistisch gedownscalten Ergebnissen sowohl von den GCMs und RCMs ähnliche Abweichungen. Dies führt zu Zweifeln an der Genauigkeit der RCM-Ergebnisse und deren direkter Verwendung. Es ist wichtig darauf hinzuweisen, dass die begrenzte Leistung der in dieser Studie verwendeten RCMs, namentlich Precis Hadley und Precis ECHAM, im Zusammenhang mit (i) der Auflösung von ca. 50 km, welche möglicherweise nicht die komplexe Orographie des

Paute-Beckens widerspiegeln kann, und (ii) dem Fehlen einer spezifischen Empfindlichkeitsanalyse der Parametrisierungen, was bewirkt, dass Sub-Grid-Effekte die Ergebnisse beeinflussen können.

Die folgenden Aspekte sind Hauptbeiträge der vorliegenden Arbeit:

- Die Bestimmung der orographischen und synoptischen Faktoren, welche uni-, bi- und tri-modale Niederschlagsregime im PB erzeugen, und auch die Dynamik der Niederschläge entlang der tropischen Anden erklären kann. Als Ergebnis wurde ein konzeptionelles Modell des Niederschlags für Bergregionen mit einer komplexen Orographie wie dem PB präsentiert.
- Die Entwicklung von hochauflösenden Niederschlagsmodellen auf der Basis von Wolkenprodukten, welche für die Regionalisierung von Niederschlagsregimen im PB verwendet wurden. Dies könnte wichtige Anwendungen in abgelegenen Regionen komplexer Orografie haben.
- Die neuartige Anwendung in den Anden von Ecuador, mit mehreren nicht-linearen statistischen Downscaling Ansätzen wie SDSM, sowie künstliche neuronaler Netze und Support-Vektor-Maschinen. Es wurde gezeigt, dass solche Techniken mesoskalige klimatische Einflüsse erfassen können, hingegen zeigten sich Mängel hinsichtlich der Darstellung der lokalen Modifikation des Klimasignals.
- Die Entwicklung einer umfassenden Sensitivitätsanalyse der Sub-Grid-Parametrisierung im PB, vor der Bewertung der hochauflösenden regionalen Klimamodellierung, z.B. WRF 15 km in den tropischen Anden. Es wurde festgestellt, dass RCM-WRF in der Lage ist mesoskalige Modifikationen des synoptischen Signals zu erfassen, wobei jedoch eine starke Überschätzung der Niederschlagsmengen beobachtet wurde.
- Die Bewertung des zusätzlichen Nutzens durch Anwendung beider, des dynamischen als auch des statistischen, Downscaling-Ansatzes in Kaskade (z. B. PRECIS und Störungsfaktor) ergab verbesserte Schätzungen des Niederschlags im PB.

CURRICULUM VITAE

PERSONAL INFORMATION

Name: Lenin Campozano

Place and Date of birth: Cuenca - Ecuador, December 12, 1976

Age: 40

Nationality: Ecuadorian

EDUCATION:

- PhD candidate, Universität Marburg, Germany. Tutor, Prof. Dr. Jöerg Bendix. From: December 12, 2011, To: present. Funding SENESCYT scholarship.

- MSc. Numerical Methods (2011), Silesian Polytechnic University. Cuenca-Ecuador.

- University Teaching Specialist (2011), University of Azuay, Cuenca - Ecuador.

- Civil Engineer (2000), University of Cuenca, Cuenca – Ecuador.

Erklärung

Ich erkläre an Eidesstatt, dass ich meine Dissertation

Climate across scales: the downscaling of precipitation for a basin in a tropical mountain region in the Andes of Southern Ecuador

selbstständig und ohne unerlaubte Hilfe angefertigt und mich dabei keinerlei anderen als der von mir ausdrücklich bezeichneten Quellen und Hilfen bedient habe.

Die Dissertation wurde in der jetzigen oder einer ähnlichen Form noch an keiner anderen Hochschule eingereicht und hat noch keinen sonstigen Prüfungszwecken gedient.

Marburg, 01.12.2016

Lenin Vladimir Campozano Parra